

A POTENTIAL FIELD FRAMEWORK FOR ACTIVE
VEHICLE LANEKEEPING ASSISTANCE

A DISSERTATION
SUBMITTED TO THE DEPARTMENT OF MECHANICAL ENGINEERING
AND THE COMMITTEE ON GRADUATE STUDIES
OF STANFORD UNIVERSITY
IN PARTIAL FULFILLMENT OF THE REQUIREMENTS
FOR THE DEGREE OF
DOCTOR OF PHILOSOPHY

Eric J. Rossetter

December 2003

© Copyright by Eric J. Rosseter 2004
All Rights Reserved

I certify that I have read this dissertation and that, in my opinion, it is fully adequate in scope and quality as a dissertation for the degree of Doctor of Philosophy.

J. Christian Gerdes
(Principal Adviser)

I certify that I have read this dissertation and that, in my opinion, it is fully adequate in scope and quality as a dissertation for the degree of Doctor of Philosophy.

Oussama Khatib
(Computer Science)

I certify that I have read this dissertation and that, in my opinion, it is fully adequate in scope and quality as a dissertation for the degree of Doctor of Philosophy.

Günter Niemeyer

Approved for the University Committee on Graduate Studies.

This thesis is dedicated to my wife, Sara.

Abstract

In 2001, over 18000 deaths in the United States were caused by automobiles leaving the lane and colliding with a fixed object in the environment. Despite recent advances in vehicle safety, the responsibility for avoiding collisions with objects in the environment remains solely with the driver. Though humans are quite adept at this task, they are far from infallible. This work presents a potential field framework for active lanekeeping assistance that seeks to prevent accidents from lane departures. This control concept assumes by-wire technology to add control inputs (steering and braking) on top of the driver commands. The potential field concept passively couples the vehicle to the environment, seamlessly adding control inputs when necessary to aid in the lanekeeping task. For a lanekeeping assistance system, safety is of primary importance. The potential field framework provides mathematical safety guarantees for the lanekeeping performance while creating a system that works cooperatively with the driver.

This thesis covers the general control structure, a method of incorporating stability and performance objectives in the potential field framework, and a Lyapunov-based method for bounding the lateral motion of the vehicle subjected to time-varying disturbances. This bounding technique is extremely general and is applicable to a wide variety of dynamic systems. The technique provides an excellent bound on the lateral motion of the vehicle in the presence of road curvature disturbances. The potential field controller is implemented on a 1997 Corvette C5 modified to include steer-by-wire. The experimental results validate the theoretical lanekeeping performance of the system. The results also show that the theoretical bounds are a useful tool for the design of a potential field controller and quantitatively guarantee the nominal safety

of the lanekeeping system.

Acknowledgements

There are many people who have helped and supported me throughout my time as a Ph.D. student. No one has been more influential during this process than my advisor, Chris Gerdes. Chris is an excellent mentor and significantly influenced my intellectual path at Stanford. I've enjoyed sharing his first years at Stanford and helping develop the lab. I also want to thank Chris for providing an extremely cool testbed for implementing my research on. Not many students get to drive a Corvette around all day and call it work.

I would also like to thank my reading committee, Günter Niemeyer and Oussama Khatib, for taking their time to read and critique this thesis. Thanks also to Claire Tomlin and Mark Cutkosky for volunteering to be on my defense committee.

I have also had the great privilege of working in the Dynamic Design Lab with many other intelligent and interesting individuals. Our workplace is a truly unique environment with epic battles of PIG, a constant barrage of wise-ass remarks, and of course sake bomb cleaning day. A few friends in the lab deserve some special recognition. Chris Carlson, although I didn't know you at U.C. Davis I'm glad to have met you at Stanford. We have had quite a journey at Stanford and at the end I think we've actually learned something (like linear algebra). You are a brilliant person and I hope we continue our quarterly traditions wherever our lives may take us. I would like to thank Greg Shaver for all of his insightful commentary and truly witty mom jokes. Thanks to Mike Prados for creating an exciting lab environment, especially when high voltage or electrolytic capacitors were involved. Finally, I want to thank Josh Switkes who's enthusiasm for vehicle testing is unmatched by anyone in the lab. I also would like to thank him for his cat-like reflexes on the day he earned

the nickname '1g' Switkes.

I want to thank all my friends outside the lab who have been there throughout my time at Stanford. Special thanks to Joel, Brucek, and Chris Barnes for all the fun times we've had throughout the years. Graduate school would not have been the same without you guys. Finally, I would like to thank Shannon and Carlson for all the memorable times we've had.

I want to thank all my family; mom, dad, Jane, Vince, and my sisters, Sandra and Beth for always being there to support and encourage me. Most of all I want to thank my wife, Sara, for all her love and encouragement. You have been there from the beginning of my academic career and we are finally both doctors!

Contents

	iv
Abstract	v
Acknowledgements	vii
1 Introduction	1
1.1 Motivation	2
1.2 Related Work	4
1.3 Thesis Contributions	6
1.4 Thesis Outline	6
2 Potential Fields for Vehicle Control	8
2.1 Previous Work	9
2.2 Tire and Vehicle Modeling	10
2.2.1 Tire Force Generation	10
2.2.2 Vehicle Dynamics	13
2.3 General Potential Field Approach	18
2.3.1 Control Law	20
2.4 A Lanekeeping System Example	24
2.4.1 Potential Field Design	24
2.4.2 Simulation Evaluation	25
2.5 A Closer Look at Dynamic Response	29

3	Lanekeeping Stability and Performance	32
3.1	Previous Work	33
3.2	Virtual Force Analogy for Control	35
3.3	Linearization of Vehicle Dynamics	38
3.3.1	Vehicle Stability without Control	40
3.4	Stability with Virtual Forces	41
3.4.1	Virtual Force at the C.G.	42
3.4.2	Shifting the Virtual Force	45
3.5	Incorporating Lookahead	50
3.6	Controller Damping	53
3.7	Concluding Remarks	56
4	Bounding Lateral Motion	58
4.1	Potential Field Control Structure	59
4.2	Bounding Lateral Motion	61
4.2.1	Passivity with Lookahead	61
4.2.2	A New Bound for Lanekeeping	64
4.2.3	Simulation Example	73
4.3	Road Curvature	75
4.4	Bounding Time-Varying Disturbances	77
4.5	Application for Lanekeeping	84
4.5.1	Simulation with Lateral Bounds	87
4.6	Concluding Remarks	90
5	Implementation of the Lanekeeping System	92
5.1	Potential Field Control with Front Steering	92
5.2	Control System Structure	94
5.3	Sensing and Actuation	95
5.3.1	Position and Attitude Sensing	95
5.3.2	Steer-by-wire	96
5.3.3	Computing	97
5.4	Kalman Filters	97

5.4.1	Overview	97
5.4.2	Heading	99
5.4.3	Position	101
5.5	Precision Maps	103
5.5.1	Error Finding	105
5.6	Results and Simulation	106
5.6.1	Test Setup	106
5.6.2	Lanekeeping Performance	107
5.7	Concluding Remarks	109
6	Conclusion	112
6.1	Summary	112
6.2	Future Work	114
A	The Dugoff Tire Model	116
B	Solving for the Control Inputs	119
C	A Simple Stability Controller	124
C.0.1	Avoidance Maneuver	126
D	Map Making	129
	Bibliography	133

List of Tables

2.1	Vehicle Parameters, Variables and Inputs	26
2.2	Driver Model Parameters	28
3.1	Vehicle Parameters: Chapter 3	44
3.2	Eigenvalues and Damping	54
4.1	Vehicle Parameters for Simulation 1	73
4.2	Vehicle and Controller Parameters for Simulation 2	87
5.1	Test Vehicle and Road Parameters	108
5.2	Controller Parameters for Moffett Field Testing	108

List of Figures

1.1	Crashes from Lane Departures	2
1.2	Lanekeeping Potential	3
2.1	Tire Velocities	11
2.2	Lateral and Longitudinal Tire Forces	12
2.3	Planar Model of Vehicle Dynamics	13
2.4	Tire Velocities	14
2.5	Cross Section of Potential Function	19
2.6	Global Coordinates	21
2.7	Section of Lanekeeping Potential Function	22
2.8	Response with Lateral Disturbance	27
2.9	Gentle Lane Change Response	29
2.10	A Possible Response	30
2.11	Lanekeeping Behavior for Varying C.G. Location	31
3.1	Lanekeeping Analogy	35
3.2	Virtual Bumper Concept	36
3.3	Virtual Force Analogy	37
3.4	Lookahead	38
3.5	Simulation: Virtual Force at C.G.	45
3.6	Shifting the Control Force	46
3.7	Vehicle Response to the Virtual Force	47
3.8	Simulation: Virtual Force at Neutral Steer Point	49
3.9	Oversteering Vehicle Eigenvalues as Application Point Shifts Forward	49

3.10	Understeering Vehicle Eigenvalues as Application Point Shifts Forward	50
3.11	Eigenvalues as the Lookahead Distance is Varied from 0-60m: Understeering Vehicle	52
3.12	Eigenvalues as the Lookahead Distance is Varied from 0-60m: Oversteering Vehicle	53
3.13	Understeering Vehicle Response with Varying Lookahead	54
4.1	Important Locations	60
4.2	Global Coordinates	65
4.3	Level Set	72
4.4	Lyapunov Function	74
4.5	Vehicle Lateral Position	75
4.6	Road Curvature Disturbance	76
4.7	Road Curvature	76
4.8	Optimal ϵ	88
4.9	Road Profile	89
4.10	Road Curvature	90
4.11	Lateral Error with Bounds	91
5.1	Control Structure for Vehicle Lanekeeping	94
5.2	Steer-by-Wire Corvette	95
5.3	Heading: GPS and Kalman filter Output	100
5.4	East Position: Raw GPS and Kalman Filter Output	103
5.5	North Position: Raw GPS and Kalman Filter Output	104
5.6	Moffett Map with Segment Boundaries	105
5.7	Error Finding	106
5.8	Corvette Test Vehicle at Moffett Field	107
5.9	Lateral Error: Simulation vs. Experiment with $k=15000$	109
5.10	Difference in Lateral Error between Simulation and Experiment	110
5.11	Lateral Error with $k=10000$	111
A.1	Tire Velocities	117

A.2	Lateral and Longitudinal Tire Forces	118
B.1	Equivalent Forces Concept	120
B.2	Differential Braking Distribution	122
B.3	Front/Rear Brake Distribution	123
C.1	Stability Control Regions of Operation	125
C.2	Avoidance Maneuver Response	127
D.1	Map of Lane Center Showing Segment Boundaries	130

Chapter 1

Introduction

Today, automobiles are an indispensable part of everyday life. Cars provide a level of freedom and autonomy that has come to be expected in our daily routine. We rely on cars for all types of travel, from the daily commute to work, to a Sunday afternoon drive. Due to the prevalence of vehicles in our society, passenger safety is of primary importance. Over the past few decades, passive safety features such as crumple zones, seat belts, and airbags have become standard automobile features, saving thousands of lives per year. More recently, active control has been used to assist the driver in avoiding accidents by preventing unstable vehicle behavior. Anti-lock brake systems designed to prevent wheel lock-up are now common and stability control programs designed to prevent skidding are seeing increased popularity. Despite these advances in active safety, the responsibility for avoiding collisions with objects in the environment remains solely with the driver. Though humans are quite adept at this task, they are far from infallible; in 2001, for instance, the first harmful event for 43% of fatal crashes in the United States was a collision with a fixed object in the environment (NHTSA [41]). In 2001, this accounted for over 18,000 deaths in the United States. Figure 1.1 shows some typical accidents from lane departures. The crash in the left photo resulted from a diabetic driver who lost consciousness while the other was simply caused by driver inattentiveness.



Figure 1.1: Crashes from Lane Departures

1.1 Motivation

The work presented in this thesis aims at preventing accidents from lane departures. There are many approaches to aid the driver in lanekeeping. On one end of the spectrum, passive approaches use auditory, visual, or haptic feedback to warn the driver of an impending lane departure. At the other extreme, fully autonomous systems remove the driver completely from any lanekeeping tasks. There are tradeoffs and advantages to both approaches. Passive systems are the easiest to implement and only require lane sensing technology and a method of warning the driver. With passive systems the lanekeeping ability of the system, however, still relies on the driver and his or her response to the warning. On the other hand, fully autonomous vehicles require extensive modification to handle both the road sensing and the control of the vehicle. The advantage is that the driver is completely removed from the lanekeeping task, eliminating any possibility of driver errors. Of course, without a driver the lanekeeping system requires an extremely high degree of robustness, which is a significant barrier for this system reaching production in the near future. The method taken in this thesis focuses on the middle ground between these two approaches. This work looks at using active control to assist the driver in the lanekeeping task.

The design of this system has two main objectives. The first is the ability to keep the vehicle in the lane, while the second is to have a system that works cooperatively

with the driver. These are often competing objectives. If a perfect lane tracking system is created, satisfying the first objective, the system will most likely be overly intrusive during normal driving. On the other hand, creating a system with low control authority that does not interfere with normal driving might fail to maintain the lane in the absence of driver inputs.

This thesis presents a framework for lanekeeping assistance that provides analytical safety guarantees for the system while providing a comfortable and predictable driving environment. The approach for the driver assistance system is based on artificial potential fields, first introduced in the context of robotic control by Khatib [34] and Hogan [32]. The general potential field approach assumes a vehicle with steer-by-wire and brake-by-wire, which are controlled to recreate the effect of a potential field acting on the vehicle. The potential function is an intuitive way to represent the level of hazard experienced by the vehicle. An exaggerated representation of a lanekeeping potential is shown in Figure 1.2 where the potential function minimum is close to the road center with height increasing towards the lane edges.

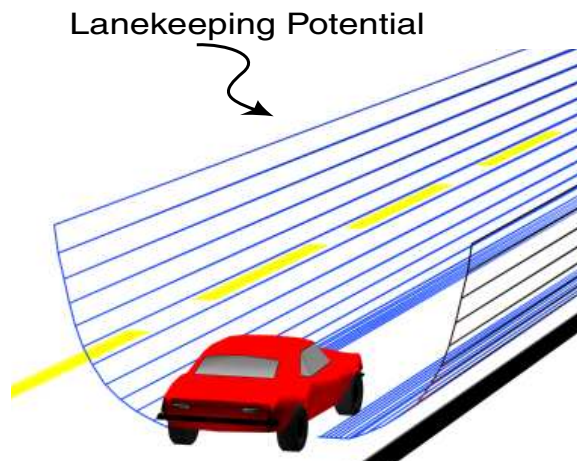


Figure 1.2: Lanekeeping Potential

The potential field approach provides a compact mathematical framework that addresses important issues for driver assistance systems. The system is designed to work with the driver and does not alter the underlying handling characteristics of

the vehicle. As a result, the vehicle responds as expected to driver inputs. Another extremely important feature is the ability to provide mathematical bounds on the lanekeeping performance of the system. These bounds can be used to design a potential field controller capable of keeping the vehicle in the lane while working cooperatively with the driver.

1.2 Related Work

There is a large body of related work for lanekeeping systems and the use of potential fields for control applications. This section presents a brief overview of previous work in lanekeeping assistance systems where the driver plays an active role in the lanekeeping task. A background of similar impedance control strategies for robotic and vehicle control is covered in Chapter 2. Chapter 3 discusses related work in vehicle control and dynamics while Chapter 5 presents previous work that incorporates GPS for automotive controls.

As mentioned earlier, there are two main approaches for lanekeeping assistance: passive and active. Both methods require sensing technology to determine the vehicle's road position. Vision has been used most extensively for this task, identifying lane markings to determine the vehicle's position and orientation. Vision for lanekeeping assistance is being researched at major automotive companies and academic institutions. A few examples of current vision based lane recognition systems are presented in work by Gehrig et al. [20], Paetzold et al. [45], and Lee et al. [39]. Gern et al. [24] looked at increasing lane detection robustness by combining information from vision and radar sensors. This system used radar to infer road position from a leading vehicle, supplementing the information from the vision system. Vision systems that incorporate obstacle detection are discussed in work by Handmann et al. [29], Stiller et al. [64], and Franke et al. [17]. All of these systems provide adequate lane recognition for lanekeeping assistance. The global positioning system (GPS) and digital maps also provide a method for obtaining lane position. This is the sensing technology used in our test vehicle and more detail is provided in Chapter 5.

Passive lanekeeping methods use this information to try and warn the driver of an

impending lane departure. These systems require a method for determining whether a lane departure is eminent. Work by Kwon and Lee [37] proposed heuristic methods for determining lane departure based on the vehicle's lateral offset and an estimate of the lane departure time. Once a lane departure is sensed, the driver is warned with visual, tactile, or auditory signals. Feng et al. [14] used visual feedback to provide road information along with the vehicle's current and future position to aid the driver in adverse conditions. Lane departure warning systems by Lee et al. [39] used voice warning while Suzuki and Jansson [66] compared auditory and haptic feedback for lane departure warnings.

In contrast, active control takes a more aggressive role in preventing lane departure. This approach utilizes some type of control authority to steer the vehicle back towards the lane center. Actuation of the wheels is accomplished in one of two ways. The first involves coupling a motor directly to the steering column, providing extra torque at the steering wheel to aid the driver in the lanekeeping task. In this type of system, as the vehicle leaves the lane the motor attempts to turn the steering wheel in the opposite direction. This approach is problematic because it resists the driver commands and is often viewed as an annoyance during normal driving. Another approach is to completely decouple the hand wheel from the front wheel actuation. In these 'steer-by-wire' systems, the steering wheel angle is measured by a control computer which then commands the desired angle at the road wheels. The term 'x-by-wire' refers to any driver controlled system that does not have a mechanical connection between the driver's control interface and the actuator. Brake-by-wire and throttle-by-wire are currently used in production vehicles with steer-by-wire in the development phase.

With these by-wire technologies it is possible to alter the vehicle's path independently from the driver. Fujioka et al. [18] developed a system, assuming steer-by-wire, that used the input from the driver along with the command from a 'virtual' driver to determine the total steering command. This approach was tested using a fixed based driving simulator, showing that the driver acceptance was inversely related to the 'virtual' drivers influence. Work by LeBlanc et al. [38] used differential braking to apply moments to the vehicle aiding in lanekeeping. Human centered designs have

also been done by Reichelt and Frank [49]. Although intriguing, these approaches to driver assistance have no quantitative way of guaranteeing safety (in terms of lane-keeping performance) while smoothly combining the driver and controller objectives.

1.3 Thesis Contributions

The contributions of this thesis are:

- A general potential field framework for incorporating collision avoidance as a driver assistance system.
- A unique method for obtaining lateral vehicle stability requirements that incorporates a wide variety of actuator and sensor configurations.
- A technique for obtaining tight bounds on the lateral motion of the vehicle using a Lyapunov function related to a subset of the system energy that is pertinent for lanekeeping.
- A method for bounding the lateral vehicle motion in the presence of time-varying disturbances. The technique is extremely general and applies to a large class of Lagrangian dynamic systems.
- Implementation and validation of the potential field controller on a steer-by-wire test vehicle.

1.4 Thesis Outline

Chapter 2 gives a brief introduction to vehicle dynamics followed by the development of the general potential field control law. This control framework utilizes the natural damping characteristics of the vehicle dynamics to form a passive system that conserves overall energy. A simple example illustrates the design of a lanekeeping system using the potential field concept.

Chapter 3 focuses on the lanekeeping stability of the system. The analysis in this chapter treats the control force as a ‘virtual’ force applied to the vehicle and

develops important stability requirements for the lanekeeping system. This virtual force analogy is an intuitive way to view many types of lateral vehicle controllers.

Chapter 4 incorporates the stability requirements developed in Chapter 3 into the potential field control structure. With these stability requirements, the overall system still maintains passive properties. However, in order to ensure safety of the lanekeeping system a useful method for bounding the lateral motion is required. Chapter 4 develops a Lyapunov function based on a subset of the system energy related to only the lateral and rotational dynamics. This function provides excellent bounds on the lateral motion of the vehicle. By design, the potential field approach passively couples the vehicle to the environment and does not attempt to track a desired trajectory. As a result, disturbances such as road curvature will alter the vehicle motion. The second part of this chapter develops a general bounding technique that handles time-varying disturbances. This technique is applied to the vehicle system with road curvature disturbances, providing an excellent bound for the vehicle's lateral motion. This bounding technique is quite general and is applicable to a wide variety of dynamic systems.

Chapter 5 presents experimental results for the lanekeeping system. This chapter gives a description of the experimental test bed and the control structure used for implementation of the potential field control law. The test vehicle is a 1997 Chevrolet Corvette modified to a steer-by-wire format. The lane information is obtained using Global Positioning System (GPS) information combined with a digital road map. The system performed almost exactly as predicted by simulation, giving confidence in the vehicle model and the theoretical bounds. The results verify that these bounds provide a safety guarantee for the lanekeeping system that is not overly conservative.

Chapter 6 provides a summary of the thesis. This is followed by possible directions for future work in active lanekeeping assistance.

Chapter 2

Potential Fields for Vehicle Control

This chapter presents a potential field framework for incorporating active vehicle safety systems (such as lanekeeping) to assist the driver. The work presented here envisions vehicle control as a means of fundamentally altering the dynamic relationships between the vehicle and surrounding environment, creating a system that is still enjoyable to drive while providing some level of increased safety. Instead of viewing driver assistance as a collection of individual functions, this approach treats it as a redesign of the driving experience. Ultimately, a successful redesign will make the driving experience safer, more fun, and tunable to individual driving styles or preferences.

The dynamics of high speed vehicles with pneumatic tires play an important role throughout this thesis. Before discussing the potential field controller, a vehicle model is introduced that captures the relevant dynamics of high speed vehicles. Vehicle dynamics are governed by the forces created between the tires and the road surface. Therefore, it is important to understand the basic properties of tire force generation and the way these forces are controlled by the driver. The rest of the chapter outlines the basic potential field approach and presents a proof of the nominally safe behavior provided by the system. To illustrate the potential field concept, a simple lanekeeping example is presented.

2.1 Previous Work

The paradigm chosen for creating this new relationship between the vehicle and the environment is that of an artificial potential field. First proposed by Khatib [34] for robotic manipulator control and by Hogan [32] in the general context of impedance control, potential fields have seen considerable application to obstacle avoidance and mobile robots. The basic concept uses control to recreate the effect of potential energy. Obstacles (or hazards) are represented by large potentials whereas desired locations correspond to low potential function values. In robotics, the underlying dynamics are often cancelled so that the dynamics of the control point are equivalent to a point mass subjected to the potential field force. For driver assistance, however, the control forces are added on top of the existing dynamics creating a passive coupling between the vehicle and the environment. Therefore the system behaves in a predictable manner to the driver inputs while providing extra control forces as needed to aid in the lanekeeping task.

Similar impedance approaches have been used in the design of autonomous passenger cars and heavy trucks. Reichhardt and Schick [48] proposed an electric field interpretation for autonomous vehicle control based upon a risk map. The risk map assigned a value corresponding to the relative hazard to every point in a two-dimensional description of space. The hazard at each point, interpreted as a charge, exerted a force on the vehicle (interpreted as an electron) with the resultant force from all charges in the environment determining the path of the autonomous vehicle. Since the vehicle dynamics were not considered, this approach resulted in desired motions that were unachievable by the vehicle. Reichardt [47] later merged lanekeeping, obstacle avoidance and traffic sign recognition into the construction of the risk map. Hennessey *et al.* [31] used a spring analogy to define “virtual bumpers” for two-dimensional collision avoidance, in effect attaching an impedance or potential field to the vehicle. This controller was coupled with a heuristic lane change controller for collision avoidance (Schiller *et al.* [58]) and demonstrated on an autonomous land vehicle (Schiller *et al.* [57]). Like the work of Reichardt and Schick [48], these results did not explicitly incorporate the vehicle dynamics.

In this chapter, the driver assistance system is formed from potential fields and generalized damping functions added to the existing vehicle dynamics and driver inputs. Viewed within the language of impedance control (Hogan [32]), the potential fields and damping turn the environment into an impedance, providing restoring forces that move the vehicle towards safer regions of the state space. The controller does not attempt to interpret driver intent, but merely presents a safe, predictable, dynamic response to the driver. Leaving the inherent dynamics in place is a novel approach to creating a driveable system where the control forces are smoothly combined with the vehicle dynamics as needed. By leaving the driver in the loop, high-level tasks such as path planning remain the province of the driver, thereby avoiding the difficulties of local minima which can arise with potential field controllers. The local nature of the control design allows the system to use a local representation of the environment, avoiding the computational difficulties noted by Reichardt and Schick [48].

2.2 Tire and Vehicle Modeling

2.2.1 Tire Force Generation

The pneumatic tires on a vehicle can create both lateral and longitudinal forces, allowing the car to accelerate and turn. These forces are a function of the tire properties (material, tread pattern, tread depth, profile, etc.), the normal load on the tire, and the velocities experienced by the tire. The relationship between these factors is extremely complex and nonlinear. Several models have been developed that predict the behavior of tires remarkably well. One of the most common is Pacjeka's "Magic Formula" [5], which does an excellent job of predicting real tire behavior, but requires a large number of tire specific parameters that are usually unknown. Another commonly used model is the Dugoff tire model [28] (Appendix A), which groups all the tire property parameters into two constants, C_x and C_y , referred to as the longitudinal and cornering (or lateral) stiffness of the tire. Along with the cornering and longitudinal stiffness, the tire forces are related to the deformation of the tire along its contact area with the ground, referred to as the tire contact patch. The longitudinal

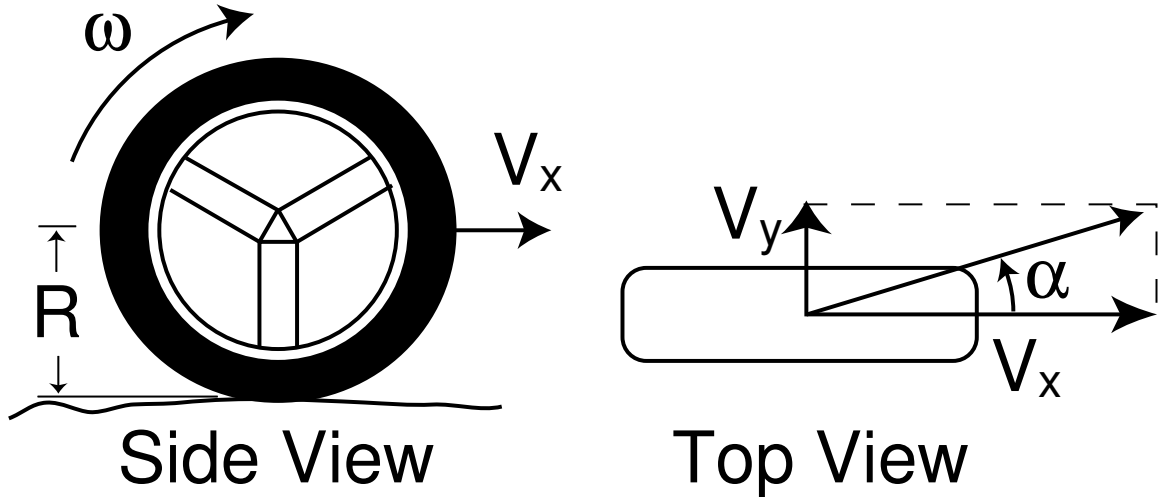


Figure 2.1: Tire Velocities

deformation is related to the tire slip, s_w , while the lateral deformation is quantified by the tire slip angle, α . Tire slip is related to the difference between the wheel's true forward velocity and the angular velocity of the tire. The tire slip angle is simply the angle between the tire's velocity direction and the longitudinal axis of the tire. The tire slip and slip angle are defined as

$$s_w = \frac{V_x - R\omega}{V_x} \quad (2.1)$$

$$\alpha = \tan^{-1} \left(\frac{V_y}{V_x} \right) \quad (2.2)$$

where V_x and V_y are the lateral and longitudinal velocity at the tire center, R is the tire radius, and ω is the angular velocity of the tire as shown in Figure 2.1.

Figure 2.2 shows typical lateral and longitudinal force profiles for pneumatic tires. These force curves are generated from the Dugoff tire model but similar profiles would be obtained from Pacjeka's formula or real tire data. The force profile for both cases is linear for small values of tire slip and tire slip angle, but eventually levels off when the tire begins to saturate. Under normal driving, the tires are well away from saturation and have small slip and slip angle values. Under these types of conditions the longitudinal and lateral forces are approximately linear functions of the slip and

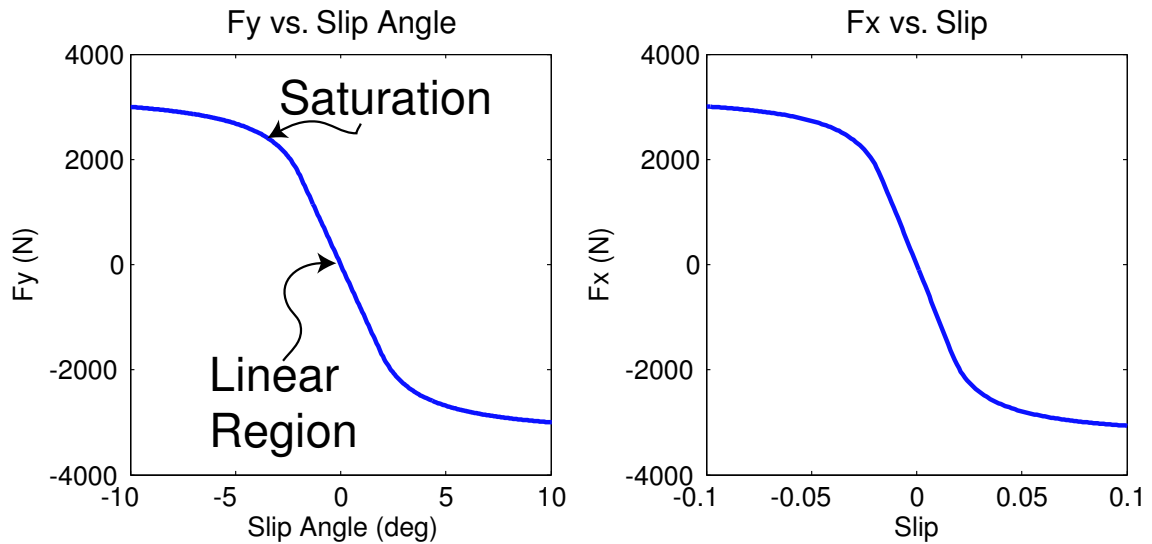


Figure 2.2: Lateral and Longitudinal Tire Forces

slip angle with a slope equal to the corresponding stiffness. As a result, it is common to use this linear approximation for the tire forces in vehicle models.

$$F_x \approx -C_x s_w \quad (2.3)$$

$$F_y \approx -C_y \alpha \quad (2.4)$$

When using these linear approximations it is important to understand the operating region of the tires for the specific application. For example, in the design of a stability controller where the vehicle tires are at the limits of adhesion, this is not a suitable approximation for predicting vehicle motion. Typically, the linear tire model predicts real tire behavior for vehicle accelerations under 0.5g, which is well within normal driving conditions. With an understanding of these basic tire properties it is relatively straightforward to develop a vehicle model that captures the important dynamics of high speed vehicles.

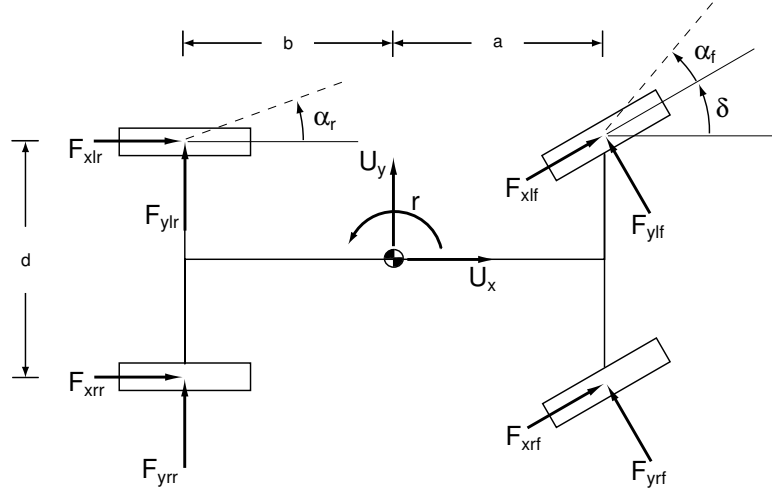


Figure 2.3: Planar Model of Vehicle Dynamics

2.2.2 Vehicle Dynamics

The vehicle model, shown in Figure 2.3, is a simple yaw plane representation with three degrees of freedom (Koepele and Starkey [35]). In the development that follows, the vehicle is assumed to have differential braking with throttle-, brake-, and steer-by-wire. This refers to the fact that the throttle, braking, and steering are all electronically controlled. The equations of motion are developed using Newton-Euler methods as follows and are expressed in terms of the vehicle fixed velocities.

$$m(\dot{U}_x - rU_y) = F_{xr} + F_{xf} \cos \delta - F_{yf} \sin \delta \quad (2.5)$$

$$m(\dot{U}_y + rU_x) = F_{yr} + F_{xf} \sin \delta + F_{yf} \cos \delta \quad (2.6)$$

$$I_z \dot{r} = aF_{xf} \sin \delta + aF_{yf} \cos \delta - bF_{yr} + \frac{d}{2}(\Delta F_{xr} + \Delta F_{xf} \cos \delta) \quad (2.7)$$

In these equations F_{xf} and F_{xr} are the longitudinal forces created by the front and rear tires. The difference between the longitudinal force on the left and right tires is captured in ΔF_{xf} and ΔF_{xr} . These terms account for the moments created by differential braking.

$$F_{xf} = F_{xrf} + F_{xlf} \quad (2.8)$$

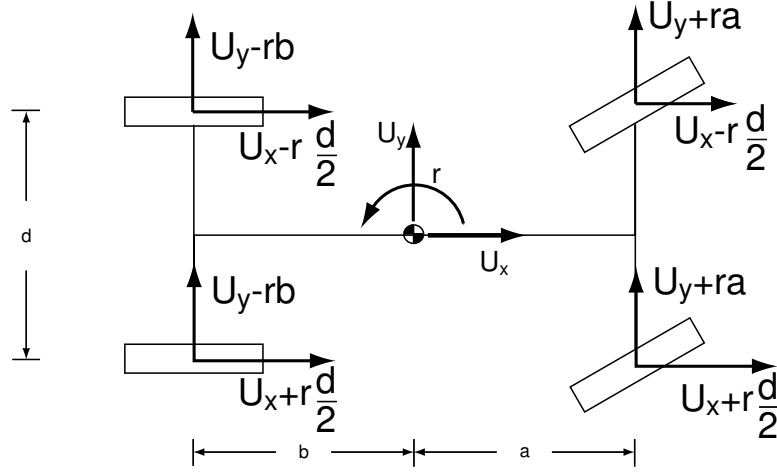


Figure 2.4: Tire Velocities

$$F_{xr} = F_{xrr} + F_{xlr} \tag{2.9}$$

$$\Delta F_{xf} = F_{xrf} - F_{xlf} \tag{2.10}$$

$$\Delta F_{xr} = F_{xrr} - F_{xlr} \tag{2.11}$$

With brake and throttle control the longitudinal forces and differential braking can be controlled. There is not, however, a direct way to control the lateral forces on the tires. As described in the previous section, the lateral forces are related to the tire slip angle, α . For this model it is assumed that the left and right tires possess the same slip angle. In general, this is not strictly true due to a longitudinal velocity component created from the yaw rate, r , crossed into half the track width, $\frac{d}{2}$, as shown in Figure 2.4. Looking more carefully at this velocity component shows that it is oppositely signed on the left and right wheels. Therefore, a force increase from this component on one tire will lead to a force decrease on the opposite tire. As a result, the left and right tires are lumped together and assumed to have a velocity that neglects this small yaw rate contribution. This assumption can also be viewed mathematically by comparing the rear slip angle on the left tire (α_{rl}) and right tire

(α_{rr}) .

$$\alpha_{rl} = \tan^{-1} \left(\frac{U_y - rb}{U_x - \frac{d}{2}r} \right) \quad (2.12)$$

$$\alpha_{rr} = \tan^{-1} \left(\frac{U_y - rb}{U_x + \frac{d}{2}r} \right) \quad (2.13)$$

The longitudinal velocity, U_x , is large while the small yaw rate term in the denominator is oppositely signed on the left and right tires. As a result, the total lateral rear force, F_{yr} , is approximately.

$$F_{yr} = -C_{rl}\alpha_{rl} - C_{rr}\alpha_{rr} \approx -(C_{rl} + C_{rr})\tan^{-1} \left(\frac{U_y - rb}{U_x} \right) = -C_r\alpha_r \quad (2.14)$$

where C_r is the sum of the rear cornering stiffnesses. This vehicle model is sometimes referred to as the ‘bicycle’ model because of this grouping of left and right tires into one tire at the front and one at the rear. Despite the name, this model does not predict the behavior of a two-wheeled vehicle (i.e. a bicycle) because it does not include any roll dynamics. Using this bicycle model, the front and rear slip angles are given by

$$\alpha_f = \tan^{-1} \left(\frac{U_y + ra}{U_x} \right) - \delta \quad (2.15)$$

$$\alpha_r = \tan^{-1} \left(\frac{U_y - rb}{U_x} \right) \quad (2.16)$$

The wheel angle, δ , is one of the available control inputs and only contributes to a portion of the lateral force at the front wheels. The remaining terms develop through the dynamics and determine the vehicle’s handling properties. Grouping the tire forces into controlled and uncontrolled portions yields

$$M_3\ddot{q}_3 = f_3(\dot{q}_3) + g(u_c) \quad (2.17)$$

where the velocity and control vectors are defined as

$$\dot{q}_3 = [U_x \ U_y \ r]^T \quad (2.18)$$

$$u_c = [\delta \ F_{xr_f} \ F_{xl_f} \ F_{xrr} \ F_{xlr}]^T \quad (2.19)$$

The matrix M_3 is the mass matrix, f_3 contains all the uncontrolled or drift terms and g contains all the controlled components.

$$M_3 = \begin{bmatrix} m & 0 & 0 \\ 0 & m & 0 \\ 0 & 0 & I_z \end{bmatrix} \quad (2.20)$$

$$f_3 = \begin{bmatrix} mrU_y \\ F_{yr} - mrU_x + \hat{F}_{yf} \\ -bF_{yr} + a\hat{F}_{yf} \end{bmatrix} \quad (2.21)$$

$$g = \begin{bmatrix} F_{xr} + F_{xf} \cos \delta - F_{yf} \sin \delta \\ F_{xf} \sin \delta + F_{yf} \cos \delta - \hat{F}_{yf} \\ aF_{xf} \sin \delta + aF_{yf} \cos \delta - a\hat{F}_{yf} + \Delta F_{xr} \frac{d}{2} + \Delta F_{xf} \frac{d}{2} \cos \delta \end{bmatrix} \quad (2.22)$$

where

$$\hat{F}_{yf} = -C_f \left(\frac{U_y + ra}{U_x} \right) \text{sgn}(U_x) \quad (2.23)$$

for some effective front cornering stiffness, $C_f \geq 0$. This separates the dynamics into a drift vector depending only on \dot{q}_3 and a control vector involving components of u_c . The sgn term is added to account for the sign change when $U_x < 0$, which is lost in the small angle approximation. It is unlikely, but possible to have a negative U_x in emergency situations such as an uncontrolled spin. This linear definition for tire force is, however, undefined at $U_x = 0$.

The inclusion of the term \hat{F}_{yf} can be motivated as follows. As a first approximation, the lateral force of a tire can be approximated as a linear function of the slip angle

$$F_{yf} = -C_f \alpha_f \quad (2.24)$$

where C_f is the effective cornering stiffness of the tire (“effective” since it may involve modification for combined slip characteristics as described in the Dugoff tire model described in Appendix A). Using small angle assumptions,

$$F_{yf} \cos \delta \approx -C_f \left(\frac{ra + U_y}{U_x} \right) + C_f \delta \quad (2.25)$$

\hat{F}_{yf} thus represents an approximation to the part of the tire force that does not include the steering angle δ . With \hat{F}_{yf} , therefore, the portion of the nonlinear term $F_{yf} \cos \delta$ that does not include a control input is properly assigned to the drift vector, at least approximately.

Using this definition, the drift term f_3 is a dissipative term due to the inherent energy dissipation of the tires. Under the assumption that the tire force and the slip angle are oppositely directed,

$$\begin{aligned} \dot{q}_3^T f_3 &= F_{yr}(U_y - br) + \hat{F}_{yf}(U_y + ra) \\ &= F_{yr}(U_y - br) - C_f \frac{(U_y + ra)^2}{|U_x|} \\ &\leq 0 \end{aligned}$$

This damping characteristic of tires was demonstrated using a linear model by Chen and Tomizuka [9] and Gerdes and Rossetter [21]. The treatment here underscores that this observation is not a result of linearization, but rather follows from the basic physics of the problem. The key idea is that the tire force acts in a direction opposite that of the slip angle that produces it (which, with the possibility of a slight offset, must be true given the mechanisms of deformation and friction that produce tire forces). While a specific tire model is necessary for the implementation of the potential field controller, the damping nature of the drift term is independent of model choice. The damping property of the drift vector plays an important role in the formulation of the potential field control law: since this term always results in a net loss of energy from the system, cancellation of these dynamics is not necessary to create a passive system that conserves overall energy.

2.3 General Potential Field Approach

Robotic control using artificial potential fields was originally motivated by the desire to move some of the responsibility for collision avoidance from a high-level (and consequently slow) planning task to the lowest (and fastest) level of control (Khatib [34]). By directly coupling sensing to certain types of actuation, fast environmental hazards could be handled instinctively, rather than by high-level planning. This analogy transfers well to driver assistance systems. By keeping the driver in the loop, human capacity for high-level planning remains central to the driving experience while advanced control systems provide added convenience or faster response to hazards.

The unifying principle behind this approach is to consider each vehicle control system as assessing some penalty, or level of hazard, on different regions of the state space. The potential function is determined by summing the hazard assessed by each system on the position variables. The damping function, in turn, penalizes velocity variables. The controller (or controllers, when multiple systems are involved) then provides a level of restoring force corresponding to the gradient of the potential function (referred to as the potential field) along with the artificial damping. The vehicle therefore exhibits a natural tendency to return to areas of the state space with low levels of hazard, assisting the driver with low-level control tasks. With this approach, sensor fusion is captured systematically by the creation of the potential and damping functions and coordination among different actuators is embodied in the generation of the restoring force.

The following examples serve to better explain this concept of an artificial potential field defined by degree of hazard. Figure 2.5 illustrates a cross section of the environmental hazards seen by the car in the right lane in the manner envisioned by Reichardt [47]. Should the driver drift so that lane departure or a collision with the other vehicle becomes likely, the potential hazard increases and the controller provides a greater restoring force to move the vehicle to a safer region (in this case, the center of its lane).

Expressing driver assistance systems in terms of potential and damping functions offers several insights. Since artificial potential fields represent a complete redesign

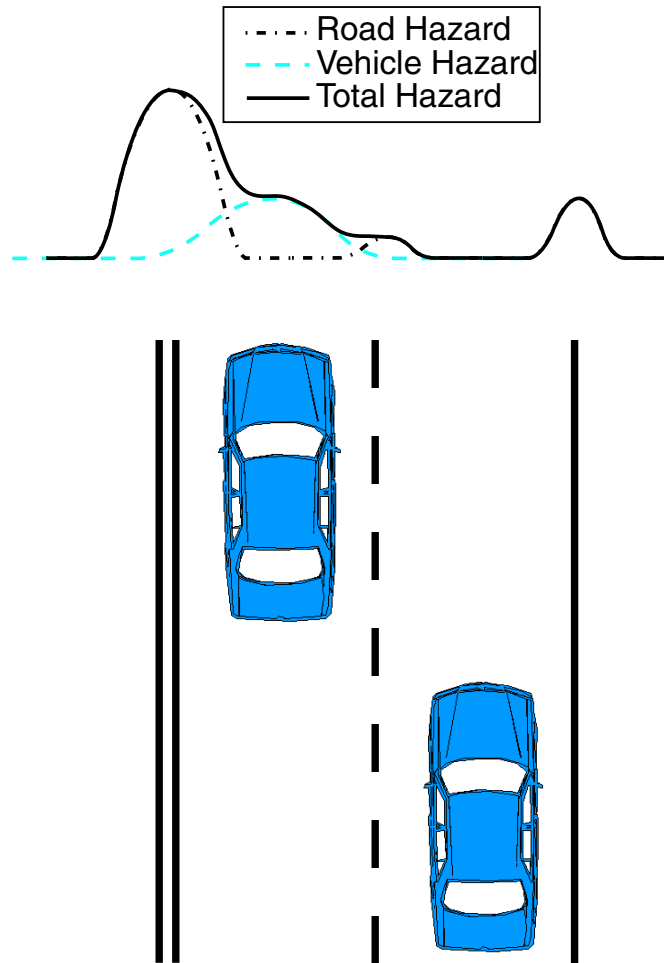


Figure 2.5: Cross Section of Potential Function

of the dynamic relationship between a system and its environment, this view opens up new possibilities for the design of the driving experience. This is especially true for interactions between systems that react primarily to environmental stimuli (like collision avoidance or lanekeeping) and those which react primarily to the vehicle state (such as stability control). While such systems have been developed separately, it is not hard to envision interactions involving, for instance, a choice between skidding and lane departure (this is particularly true if the scope is extended to heavy trucks with multiple trailers). Finally, the level of assistance provided can be adjusted by simple scaling of the potential function. Increasing the “height” of the potential function peaks relative to the valleys creates a greater restoring force in response to a given hazard, thus providing a higher level of assistance (or intrusiveness).

2.3.1 Control Law

In general, it is convenient to express fixed hazards in the environment (i.e. a lane edge) relative to road coordinates. The road fixed position vector of the vehicle is defined as $w = [s \ e \ \psi]^T$ representing the distance down the roadway, the lateral offset from the center of the lane, and the heading angle error, respectively (Figure 2.6). The state vector of the system is therefore given in terms of the position variables, w and the velocity vector \dot{q}_3 . Transformation between the road fixed velocities, \dot{w} , and the velocity vector of the vehicle, \dot{q}_3 is given by:

$$\frac{\partial \dot{w}}{\partial \dot{q}_3} = \frac{\partial w}{\partial q_3} = \begin{bmatrix} \cos \psi & -\sin \psi & 0 \\ \sin \psi & \cos \psi & 0 \\ 0 & 0 & 1 \end{bmatrix} \quad (2.26)$$

With the assumption of throttle-, brake- and steer-by-wire, the control vector u_c must combine commands from the driver and the assistance system. The control vector must therefore solve

$$g(u_c) = g(u_{driver}) + F(\dot{q}_3) - \left(\frac{\partial V_c}{\partial w} \frac{\partial w}{\partial q_3} \right)^T \quad (2.27)$$

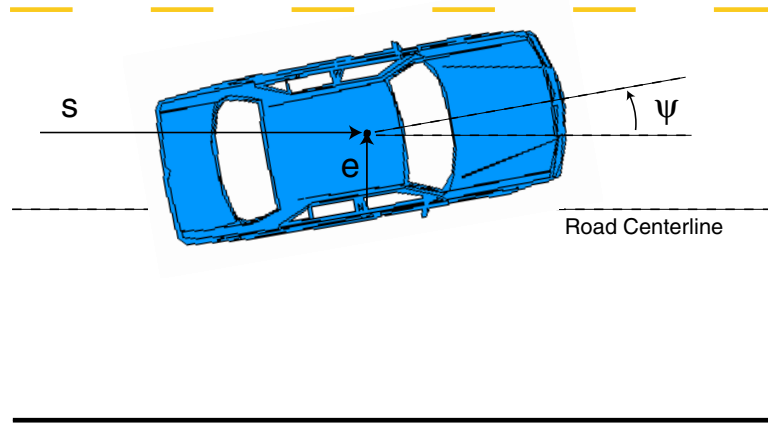


Figure 2.6: Global Coordinates

where $g(u_{driver})$ is the portion corresponding to the driver input and the remaining two terms come from the assistance system. $V_c(w)$ is the potential function describing the overall hazard in the environment and $F(\dot{q}_3)$ is a generalized damping term. This term can be any vector function that satisfies

$$\dot{q}_3^T F(\dot{q}_3) \leq 0 \quad (2.28)$$

Several constraints on the potential function are required to produce an appropriate design for lanekeeping. First, the potential function value is small near the center of the lane to give the driver the opportunity to maneuver without intrusion. Second, the potential function derivative should be continuous to prevent any discontinuities in the controlled dynamics. Finally, the peak value of the field in each section is scaled to correspond to the energy required to overcome the field. The profile of the lanekeeping potential used in the following simulation example is shown in Figure 2.7. This potential is designed for two lanes of traffic flowing in the same direction. The potential is largest on the left, which is the boundary with oncoming traffic, smallest between the lanes, and relatively large at the road edge on the right.

The driver commands, u_{driver} , consist of the steering wheel, δ_{driver} , the accelerator

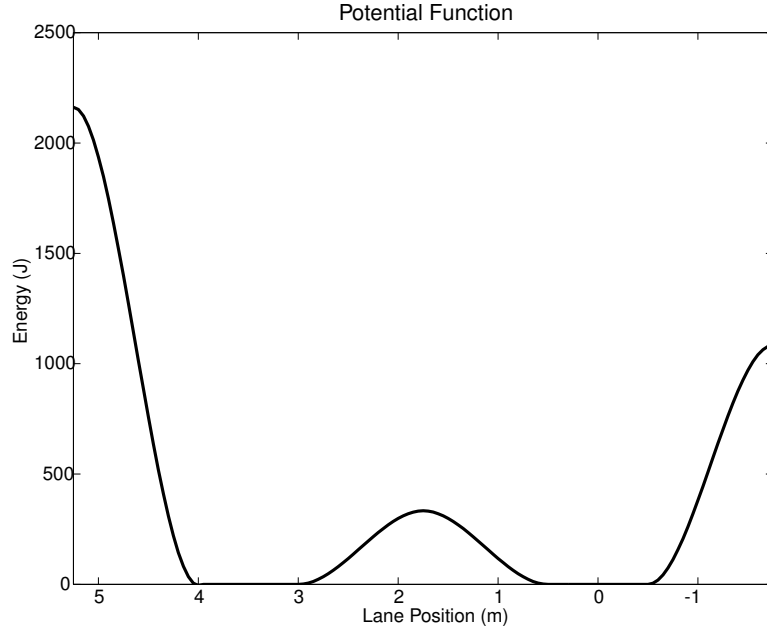


Figure 2.7: Section of Lanekeeping Potential Function

pedal, F_{ad} , and the brake pedal, F_{bd} . If we set the driver controlled terms to be

$$g(u_{driver}) \doteq g\left(\begin{array}{c} \delta_{driver} \\ -\frac{F_{bd}}{4} \\ -\frac{F_{bd}}{4} \\ \frac{F_{ad}}{2} - \frac{F_{bd}}{4} \\ \frac{F_{ad}}{2} - \frac{F_{bd}}{4} \end{array}\right) \quad (2.29)$$

then the vehicle will respond to driver inputs as if it had rear-wheel drive and standard connections (ignoring brake proportioning). With full x-by-wire capability, other mappings from driver inputs to control inputs are possible but this represents the simplest choice.

The equations of motion given in Equation 2.17 can be expressed as

$$M_3\ddot{q}_3 = f_3(\dot{q}_3) + g(u_{driver}) + F(\dot{q}_3) - \left(\frac{\partial V_c}{\partial w} \frac{\partial w}{\partial q_3}\right)^T \quad (2.30)$$

With a differentiable potential function, $V_c(w)$, and a damping function that satisfies

Equation 2.28, the system will exhibit a nominally safe behavior.

Proposition 2.3.1 [*Nominally Safe Behavior*] *If the potential function $V_c(w)$ is interpreted as a level of hazard applied to system states, then in the absence of driver input, the system hazard is bounded by:*

$$E_{max} = \frac{1}{2} \dot{q}_3(0)^T M_3 \dot{q}_3(0) + V_c(w(0))$$

where $w(0)$ and $\dot{q}_3(0)$ are the values at the initial time $t = 0$.

Proof Defining an effective energy as the sum of the vehicle's kinetic energy and the artificial potential energy from the potential field yields:

$$E = \frac{1}{2} \dot{q}_3^T M_3 \dot{q}_3 + V_c(w)$$

The rate of change of energy is:

$$\begin{aligned} \dot{E} &= \dot{q}_3^T M_3 \ddot{q}_3 + \frac{\partial V_c}{\partial w} \frac{\partial w}{\partial q_3} \dot{q}_3 \\ &= \dot{q}_3^T [f_3(\dot{q}_3) + g(u_c)] + \frac{\partial V_c}{\partial w} \frac{\partial w}{\partial q_c} \dot{q}_3 \\ &= \dot{q}_3^T \left[f_3(\dot{q}_3) + F(\dot{q}_3) - \left(\frac{\partial V_c}{\partial w} \frac{\partial w}{\partial q_3} \right)^T \right] + \frac{\partial V_c}{\partial w} \frac{\partial w}{\partial q_3} \dot{q}_3 \\ &= \dot{q}_3^T \left[f_3(\dot{q}_3) + F(\dot{q}_3) - \left(\frac{\partial V_c}{\partial w} \frac{\partial w}{\partial q_3} \right)^T \right] + \frac{\partial V_c}{\partial w} \frac{\partial w}{\partial q_3} \dot{q}_3 \\ &= \dot{q}_3^T f_3(\dot{q}_3) + \dot{q}_3^T F(\dot{q}_3) \\ &\leq 0 \end{aligned}$$

Since the effective energy cannot increase

$$E \leq E_{max} = \frac{1}{2} \dot{q}_3(0)^T M_3 \dot{q}_3(0) + V_c(w(0))$$

bounds the hazard experienced by the system.

□

This proof utilizes the fact that the drift terms in the dynamics are always removing energy. This is important because even without additional damping in the controller, the overall system still conserves energy. The equilibrium configuration of the controlled vehicle system in the absence of driver inputs is at the minimum of the artificial potential function, $V_c(w)$.

2.4 A Lanekeeping System Example

To demonstrate the potential field concept, a simple lanekeeping system is developed. This example is intended to highlight some of the functionality that can be achieved by simply adding a potential field to the existing vehicle dynamics. Although this simulation illustrates the potential field framework for lanekeeping, it is not difficult to include other control objectives in this framework. Appendix C incorporates a simple stability controller in the potential field framework through the addition of artificial damping.

2.4.1 Potential Field Design

As we have formulated the problem, it is not hard to develop the control law or to guarantee that the system tends to move towards “safer” states (as defined by the overall energy of the system) in the absence of driver inputs. In a vehicle system, some other criteria can be formulated:

- In the absence of driver inputs the potential field should be large enough to prevent lane departures in the presence of disturbances.
- The driver should be able to change lanes in a manner qualitatively similar to the uncontrolled system.

The first can be met analytically in the development of the potential fields. The second is evaluated through simulation with a simple driver model. It is important to keep in mind that this approach to driver assistance does not treat driver inputs as disturbances, rather it simply adds control commands to move the vehicle states

to a “safer” region. The driver can choose to cancel the effects of these control inputs through his or her control authority (much like maintaining the lane in the presence of a sidewind or banked road). The potential field will affect a driver’s response, but this should be minimal in cases such as changing lanes.

Generally speaking, there are two critical parameters to consider in the potential function. One is the energy or height of the function and the other is the function’s maximum slope. In order to avoid a “hazardous” object, the potential function must be able to store at least the kinetic energy of the system which lies along the gradient of the function. This specifies the height of the potential function. Achieving this height in a given distance (i.e. from the vehicle’s current location to the object), places a lower bound on the slope of the function. Since the slope of the potential function corresponds to the control force required by the vehicle, tire saturation places an upper bound on the slope. Therefore, it is crucial to balance the slope of the potential field between the safety requirements and the saturation limits of the vehicle. In almost all situations, lanekeeping can be accomplished without approaching the limits of tire adhesion. As a result, the focus in the potential field design is on scaling the potential function gain to provide adequate lanekeeping performance while not making it so large that it hinders normal driving.

2.4.2 Simulation Evaluation

Although the system presented here is straightforward to design and amenable to analysis, there is no evidence that the resulting dynamics are well behaved and easily controlled by a driver. To examine this, simulation results show the response of the system to a disturbance (with no driver input) and the performance in two different lane change maneuvers. The purpose of these simulations is to show that this approach handles the conflicting goals of rejecting disturbances while minimally impacting the ability of the driver to maneuver within the potential. The simulation uses a non-linear Dugoff tire model (Appendix A), the vehicle dynamics given in Equation 2.17, and the potential shown in Figure 2.7. Please see Table 2.1 for further explanation and the numerical values used in this example.

Parameter or Variable	Symbol	Value
Front Cornering Stiffness	C_{yf}	145,000 N/rad
Rear Cornering Stiffness	C_{yr}	145,000 N/rad
Front Longitudinal Stiffness	C_{xf}	300,000 N
Rear Longitudinal Stiffness	C_{xr}	300,000 N
Wheelbase	l	2.8 m
Distance from c.g. to Front Tire	a	1.37 m
Distance from c.g. to Rear Tire	b	1.43 m
Track width	d	1.5 m
Vehicle mass	m	1860 kg
Moment of Inertia	I_z	3100 kg m ²
Distance Along Roadway (state)	s	-
Lateral Position (state)	e	-
Yaw Angle (state)	ψ	-
Driver Braking Force (driver input)	F_{bd}	-
Driver Acceleration Force (driver input)	F_{ad}	-
Driver Steering Command (driver input)	δ_{driver}	-
Right Differential Braking Force (input)	F_{br}	-
Left Differential Braking Force (input)	F_{bl}	-
Controller Steering Command (input)	δ_c	-

Table 2.1: Vehicle Parameters, Variables and Inputs

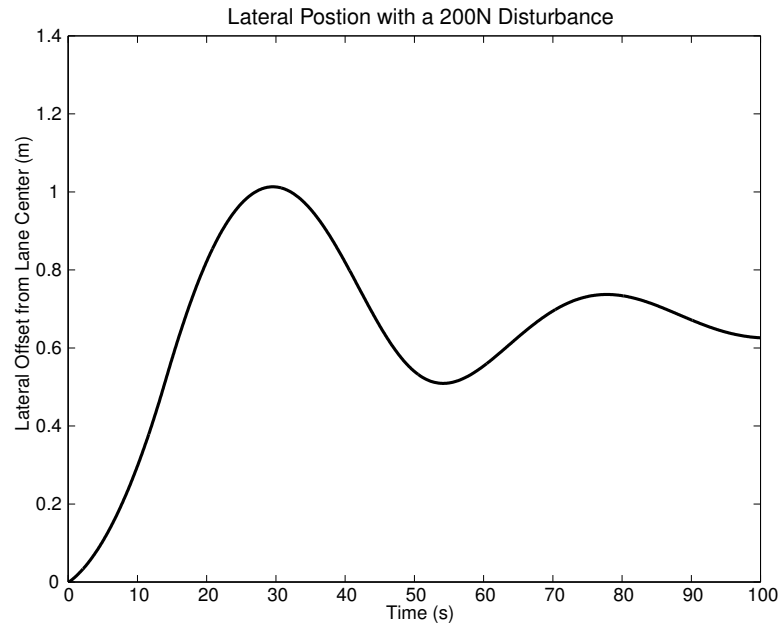


Figure 2.8: Response with Lateral Disturbance

Disturbance Rejection

Figure 2.8 shows the system response for a lateral step disturbance of 200N applied to the vehicle without driver inputs. This disturbance approximates the force from gravity due to the crown angle on a four lane road (approx. 0.6 degrees) or a side wind. From the highway design manual published by the California Department of Transportation [42], a standard freeway lane is 3.6m wide. The vehicle width used in the simulation is 1.5m, leaving a little over a meter between the side of the vehicle and the lane edge. As can be seen from the plot, the vehicle remains within the lane with this disturbance. The trajectory does move close to the lane edge, but it is important to remember that the center potential field is fairly small in order to allow the driver to change lanes. In order to maintain lane composure in the presence of larger disturbances, the field can be increased appropriately to remove the necessary energy. The response shows a very slow oscillation that can easily be controlled by the driver. Designing the dynamic response to remove unwanted oscillations is covered in the following chapter.

Parameter	Symbol	Value
Gain	K_{drv}	0.035
Time delay	τ_d	0.2 s
Neuromuscular Lag	τ_n	0.2 s
Lead Constant	τ_1	10 s
Lag Constant	τ_2	0 s
Steering Ratio	K_{steer}	19.6

Table 2.2: Driver Model Parameters

Lane Change

To evaluate the effect of the potential field during normal driving a simple driver model from Cooke *et al.* [10] is used. The transfer function is given by:

$$\frac{\Delta_d(s)}{E_d(s)} = K_{drv} \left(\frac{\tau_1 s + 1}{\tau_2 s + 1} \right) \left(\frac{1}{\tau_n(s) + 1} \right) e^{-\tau_d s} \quad (2.31)$$

where $\Delta_d(s)$ is the Laplace transform of δ_d and $E_d(s)$ is the Laplace transform of the tracking error used by the driver. The tracking error used is $e_d = e + 14\psi$ where e is the lateral offset and ψ is the heading angle, which is multiplied by a preview distance of 14m. Using this preview distance makes intuitive sense because drivers look forward while driving, utilizing future information to help in the lanekeeping task. Using no preview distance (or lookahead) makes the tracking task extremely difficult (imagine trying to drive by sticking your head out the window and looking straight down at the lane markings). This use of future information for lanekeeping is extremely important and later chapters utilize this concept in the potential field design.

The parameters in Table 2.2 are used to generate an estimate of the wheel angle needed to follow a desired trajectory. To evaluate the driveability of the controlled system, a sinusoidal lane change trajectory was fed through the driver model at a speed of 20 m/s. Figure 2.9 compares the lateral position and driver input for the uncontrolled vehicle and the vehicle with potential fields added. The two responses are strikingly similar. This result suggests that driving in the potential field does not

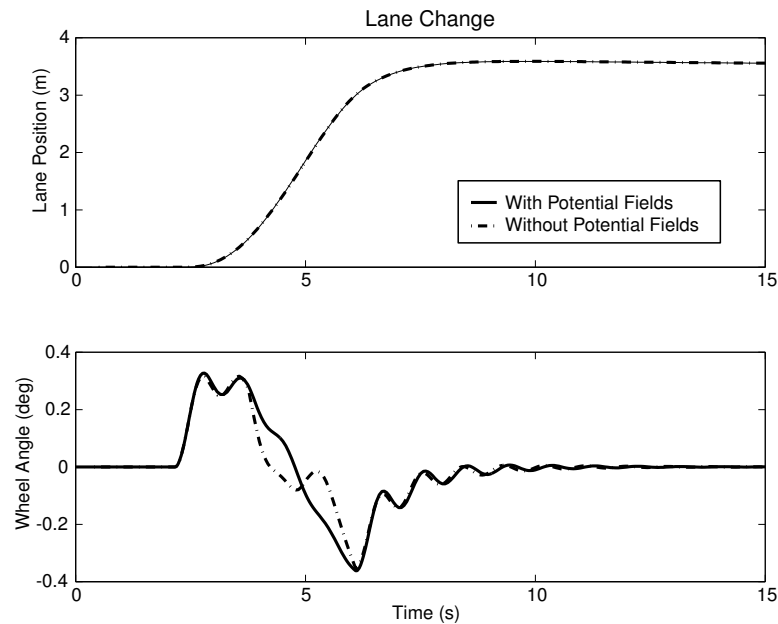


Figure 2.9: Gentle Lane Change Response

require or provoke a substantially different response from the driver (to the extent that the driver model incorporated here reflects a true human response). The trajectory is also quite similar, suggesting that a potential field capable of lanekeeping in the presence of small disturbances is not overly obtrusive in normal driving. Qualitatively, initial experiences with driving a vehicle equipped with this controller (Chapter 5) verify that it is indeed possible to have a system capable of lanekeeping, in the absence of driver inputs, while allowing the driver to easily maneuver within the potential.

2.5 A Closer Look at Dynamic Response

This chapter introduced a general potential field approach for incorporating collision avoidance for driver assistance. This is a novel and unique way of looking at driver assistance because it offers an intuitive means of creating a nominally safe operating environment for the vehicle while keeping the driver in control. The potential field approach integrates vehicle control systems with the vehicle dynamics through simple addition of potential and damping functions. The simple example illustrated the

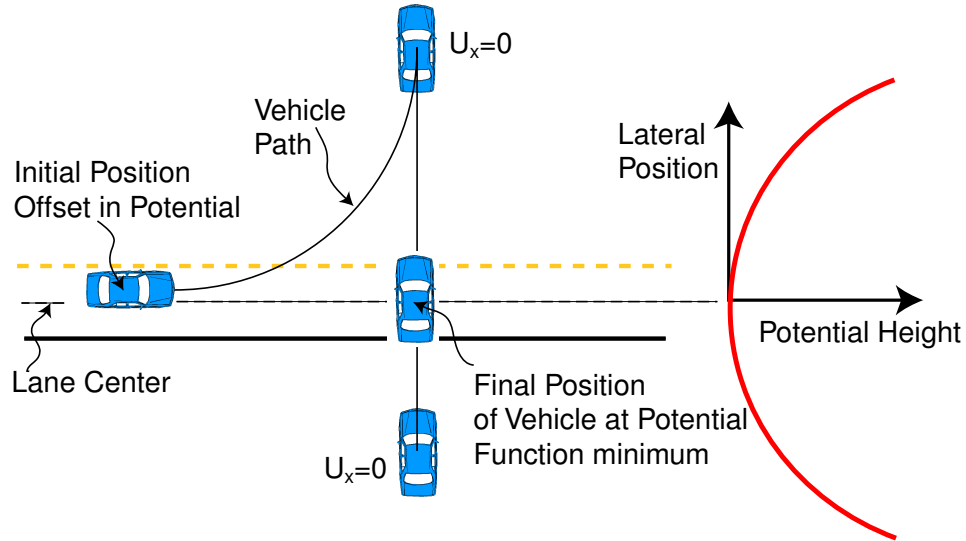


Figure 2.10: A Possible Response

design of a lanekeeping controller under this framework.

The remaining chapters focus on using the potential field framework developed in this chapter for lanekeeping assistance. The general framework incorporates the lateral, longitudinal, and yaw motions of the vehicle to create a system that dissipates overall energy. For lanekeeping, the motion of interest is the lateral motion of the vehicle relative to the lane center which, in general, is coupled with the yaw rate (in order to move laterally the car must rotate). Under normal driving the energy in these directions is orders of magnitude smaller than the longitudinal energy of the vehicle.

$$\frac{1}{2}mU_x^2 \gg \frac{1}{2}me^2 + \frac{1}{2}I_z\dot{\psi}^2 \quad (2.32)$$

Although overall energy is conserved, the energy in the lateral and yaw modes of the vehicle can increase significantly if the longitudinal energy is transferred into these directions. As a result, conserving overall energy does not guarantee much about the performance or stability (in the sense of staying close to the minimum of the potential) of a lanekeeping system. For example, under the general framework it is possible that the vehicle could rotate into the lanekeeping potential until the longitudinal axis is perpendicular to the gradient of the potential function. The control force from

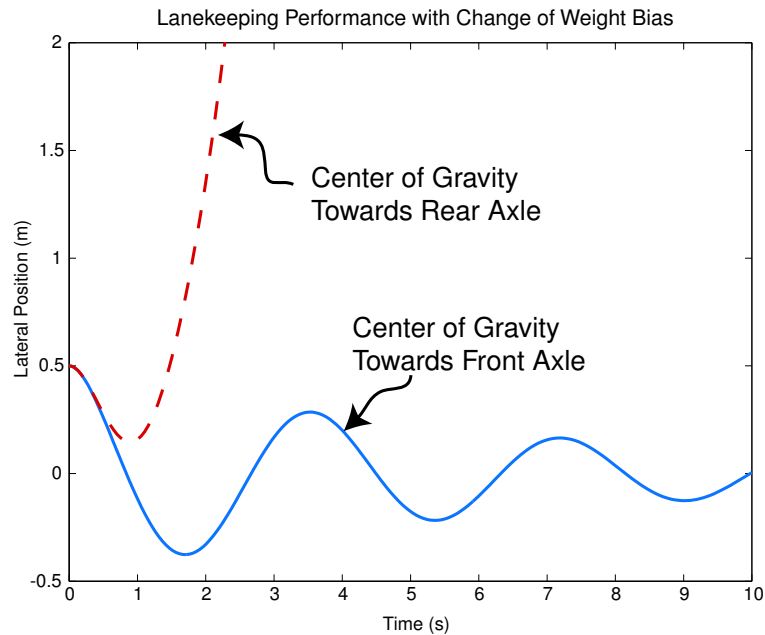


Figure 2.11: Lanekeeping Behavior for Varying C.G. Location

the potential would slow the vehicle down until it stops and then it would move backwards eventually ending up at the center of the lane (Figure 2.10). Although this type of behavior was not observed in the previous lanekeeping example, different vehicle parameters can significantly alter the vehicle's response. Figure 2.11 shows a simulation for two different weight distributions using a simple quadratic potential. The vehicle is started with a $0.5m$ initial offset from lane center and the response is shown without any driver input. In the case with the center of gravity towards the front axle, the vehicle response is similar to the one shown earlier in Figure 2.8. If, however, the center of gravity is shifted rearward, the response is completely different. This is the case where the vehicle rotates into the potential. Clearly, this type of response is not desirable for a lanekeeping system.

In order to avoid undesirable dynamic behavior it is crucial to understand the interaction between the potential field control force and the tire forces governing the lateral and yaw dynamics. The following chapter focuses on the stability and performance of these dynamics under the potential field framework.

Chapter 3

Lanekeeping Stability and Performance

This chapter presents a linear analysis of lateral vehicle stability under the potential field framework. Although the general potential field controller creates a system that dissipates overall energy, the resulting dynamic behavior can change significantly depending on the vehicle parameters. For lanekeeping, it is extremely important to understand the system behavior to create a response that remains in the lane and is predictable for the driver. This chapter treats the control force from the potential field controller as a ‘virtual’ force applied to the vehicle. The overall response of the vehicle is determined by the interaction between the virtual control force from the potential and the inherent vehicle dynamics.

There is a significant amount of research on lateral control for autonomous lanekeeping and collision avoidance [61] [15]. Research in lateral control has focused on four main factors that influence system performance: vehicle handling characteristics, preview distance, actuator capability, and controller design. Understanding the interaction of all these factors is crucial in the design of a lanekeeping system. This chapter illustrates the influence of the following attributes on the stability and performance of lateral vehicle control:

- Vehicle Handling Properties (Amount of Understeer/Oversteer)

- Virtual Force Application Point (Coordination of Steering and Braking)
- Sensing Location (Amount of Lookahead)
- Controller Damping

The stability results presented in this chapter clearly illustrate that the virtual control force must be applied in front of the neutral steer point for stability. This point is a physical point on the vehicle where an external force creates no steady state yaw rate. This location is significant in vehicle design in order to ensure appropriate vehicle response to side-wind disturbances or gravity forces from banked roads. By abstracting the control force as a virtual force applied to the vehicle, the intuition used in the mechanical design of automobiles is easily transferred to the control system design.

Although application of the control force in front of the neutral steer point is necessary for stability it is not sufficient. To ensure high speed stability, the control force must be based on a projection into the potential function. This idea is analogous to the preview distance used in the driver model from the previous chapter. Finally, the combination of lookahead and controller damping allows complete control over the system response. The results presented in this chapter provide useful stability requirements for the potential field controller.

3.1 Previous Work

Vehicle handling characteristics are a key component in control system design. Open-loop vehicle stability is well understood and research in this area dates back to the early 1930's. At this time, researchers at General Motors first noticed that some steering geometries created a tendency for the vehicle to 'oversteer' the desired trajectory. Shortly after this discovery, the same 'oversteering' behavior was noticed with vehicles that had underinflated rear tires or a rearward weight bias. This inspired the study of tire dynamics and their influence on vehicle handling. Stonex [65] was one of the first to study steady-state vehicle stability and explore understeering and oversteering behavior. This led to the development and analysis of dynamic vehicle

models, resulting in a mathematical understanding of understeering and oversteering dynamics [60]. The results showed that understeering vehicles are always stable, but damping decreases with increasing speed. Oversteering vehicles, however, are stable with increasing damping up to a critical speed where the vehicle becomes unstable [40] [25]. The simple models that yield these results are still used in the design of most vehicle lateral controllers.

With sensor and computer advances, the capability for vehicle control became possible. Fenton [16] did initial work in vehicle lateral control by using an electric wire as a reference. In this work, the vehicle only had knowledge of its current lateral position, which created instability at high speeds. These look-down reference systems were also studied by researchers at PATH [70] and later by Guldner et al. [27], but still had instabilities well below freeway speeds ($30m/s$). In order to achieve speeds appropriate for highway travel, it is necessary to incorporate a look-ahead reference. The advantage of incorporating a preview distance was shown theoretically by Peng and Tomizuka [46] and experimentally by Alleyne and DePoorter [4]. Guldner et al. [26] created a ‘virtual’ preview distance for high speed stability using a look-down reference at the front and rear of the vehicle.

With additional actuators such as four wheel steering or differential braking, it is possible to change the coupling between the vehicle’s lateral and rotational dynamics. Ackermann [1] developed control algorithms to decouple the lateral and yaw dynamics, making the driving experience safer and more comfortable. Alleyne [3] looked at lateral control of a vehicle using various combinations of steering and differential braking for improved lanekeeping. The ability to alter the coupling between the yaw and lateral modes gives more freedom in the control system design.

Although past work has studied vehicle stability for each of these effects, the analysis presented in this chapter incorporates all of these factors in the stability analysis. In order to study the interaction of all these different variables it is convenient to look at control from a virtual force standpoint. In essence, most control laws can be viewed as the combination of external forces and torques applied at the center of gravity. This can be combined into a single virtual control force acting at some point along the longitudinal axis of the vehicle. This virtual force concept gives

physical insight into the design of the potential field controller for lanekeeping. This technique is also extremely useful as a general design tool for vehicle control systems.

3.2 Virtual Force Analogy for Control

The potential field approach developed in Chapter 2 is analogous to having a conservative force from an imaginary spring attached to the vehicle's center of gravity as shown in Figure 3.1. This spring analogy is similar to work done by Hennessey et

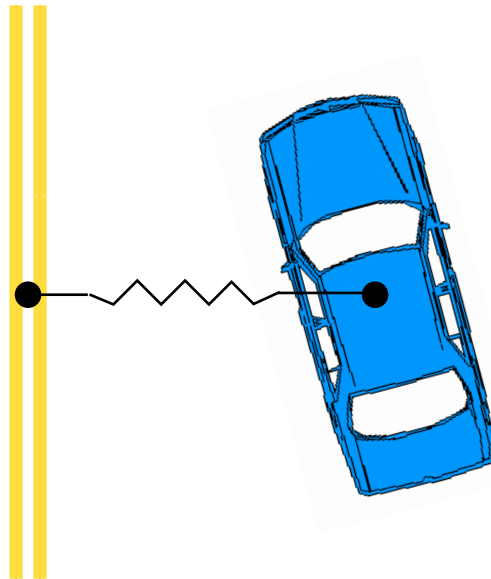


Figure 3.1: Lanekeeping Analogy

al. [31] and Schiller et al. [58][57] in the design of a ‘virtual bumper’ (Figure 3.2). If an obstacle penetrates the bumper, imaginary springs and dampers are compressed applying a virtual force to the vehicle. The main difference in our approach is that the spring is attached to the environment instead of the vehicle. This associates the control force with the hazard and avoids the scaling issues encountered by fixing the potential on the vehicle. In the virtual bumper approach, the springs and dampers must be scaled appropriately based on the object penetrating the bumper. For example, a fast moving obstacle, such as another vehicle, requires a much stiffer spring

compared with a fixed obstacle that the vehicle is drifting towards such as a lane edge.

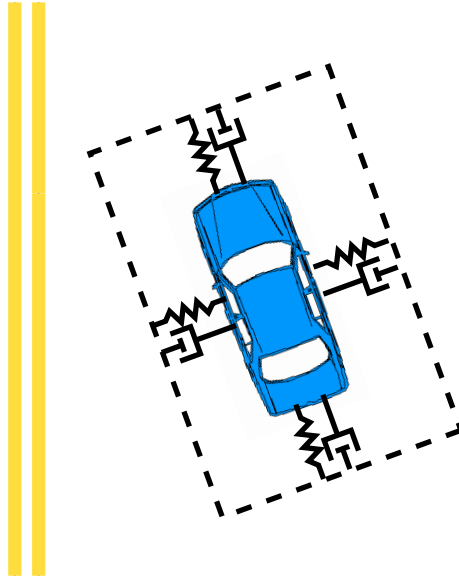


Figure 3.2: Virtual Bumper Concept

In this chapter, the potential field control force is viewed as a virtual control force applied to the vehicle. Physically, this control force is realized through the tire forces that can be directly controlled. Figure 3.3 shows how forces generated from a combination of longitudinal forces and front steering can be thought of as a virtual control force. This is accomplished by creating an equivalent force system consisting of a longitudinal and lateral force on the vehicle. For lateral control, the longitudinal force is small and disappears in the linearization of the system dynamics (Section 3.3). The ability to manipulate the coupling between lateral and yaw modes allows movement of the virtual control force along the longitudinal axis of the vehicle. For example, if differential braking is unavailable ($\Delta F_{xf} = \Delta F_{xr} = 0$), the virtual control force from the steering angle is constrained at the front axle. With differential braking, the moment equation can be influenced independently from steering inputs, effectively shifting the location of the virtual force from the front axle. This virtual force analogy is a convenient way of looking at actuator coordination and its influence on the vehicle behavior.

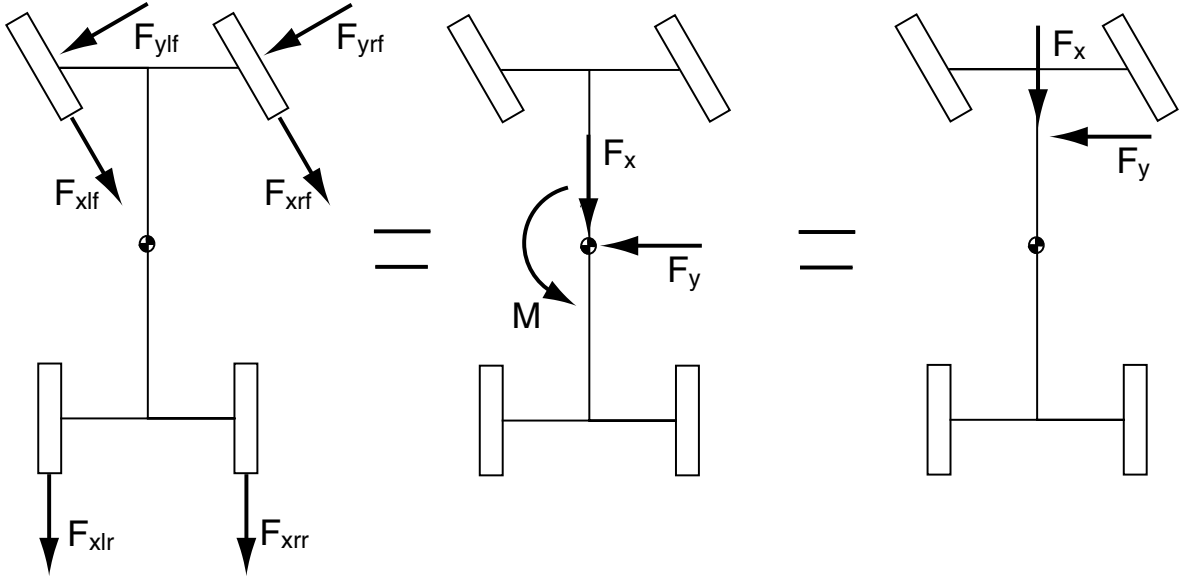


Figure 3.3: Virtual Force Analogy

In order to incorporate various sensor locations, the virtual force is based on a projected lateral offset from the control force location (Figure 3.4). This is accomplished by projecting a distance, x_{la} , in front of the vehicle's center of gravity and using the lateral offset at this location. This lookahead concept can be viewed as a projection into the potential.

Creating a control force from a projection into the potential and allowing it to shift a distance, x_{cf} , from the center of gravity yields a control force that affects both the lateral and rotational dynamics of the vehicle. The force components in the lateral and rotational directions are given by

$$F_{virtual} = \begin{bmatrix} -\frac{\partial V_c(e_{la})}{\partial e} \\ -\frac{\partial V_c(e_{la})}{\partial e} x_{cf} \end{bmatrix} \quad (3.1)$$

This control force, however, does not necessarily fall into the spring analogy discussed earlier because of using lookahead and allowing manipulation of the control force location. The passivity of the overall dynamics using this control force is discussed in Chapter 4.

The set of nonlinear differential equations for the controlled dynamics (Equation

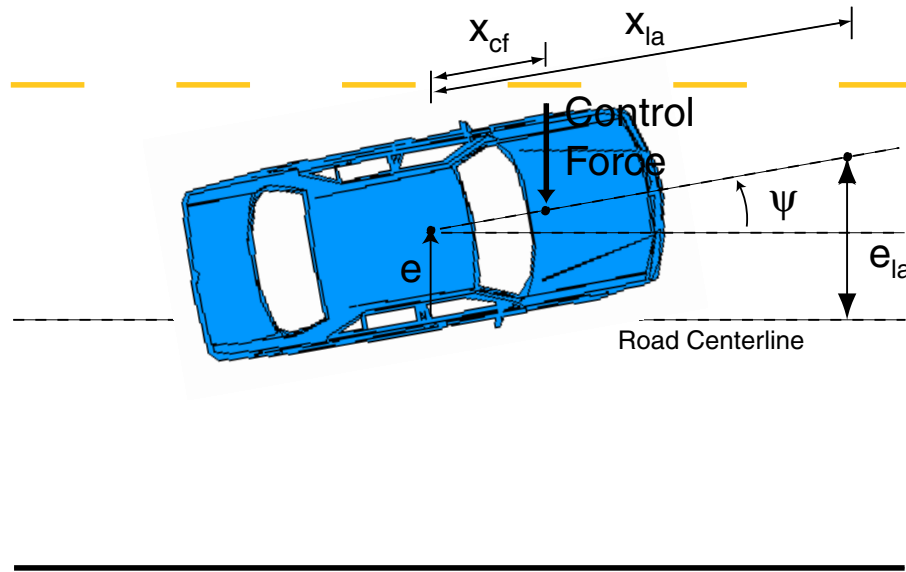


Figure 3.4: Lookahead

2.30) is the focus of the following analysis. The behavior in question is the stability of the vehicle with respect to a desired trajectory consisting of a constant longitudinal velocity in the center of the road. Since the interesting behavior is in global coordinates, it makes sense to transform the equations of motion into global states and then linearize the system about the desired trajectory.

3.3 Linearization of Vehicle Dynamics

The goal of the stability analysis is to study the vehicle's response to small excursions from the lane center. The basic idea is to transform the equations of motion from body fixed coordinates to road fixed coordinates. Recall that the longitudinal, lateral, and rotational velocities in the vehicle fixed frame are given by \dot{q}_3 . The velocities in the road fixed frame are given by \dot{w} , which contains the velocity down the road, the lateral velocity relative to the road, and the rotational velocity of the vehicle relative to the road.

$$\dot{q}_3 = \begin{bmatrix} U_x & U_y & r \end{bmatrix} \quad (3.2)$$

$$\dot{w} = \begin{bmatrix} \dot{s} & \dot{e} & \dot{\psi} \end{bmatrix} \quad (3.3)$$

Transformation between the road fixed frame and the vehicle fixed frame is given by

$$\frac{\partial \dot{w}}{\partial \dot{q}_3} = \frac{\partial w}{\partial q_3} = \begin{bmatrix} \cos \psi & -\sin \psi & 0 \\ \sin \psi & \cos \psi & 0 \\ 0 & 0 & 1 \end{bmatrix} \quad (3.4)$$

As presented in the last chapter, the uncontrolled vehicle dynamics are contained in the drift term

$$M_3 \ddot{q}_3 = f_3(\dot{q}_3) \quad (3.5)$$

Assuming a linear tire model for the lateral force (Equation 2.4), these equations of motion can be written as

$$m\dot{U}_x = mrU_y \quad (3.6)$$

$$m\dot{U}_y = -C_r \alpha_r - C_f \alpha_f - mrU_x = -C_r \left(\frac{U_y - rb}{U_x} \right) - C_f \left(\frac{U_y + ra}{U_x} \right) - mrU_x \quad (3.7)$$

$$I_z \dot{r} = C_r b \alpha_r - C_f a \alpha_f = C_r b \left(\frac{U_y - rb}{U_x} \right) - C_f a \left(\frac{U_y + ra}{U_x} \right) \quad (3.8)$$

Transforming these equations of motion to road fixed coordinates yields

$$m\ddot{s} = -(C_f + C_r) \left(\frac{\dot{e} \cos \psi - \dot{s} \sin \psi}{\dot{s} \cos \psi + \dot{e} \sin \psi} \right) \sin \psi + (C_r b - C_f a) \left(\frac{\dot{\psi}}{\dot{s} \cos \psi + \dot{e} \sin \psi} \right) \sin \psi \quad (3.9)$$

$$m\ddot{e} = -(C_f + C_r) \left(\frac{\dot{e} \cos \psi - \dot{s} \sin \psi}{\dot{s} \cos \psi + \dot{e} \sin \psi} \right) \cos \psi + (C_r b - C_f a) \left(\frac{\dot{\psi}}{\dot{s} \cos \psi + \dot{e} \sin \psi} \right) \cos \psi \quad (3.10)$$

$$I_z \ddot{\psi} = (C_r b - C_f a) \left(\frac{\dot{e} \cos \psi - \dot{s} \sin \psi}{\dot{s} \cos \psi + \dot{e} \sin \psi} \right) - (C_r b^2 + C_f a^2) \left(\frac{\dot{\psi}}{\dot{s} \cos \psi + \dot{e} \sin \psi} \right) \quad (3.11)$$

Since the behavior in question is the vehicle's lateral and heading error dynamics, these nonlinear equations are linearized about a trajectory corresponding to the equilibrium configuration of the system. This consists of driving down the center of the road ($e = \dot{e} = \psi = \dot{\psi} = 0$) at a constant rate, $\dot{s} = S$. Performing Jacobian linearization yields the following linear equation for the lateral and heading error of the

vehicle.

$$\delta\dot{x} = A\delta x \quad (3.12)$$

where $\delta x = [\delta e \ \delta\dot{e} \ \delta\psi \ \delta\dot{\psi}]^T$ are perturbations away from the nominal states and

$$A = \begin{bmatrix} 0 & 1 & 0 & 0 \\ 0 & \frac{-(C_f+C_r)}{mS} & \frac{C_f+C_r}{m} & \frac{(-aC_f+bC_r)}{mS} \\ 0 & 0 & 0 & 1 \\ 0 & \frac{(-aC_f+bC_r)}{I_zS} & \frac{(aC_f-bC_r)}{I_z} & \frac{-(a^2C_f+b^2C_r)}{I_zS} \end{bmatrix} \quad (3.13)$$

3.3.1 Vehicle Stability without Control

For completeness, the stability properties of a vehicle without any control are presented below (Equation 3.13). Taking the determinant of $(\lambda I - A)$ yields the characteristic equation of the system.

$$\lambda^2 (\lambda^2 + \lambda a_1 + a_2) = 0 \quad (3.14)$$

where,

$$a_1 = \frac{(C_f + C_r)I_z + (a^2C_f + b^2C_r)m}{I_z m S}$$

$$a_2 = \frac{C_f C_r (a + b)^2 + (bC_r - aC_f)mS^2}{I_z m S^2}$$

From the above equation, there are four eigenvalues. Two of these eigenvalues determine the vehicle handling and the two zero eigenvalues arise from the integrators for the positional states. The zero eigenvalues simply show that the positional states will not necessarily be driven to zero.

The characteristic equation shows that the vehicle dynamics are a function of the front and rear cornering stiffness, C_f and C_r , the c.g. location determined by the distances a and b , the mass and moment of inertia, and the vehicle speed, S . For vehicle stability it is common to look at vehicle handling in terms of three different parameter configurations: understeering, oversteering, and neutral steering. These

terms are defined by the weight distribution of the car and the cornering stiffness of the front and rear tires. The definition of understeering, oversteering, and neutral steering is given below.

$$\text{Understeering: } aC_f - bC_r < 0 \quad (3.15)$$

$$\text{Oversteering: } aC_f - bC_r > 0 \quad (3.16)$$

$$\text{Neutral steering: } aC_f - bC_r = 0 \quad (3.17)$$

The names come from the behavior of the vehicle during steady state cornering relative to the path predicted by kinematics. An understeering vehicle tends to “understeer” the predicted path as speed increases while an oversteering vehicle “oversteers” the predicted path. The neutral steering vehicle, however, remains on the desired radius turn as speed increases.

For an understeering car both coefficients a_1 and a_2 are positive which, for a second order system, is sufficient to prove stability. Although the system is always stable the damping for an understeering car decreases with increasing speed. The neutral steering vehicle is also stable but the damping remains constant. In an oversteering case, the coefficient a_2 will be negative when the speed is greater than the critical speed [25].

$$S_{cr} = \sqrt{\frac{C_f C_r (a + b)^2}{(aC_f - bC_r)m}} \quad (3.18)$$

As the speed increases, however, the damping of an oversteering car also increases until the critical speed is reached. These results are well known for vehicles and are utilized to design stable vehicles with appropriate dynamics. As we will see, these vehicle parameters also play an important role in vehicle control.

3.4 Stability with Virtual Forces

Without a virtual control force, the analysis of the linear dynamics returns well-known stability results for vehicle handling, as should be expected. The following analysis assumes a quadratic potential function that in general is based on a projected lateral

offset e_{la} .

$$V_c(e_{la}) = ke_{la}^2 = k(e + x_{la}\sin\psi)^2 \quad (3.19)$$

where k is the potential function gain. Assuming small heading angles this can be approximated by

$$V_c(e_{la}) = k(e + x_{la}\psi)^2 \quad (3.20)$$

Deriving a control force from this potential and allowing it to shift a distance, x_{cf} from the center of gravity yields the following virtual control force

$$F_{virtual} = \begin{bmatrix} -\frac{\partial V_c(e_{la})}{\partial e} \\ -\frac{\partial V_c(e_{la})}{\partial e} x_{cf} \end{bmatrix} = \begin{bmatrix} -2k(e + x_{la}\psi) \\ -2k(e + x_{la}\psi)x_{cf} \end{bmatrix} \quad (3.21)$$

In order to systematically look at the effect of the control force location and lookahead we will first look at applying the virtual control force at the center of gravity without lookahead ($x_{cf} = x_{la} = 0$). This analysis raises some stability concerns that can be fixed by shifting the control force. Finally, the sensing location is taken into account to provide high speed stability. The last section looks at adding artificial damping to the control structure.

3.4.1 Virtual Force at the C.G.

Adding a virtual control force at the center of gravity yields a linear system which has the control force appearing in the lateral equation of motion. This adds one extra term to the matrix in Equation 3.13.

$$A = \begin{bmatrix} 0 & 1 & 0 & 0 \\ -\frac{2k}{m} & -\frac{C_f+C_r}{mS} & \frac{C_f+C_r}{m} & \frac{(-aC_f+bC_r)}{mS} \\ 0 & 0 & 0 & 1 \\ 0 & \frac{(-aC_f+bC_r)}{I_z S} & \frac{(aC_f-bC_r)}{I_z} & \frac{-(a^2C_f+b^2C_r)}{I_z S} \end{bmatrix} \quad (3.22)$$

The characteristic equation is now

$$\lambda^4 + \lambda^3 b_1 + \lambda^2 b_2 + \lambda b_3 + b_4 = 0 \quad (3.23)$$

where

$$\begin{aligned}
b_1 &= \frac{(C_f + C_r)I_z + (a^2C_f + b^2C_r)m}{I_z m S} \\
b_2 &= \frac{C_f C_r (a + b)^2 + (bC_r - aC_f)mS^2 + 2kI_z S^2}{I_z m S^2} \\
b_3 &= \frac{2k(a^2C_f + b^2C_r)}{I_z m S} \\
b_4 &= \frac{2k(bC_r - aC_f)}{I_z m}
\end{aligned}$$

Regardless of the vehicle's speed, the last term, b_4 , is always negative when oversteering parameters are used. Sign changes in the characteristic equation's coefficients fail the necessary conditions for stability. This instability occurs because the virtual force is applied at the center of gravity, causing the vehicle to turn into the applied force. This type of response is well known for an oversteering car with a physical force, such as a side wind, applied at the center of gravity. Since the underlying dynamics are left in this control framework, the vehicle's response to the virtual control force is exactly the same as its response to a physical force.

If the vehicle is understeering, all the coefficients are positive. Although this is a necessary condition for stability, it is not sufficient. Using the Routh array, it can be shown that the system is stable up to a critical velocity.

$$S_{cr} = \left(\frac{N}{D}\right)^{1/2} \quad (3.24)$$

where N and D are

$$\begin{aligned}
N &= -(a + b)^2 C_f C_r (a^2 C_f + b^2 C_r) (I_z (C_f + C_r) + (a^2 C_f + b^2 C_r) m) \\
D &= (C_f + C_r) I_z ((C_f + C_r) (a C_f - b C_r) I_z + 4 I_z K (a^2 C_f + b^2 C_r) \\
&\quad + (a C_f - b C_r) (a^2 C_f + b^2 C_r) m)
\end{aligned}$$

Using the understeering parameters in Table 3.1 the critical speed is $27.06m/s$. Figure 3.5 shows the understeering and oversteering response with the virtual control force

	Understeer	Oversteer
m (kg)	1640	1640
I_z (N/m ²)	3500	3500
C_f (N/rad)	100000	100000
C_r (N/rad)	160000	80000
k	2500	2500
a (m)	1.3	1.3
b (m)	1.5	1.5

Table 3.1: Vehicle Parameters: Chapter 3

applied at the center of gravity. The initial conditions for the simulation are $e = 0.5m$ and $S = 25m/s$, representing a typical driving speed and an initial offset from the lane center. All other states are initially zero and the parameters used are in Table 3.1.

The results shown in Figure 3.5 show the exact behavior predicted by the linear analysis. The understeering vehicle is stable but underdamped, oscillating about the lane center. An oversteering vehicle exhibits drastically different results. The control force initially pushes the car towards the center of the lane, but the change in the vehicle dynamics causes a rotation into the applied force.

In the above analysis, the vehicle is controlled by a virtual force applied at the c.g. of the vehicle with sensing based on the lateral position of the c.g. (i.e. no lookahead). The location of this control force results in instability for the oversteering vehicle that can only be rectified by shifting the control force forward. For the understeering vehicle, this control strategy results in stability below a critical speed. The low damping characteristics and a critical speed within the operating range of the vehicle can be attributed to the lack of lookahead. An interesting result is that without any lookahead the critical speed is fairly large compared with previous results for look-down lateral controllers. This is a result of applying the control force at a location that almost decouples the lateral and yaw modes of the vehicle.

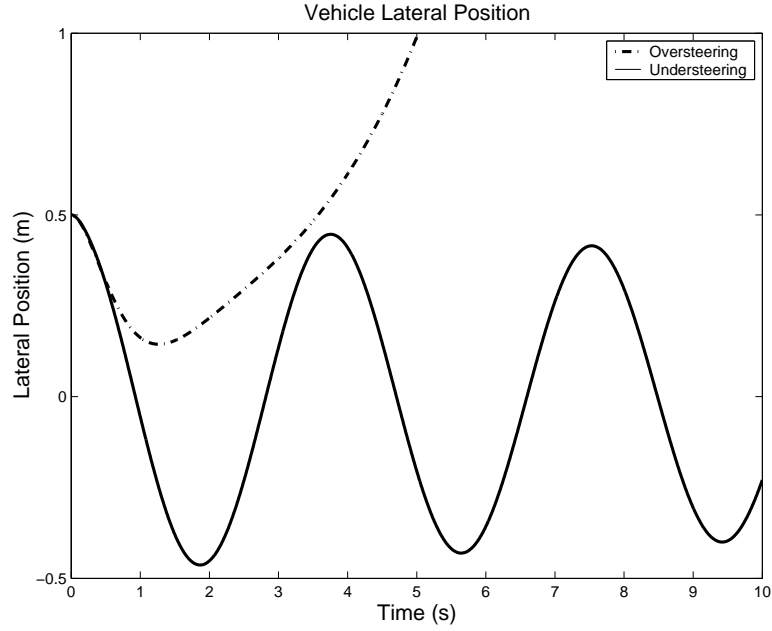


Figure 3.5: Simulation: Virtual Force at C.G.

3.4.2 Shifting the Virtual Force

This section explores the effect of shifting the virtual force a distance x_{cf} from the center of gravity (Figure 3.6). With the virtual control force acting in front of the c.g. the equations of motion have an extra term appearing in the moment equation.

$$A = \begin{bmatrix} 0 & 1 & 0 & 0 \\ -\frac{2k}{m} & \frac{-(C_f+C_r)}{mS} & \frac{C_f+C_r}{m} & \frac{(-aC_f+bC_r)}{mS} \\ 0 & 0 & 0 & 1 \\ \frac{-2kx_{cf}}{I_z} & \frac{(-aC_f+bC_r)}{I_zS} & \frac{(aC_f-bC_r)}{I_z} & \frac{-(a^2C_f+b^2C_r)}{I_zS} \end{bmatrix} \quad (3.25)$$

The characteristic equation is

$$\lambda^4 + \lambda^3c_1 + \lambda^2c_2 + \lambda c_3 + c_4 = 0 \quad (3.26)$$

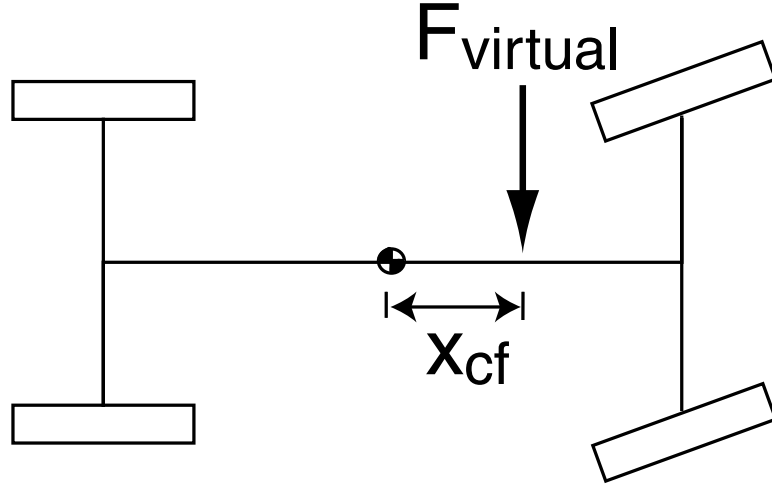


Figure 3.6: Shifting the Control Force

where

$$\begin{aligned}
 c_1 &= \frac{(C_f + C_r)I_z + (a^2C_f + b^2C_r)m}{I_z m S} \\
 c_2 &= \frac{C_f C_r (a + b)^2 + (bC_r - aC_f)mS^2 + 2kI_z S^2}{I_z m S^2} \\
 c_3 &= \frac{2k(a^2C_f + b^2C_r + x_{cf}(bC_r - aC_f))}{I_z m S} \\
 c_4 &= \frac{2k(bC_r - aC_f + x_{cf}(C_f + C_r))}{I_z m}
 \end{aligned}$$

From the last section, the final term in the characteristic equation is sensitive to changes in the handling properties of the vehicle. With the ability to shift the virtual force it is possible to negate this problem. For stability, the following inequality must be satisfied.

$$bC_r - aC_f + x_{cf}(C_f + C_r) > 0 \quad (3.27)$$

so,

$$x_{cf} > \frac{aC_f - bC_r}{C_f + C_r} \quad (3.28)$$

The right hand side of the above expression is defined as the neutral steer point and has physical significance in vehicle design. The neutral steer point is the location

on the centerline of a vehicle where an external force produces no steady state yaw velocity. This concept is often used to discuss sidewind sensitivity of a vehicle and has a natural interpretation when considering virtual forces and stability. For stability, the virtual force must be applied in front of the neutral steer point of the vehicle. This ensures that the vehicle will rotate in the same direction as the virtual control force (Figure 3.7).

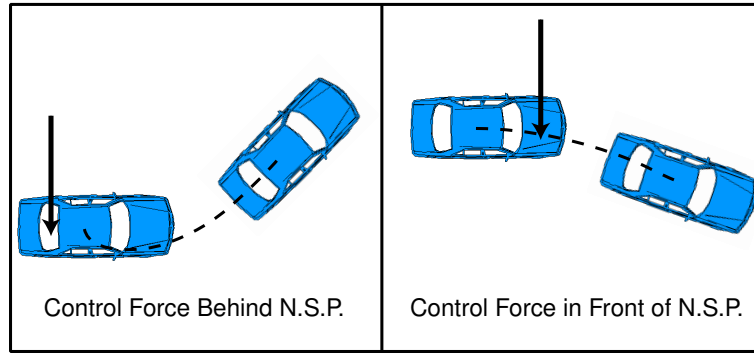


Figure 3.7: Vehicle Response to the Virtual Force

If the virtual force is applied at the neutral steer point, the system is marginally stable with three negative eigenvalues and one at the origin. The coefficients for the characteristic equation become

$$\begin{aligned}
 c'_1 &= \frac{(C_f + C_r)I_z + (a^2C_f + b^2C_r)m}{I_z m S} \\
 c'_2 &= \frac{C_f C_r (a + b)^2 + (bC_r - aC_f)mS^2 + 2kI_z S^2}{I_z m S^2} \\
 c'_3 &= \frac{2kC_f C_r (a + b)^2}{(C_f + C_r)I_z m S} \\
 c'_4 &= 0
 \end{aligned}$$

With the virtual force at the neutral steer point there is still the possibility of a critical speed. The only term in this system which can possibly go negative for an oversteering vehicle is c'_2 , but this is unlikely due to the small magnitude of the only term that can be negatively signed ($bC_r - aC_f$). From looking at the Routh array,

the critical speed of the system is given by

$$S_{cr} = \left(\frac{N}{D} \right)^{1/2} \quad (3.29)$$

where

$$\begin{aligned} N &= -(a+b)^2 C_f C_r (C_f + C_r) (I_z (C_f + C_r) + (a^2 C_f + b^2 C_r) m) \\ D &= 4(C_f + C_r)^2 I_z^2 k - I_z (a C_f - b C_r) ((C_f + C_r)^2 + 2k(b C_r - a C_f)) m \\ &\quad - (C_f + C_r) (a C_f - b C_r) (a^2 C_f + b^2 C_r) m^2 \end{aligned}$$

Using the oversteering parameters in Table 3.1, there happens to be no critical speed for the system (the solution to Equation 3.29 is imaginary, but certain oversteering parameters can give real critical speeds). By shifting the force to the neutral steer point the oversteering vehicle is marginally stable, but exhibits a nicely damped response (compare it with the understeering vehicle from the previous section shown in Figure 3.8). Since this control force location creates no steady state yaw velocity there is minimal rotation, yielding an acceptable response. Shifting the control force to the neutral steer point of the understeering vehicle gives similar results (Figure 3.8). The understeering vehicle has an overdamped response that is due to the transient behavior of the vehicle as it reaches steady state.

Figure 3.9 and Figure 3.10 show how the eigenvalues shift for an oversteering and understeering car as the virtual force is shifted from $0.5m$ behind the neutral steer point to $0.5m$ in front of the neutral steer point. The square denotes the initial position behind the neutral steer point. The eigenvalues verify that the system is unstable when the application point is behind the neutral steer point. As the virtual force is shifted forward, the system becomes stable, but as the force is moved further forward the system becomes oscillatory and eventually unstable. This instability is due to the lack of lookahead in the system and is explored in the next section.

Interestingly, in the case discussed in this section, the force is shifted to the neutral steer point but the sensing location remains at the c.g. Therefore, in the oversteering case the sensing location is actually behind the control force while in the understeering

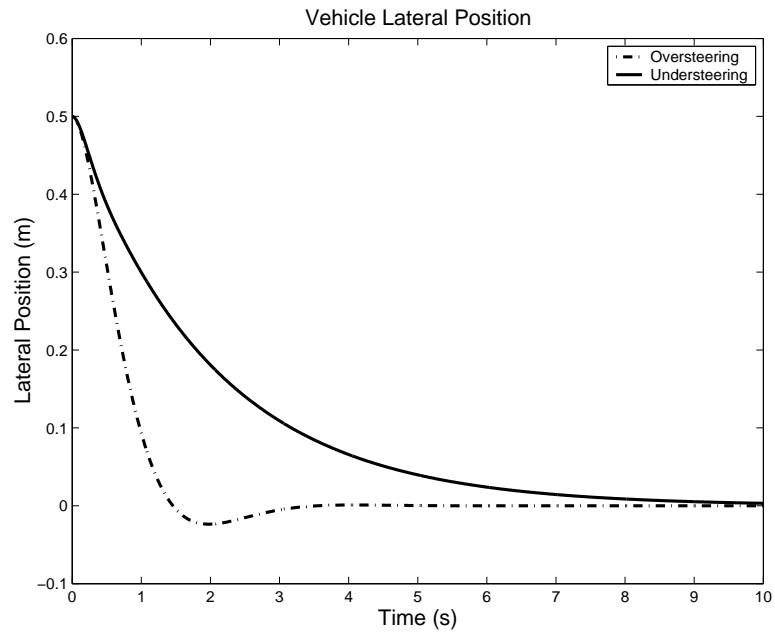


Figure 3.8: Simulation: Virtual Force at Neutral Steer Point

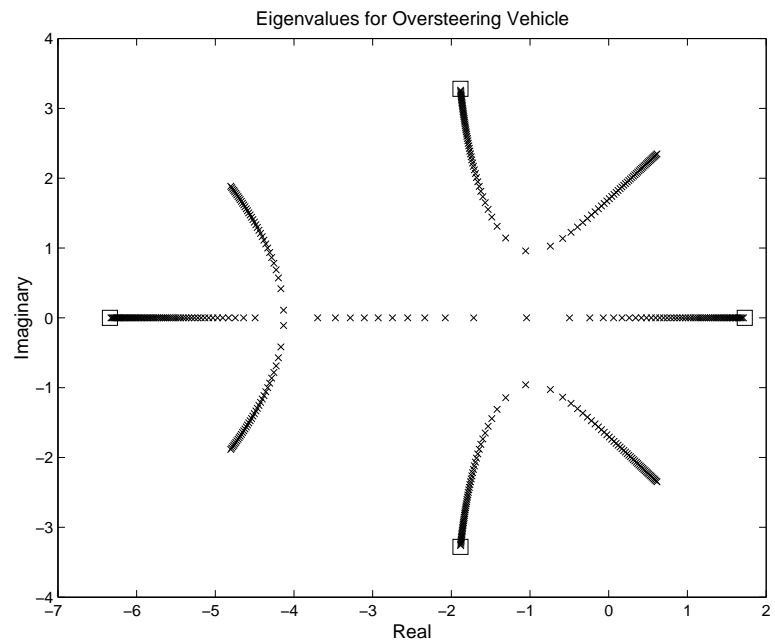


Figure 3.9: Oversteering Vehicle Eigenvalues as Application Point Shifts Forward

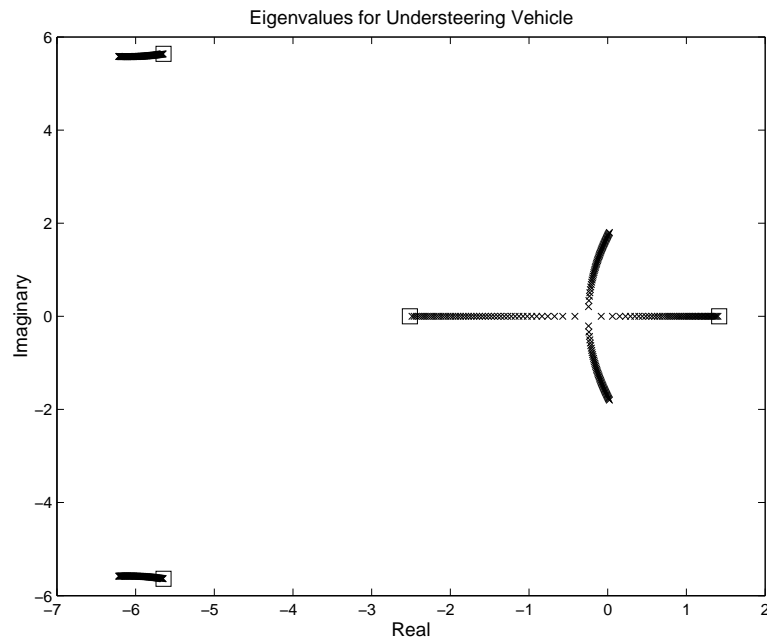


Figure 3.10: Understeering Vehicle Eigenvalues as Application Point Shifts Forward

vehicle it is slightly in front of this control force. In either case, with no lookahead the system response is excellent. The limitation is that the neutral steer point is only marginally stable, yielding an eigenvalue at zero. If the control force is moved slightly rearward, the system will become unstable. It is unlikely that the vehicle parameters can be known with the accuracy necessary to pin point this location. Even variations in vehicle loading or tire pressure can shift this point and create instability. To be robust to parameter uncertainties the control force should be shifted in front of the neutral steer point.

3.5 Incorporating Lookahead

Incorporating lookahead creates a virtual control force that depends on the lateral position at a projected distance x_{la} in front of the c.g. (Equation 3.21). Including

lookahead in the linearized vehicle model gives

$$A = \begin{bmatrix} 0 & 1 & 0 & 0 \\ -\frac{2k}{m} & \frac{-(C_f+C_r)}{mS} & \frac{C_f+C_r}{m} - \frac{2kx_{la}}{m} & \frac{(-aC_f+bC_r)}{mS} \\ 0 & 0 & 0 & 1 \\ \frac{-2kx_{cf}}{I_z} & \frac{(-aC_f+bC_r)}{I_zS} & \frac{(aC_f-bC_r)}{I_z} - \frac{2kx_{la}x_{cf}}{I_z} & \frac{-(a^2C_f+b^2C_r)}{I_zS} \end{bmatrix} \quad (3.30)$$

The characteristic equation is

$$\lambda^4 + \lambda^3 d_1 + \lambda^2 d_2 + \lambda d_3 + d_4 = 0 \quad (3.31)$$

where

$$\begin{aligned} d_1 &= \frac{(C_f + C_r)I_z + (a^2C_f + b^2C_r)m}{I_z m S} \\ d_2 &= \frac{C_f C_r (a + b)^2 + (bC_r - aC_f)mS^2 + 2kS^2(I_z + mx_{cf}x_{la})}{I_z m S^2} \\ d_3 &= \frac{2k(a^2C_f + b^2C_r + (x_{cf} + x_{la})(bC_r - aC_f)) + (C_f + C_r)x_{cf}x_{la}}{I_z m S} \\ d_4 &= \frac{2k(bC_r - aC_f + x_{cf}(C_f + C_r))}{I_z m} \end{aligned}$$

Now there are two factors affecting stability: application point of the virtual force and lookahead distance. From the previous section there are clear limitations on the application point of the control force. Note that the addition of lookahead does not affect the final term in the characteristic equation. Therefore, the instability caused by applying the virtual force behind the neutral steer point cannot be rectified using lookahead. Once stability has been achieved by applying the force in front of the neutral steer point, system response and critical speed are changed by manipulation of the sensing location.

Figure 3.11 shows how the system eigenvalues change as the lookahead is varied from the c.g. to a preview distance of $60m$ for an understeering vehicle. The speed is held at a constant $30m/s$ and the virtual force is $0.5m$ in front of the neutral steer point. Initially, the vehicle is unstable with a pair of eigenvalues in the right

half plane. As the lookahead distance is increased, these unstable poles eventually migrate into the left half plane, stabilizing the system. Increasing the lookahead by too great a margin has some negative side effects on system performance. Eventually, two eigenvalues move onto the real axis while the other two eigenvalues move towards the imaginary axis, decreasing the system damping.

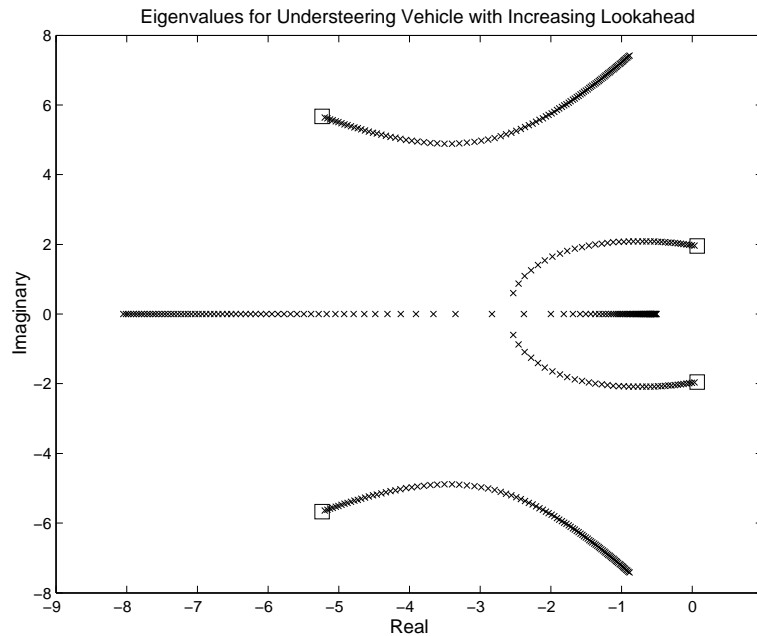


Figure 3.11: Eigenvalues as the Lookahead Distance is Varied from 0-60m: Understeering Vehicle

Figure 3.12 depicts the system eigenvalues for an oversteering vehicle using the same range of lookahead distances. As in the understeering case, the system is initially unstable with a pair of eigenvalues in the right half plane. As the lookahead is increased, this eigenvalue pair moves into the left half plane stabilizing the system. With increasing lookahead, however, the eigenvalues that were initially unstable become less damped. As with the understeering case, there is a lookahead distance that yields a stable system with appropriate damping characteristics.

Figure 3.13 shows the system states for an understeering vehicle with varying amounts of lookahead. The virtual force application point and speed are the same as those used in the eigenvalue figures and the initial condition is a lateral offset of

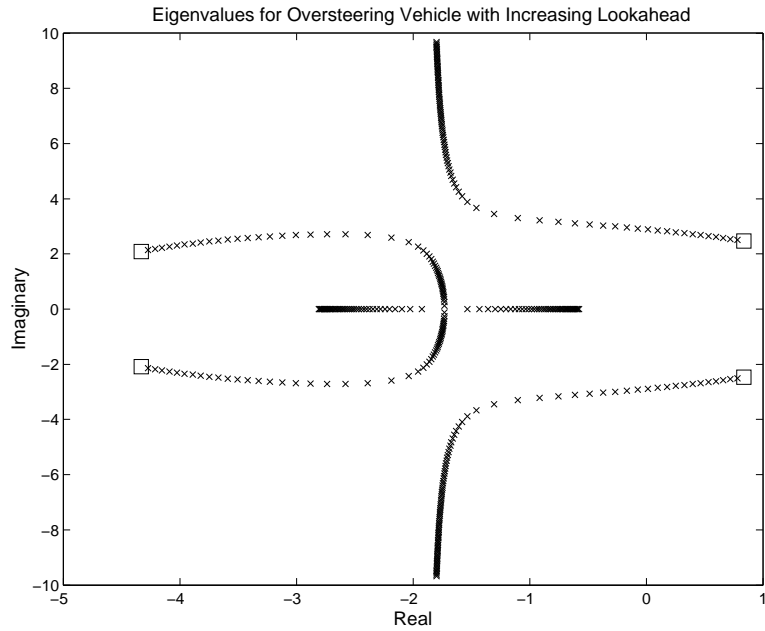


Figure 3.12: Eigenvalues as the Lookahead Distance is Varied from 0-60m: Oversteering Vehicle

0.5m from the lane center. With a lookahead of 10m the system is underdamped with a slow natural frequency. When the preview distance is increased to 30m the responses look much better. The damping has increased and all states converge to nominal values in a shorter time. Increasing the preview distance to 50m, however, creates a less desirable system response with high frequency oscillations in the states. Table 3.2 shows the eigenvalues and damping for these three cases of lookahead.

3.6 Controller Damping

Given a certain application point for the virtual force, a lookahead distance can be chosen that will create a stable, adequately damped system without any artificial controller damping (i.e. damping on \dot{e} and $\dot{\psi}$). The final way to alter the performance of the system is to include controller damping. Adding damping to the velocity states allows the designer to implement full state feedback on the system, giving the freedom to theoretically place the poles at an arbitrary location (of course, there are limits due

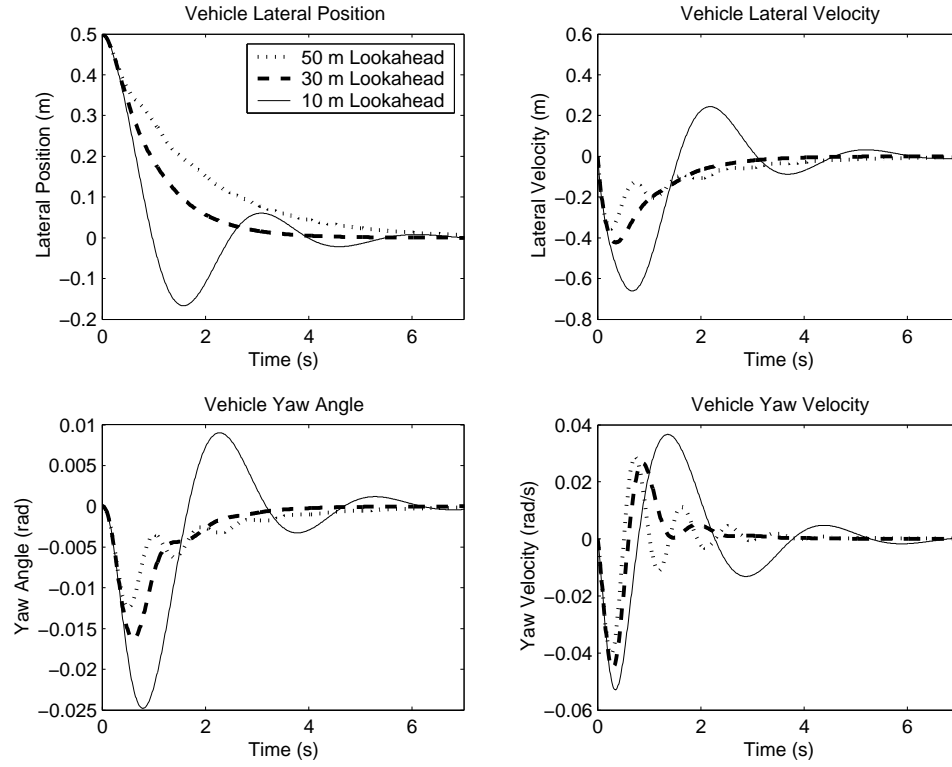


Figure 3.13: Understeering Vehicle Response with Varying Lookahead

10 m Lookahead	30 m Lookahead	50 m Lookahead
$-0.6748 + 2.0868i$	-5.1086	-0.6163
$-0.6748 - 2.0868i$	-1.1999	-7.3928
$-4.4865 + 5.1920i$	$-2.0071 + 5.7376i$	$-1.1568 + 6.9551i$
$-4.4865 - 5.1920i$	$-2.0071 - 5.7376i$	$-1.1568 - 6.9551i$
$\zeta_{1-2}=0.3077$	$\zeta_{1-2}=1.0$	$\zeta_{1-2}=1.0$
$\zeta_{3-4}=0.6538$	$\zeta_{3-4}=0.33$	$\zeta_{3-4}=0.164$

Table 3.2: Eigenvalues and Damping

to actuator capability, bandwidth, etc.). With controller damping the virtual force is now a function of the lateral position at some lookahead distance, x_{la} , the lateral velocity, \dot{e} , and the yaw rate, $\dot{\psi}$.

$$F_{virtual} = -2k(e + x_{la}\sin\psi) - D_{\dot{e}}\dot{e} - D_{\dot{\psi}}\dot{\psi} \quad (3.32)$$

where $D_{\dot{e}}$ and $D_{\dot{\psi}}$ are the damping coefficients on the lateral and yaw velocities respectively.

Incorporating the damping terms into the linear dynamics gives

$$A = \begin{bmatrix} 0 & 1 & 0 & 0 \\ -\frac{2k}{m} & \frac{-(C_f+C_r)}{mS} - \frac{\mathbf{D}_{\dot{e}}}{\mathbf{m}} & \frac{C_f+C_r}{m} - \frac{2kx_{la}}{m} & \frac{(-aC_f+bC_r)}{mS} - \frac{\mathbf{D}_{\dot{\psi}}}{\mathbf{m}} \\ 0 & 0 & 0 & 1 \\ \frac{-2kx_{cf}}{I_z} & \frac{(-aC_f+bC_r)}{I_zS} - \frac{\mathbf{x}_{cf}\mathbf{D}_{\dot{e}}}{\mathbf{I}_z} & \frac{(aC_f-bC_r)}{I_z} - \frac{2kx_{la}x_{cf}}{I_z} & \frac{-(a^2C_f+b^2C_r)}{I_zS} - \frac{\mathbf{x}_{cf}\mathbf{D}_{\dot{\psi}}}{\mathbf{I}_z} \end{bmatrix} \quad (3.33)$$

If the input is the virtual force applied at a distance, x_{cf} , from the c.g., the closed loop system can be written as

$$\delta\dot{x} = (A_{OL} - BG)\delta x \quad (3.34)$$

where A_{OL} is the open loop vehicle dynamics given in Equation 3.13 with B and G defined as

$$B = \begin{bmatrix} 0 & \frac{1}{m} & 0 & \frac{x_{cf}}{I_z} \end{bmatrix}^T \quad (3.35)$$

$$G = \begin{bmatrix} 2k & D_{\dot{e}} & 2kx_{la} & D_{\dot{\psi}} \end{bmatrix} \quad (3.36)$$

In theory, there is now complete control over the closed loop system dynamics. The poles of the system can be put at any location given the correct choice of the parameters in the virtual force expression. Of course, there are practical limits on these parameters depending on the actuation and sensing capabilities of a particular system. Ignoring these issues, the problem of lateral vehicle control now seems trivial. The gain, lookahead distance, and damping values can be chosen to give any desired

response.

In reality, however, it might be undesirable to have large damping values in the controller. With large damping values, the system is constantly losing energy when there is a lateral or yaw velocity. From an efficiency standpoint this is a poor design move. For lanekeeping assistance systems, the ability to produce adequate responses without adding any artificial controller damping on the velocity states is quite beneficial. Ideally when the driver is close to the minimum of the potential the dynamics should be equivalent to the uncontrolled vehicle. With additional damping the vehicle handling will be markedly different even near the potential field minimum (imagine driving through molasses). For driver assistance the results and intuition pertaining to the control force location and projection into the potential can be used to create a well-behaved stable response in the absence of driver inputs.

3.7 Concluding Remarks

For vehicle control, it is crucial to pay attention to the application point of virtual control forces (i.e. the coordination of the available actuators). Changes in vehicle properties can have deleterious effects on the system's performance and stability. The analysis in this chapter illustrates the instabilities that can occur when virtual control forces are applied to a vehicle. This analysis showed that there are two main factors contributing to the stability of the vehicle related to the control force location and the sensing location.

- For stability, the virtual control force must be applied in front of the neutral steer point.
- For high speed stability, the control force must be based on a projection into the potential

Although there is a great deal of research devoted to lateral stability, the virtual forces analogy is a novel and unique way of looking at vehicle stability. Abstracting the control as a force applied to the vehicle naturally incorporates the actuator coordination and the relationship between the control forces and the underlying vehicle

dynamics. This approach provides useful design rules for not only the potential field controller, but other types of lateral controllers. The virtual force concept is especially useful for the design of lateral controllers where multiple actuators are used that can alter the coupling between the lateral and yaw modes.

The results presented in this chapter provide design rules for achieving stable, well-behaved responses when using virtual forces. One question that still remains is how to scale the potential function to guarantee the lanekeeping ability of the system. As discussed in the previous chapter, the overall system energy provides a bound that can be used to scale the potential function. Using total energy, however, tells us that in the worst case all the initial energy (including the large amount in the longitudinal direction) is transferred into the lanekeeping potential. Recall that this is the case where the vehicle rotates into the potential field force. In light of the stability results presented in this chapter, this type of response is avoided by applying the control force in front of the neutral steer point and then using an appropriate amount of lookahead. Utilizing these stability results creates a system response where very little of the longitudinal energy is transferred into the lateral hazard. Lookahead, however, alters the basic potential field control structure, raising questions about the passivity of the overall system. The next chapter shows that the overall energy (with a slightly modified potential) is still dissipative, but provides a conservative bound for the vehicle's lateral motion. Utilizing the stability results from this chapter, a less conservative bound for the lateral motion is developed, providing a safety guarantee for the lanekeeping system in the presence of time-varying disturbances.

Chapter 4

Bounding Lateral Motion

For lanekeeping, the goal of the potential field approach is to smoothly combine the driver and controller commands while providing enough disturbance rejection to remain in the lane in the absence of driver commands. Scaling of the potential field is crucial in order to satisfy these two criteria. If the potential gain is too large, the system will be overly obtrusive to the driver. Conversely, erring in the other direction will create a system that is unable to keep the vehicle in the lane. The conflicting nature of these two goals was noted by Fujioka et al. [18] who developed a system that used the input from the driver along with the command from a ‘virtual’ driver to determine the total steering command. Testing on a fixed base driving simulator revealed that the driver acceptance of this approach was inversely related to the ‘virtual’ driver’s influence. The final goal in the potential field control structure is to be able to guarantee the nominal safety of the system (i.e. without driver inputs) while avoiding over scaling of the potential function.

In the potential field framework, the dynamic response of the vehicle is determined by the interaction between the underlying vehicle dynamics and the passive connection with the environment. As shown in the last chapter, guaranteeing passivity is not sufficient to ensure an appropriate lanekeeping response. To ensure a well-behaved and stable response from the driver’s perspective requires two constraints on the potential field controller.

1. The control force must be applied in front of the vehicle’s neutral steer point.

2. Adequate system response can be achieved using a projection (lookahead) into the potential.

This chapter shows that taking these factors into account in the potential field control structure still results in a passive system, providing a quantitative way of guaranteeing the lanekeeping ability of the vehicle. Using total energy, however, is a remarkably conservative bound for the lateral motion of the vehicle. With properly designed dynamics (Chapter 3) not much of the longitudinal energy, which is contained in the bound, is transferred into the lateral and rotational modes of the vehicle. With a constraint on the lookahead used in the controller, a subset of the overall dynamics, consisting of the lateral and rotational dynamics, maintains passive properties. This result is extremely powerful because the energy-like bound on these dynamics provides tight bounds on the lateral motion of the vehicle.

Up to this point, only a straight road has been treated in the development of the lateral and heading error dynamics. Although it is mathematically convenient to treat roads as being straight, they do indeed curve to give us the freedom to move globally in \mathbb{R}^2 as well as providing enjoyment for sports car owners. By design, the potential field structure passively couples the vehicle to the environment and does not attempt to track a desired trajectory. As a result, disturbances such as road curvature will alter the path of the vehicle. The last part of this chapter develops a general method of bounding Lagrangian systems in the presence of time-varying disturbances. This technique is then applied to the vehicle system with time-varying road curvature disturbances. A simulation example shows that the resulting bound on the lateral motion works remarkably well and provides a realistic safety guarantee for the lanekeeping system. The bounding technique developed in this chapter is an extremely general and powerful tool that can provide performance guarantees for a large class of Lagrangian dynamic systems.

4.1 Potential Field Control Structure

As discussed in the previous chapter, a well-behaved lateral response requires a certain amount of lookahead into the potential. Therefore, the potential used for lanekeeping

is a function of the projected lateral offset, e_{la} (Figure 4.1). In this chapter, the lookahead is defined from the application point of the control force in order to simplify the results that will follow (this is slightly different from the definition in the last chapter where the lookahead was defined from the vehicle's c.g.). The potential function used for control is given by

$$V_c(e_{la}) = ke_{la}^2 = k(e + (x_{cf} + x_{la})\sin\psi)^2 \quad (4.1)$$

where x_{cf} is the control force location and x_{la} is the lookahead distance. Using this

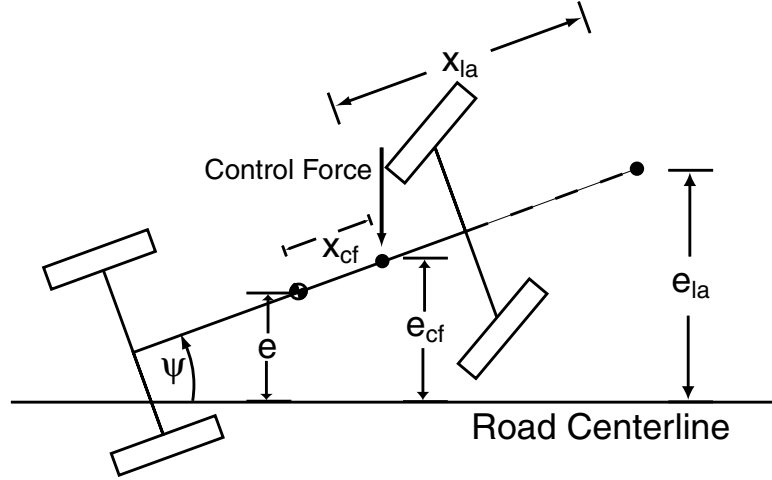


Figure 4.1: Important Locations

potential and allowing the control force to be applied at a distance, x_{cf} , from the center of gravity gives the following control law.

$$g(u_c) = g(u_{driver}) + g(u_{pf}) = g(u_{driver}) - \begin{bmatrix} \frac{\partial V_c}{\partial e} \sin\psi \\ \frac{\partial V_c}{\partial e} \cos\psi \\ x_{cf} \frac{\partial V_c}{\partial e} \cos\psi \end{bmatrix} \quad (4.2)$$

Using this control law, the equations of motion given in Equation 2.17 can be rewritten as

$$M_3\ddot{q}_3 = f_3(\dot{q}_3) + g(u_{driver}) + g(u_{pf}) \quad (4.3)$$

where $f_3(\dot{q}_3)$ are the uncontrolled vehicle dynamics, $g(u_{driver})$ are the driver controlled forces, and $g(u_{pf})$ are the control forces from the potential (or the virtual control force). Now, however, the control forces contained in $g(u_{pf})$ are related to the lookahead distance and the control force location.

4.2 Bounding Lateral Motion

4.2.1 Passivity with Lookahead

With a control force location that is not coincident with the lookahead point, which is normally the case for lateral vehicle control, the control forces cannot be entirely derived from the quadratic potential, V_c . With this control structure, however, the overall system dynamics maintain passive properties, which can be shown using a Lyapunov function composed of the vehicle's kinetic energy and a new potential energy-like term. The following proofs assume a working knowledge of Lyapunov theory, which is detailed in many nonlinear texts (Sastry [56] and Slotine and Li [62]).

Proposition 4.2.1 *Given a control force, $x_{cf} > 0$, and a lookahead distance $x_{la} \in \mathcal{L}$ where $\mathcal{L} = \left\{ x \in \mathbb{R} \mid 0 < x < \frac{2C_f C_r (a+b)^2}{k(C_f a^2 + C_r b^2)} \right\}$ a Lyapunov function for the system dynamics given in Equation 4.3 (in the absence of driver inputs) is*

$$L_3(q_2, \dot{q}_3) = T_3(\dot{q}_3) + V_3(q_2) \quad (4.4)$$

where T_3 is the total kinetic energy of the vehicle and V_3 is a potential energy-like term

$$T_3 = \frac{1}{2}mU_x^2 + \frac{1}{2}mU_y^2 + \frac{1}{2}I_z r^2 \quad (4.5)$$

$$V_3 = ke^2 + 2kx_{cf}e\psi + kx_{cf}(x_{la} + x_{cf})\psi^2 \quad (4.6)$$

Proof: In order to be a Lyapunov function, the candidate function must satisfy the following conditions:

- $L(z) > 0$
- $\|z\| \rightarrow \infty \Rightarrow L(z) \rightarrow \infty$
- $\dot{L}(z) \leq 0$

The first condition can be checked by verifying that the kinetic energy and potential energy-like term are both positive. By definition, the kinetic energy of the system is positive. In matrix form, the potential is given by

$$V_3 = q_2^T V_m q_2 \quad (4.7)$$

where $q_2 = \begin{bmatrix} e & \psi \end{bmatrix}^T$ and the matrix V_m is given by

$$V_m = \begin{bmatrix} k & kx_{cf} \\ kx_{cf} & kx_{cf}(x_{la} + x_{cf}) \end{bmatrix} \quad (4.8)$$

The positive definiteness of V_m is shown using Sylvester's theorem [62]. This theorem states that a necessary and sufficient condition for a matrix to be positive definite is for all the principal minors to be strictly positive. The first term of V_m consists of the potential field gain and is positive. Taking the determinant of V_m yields

$$|V_m| = k^2 x_{cf} x_{la} \quad (4.9)$$

$$|V_m| > 0 \quad \text{if and only if}$$

$$x_{cf} x_{la} > 0 \quad (4.10)$$

Since it will soon be shown the the lookahead must be greater than zero, this condition simply implies that the control force location must also be positive. The candidate function is a positive, quadratic function of the system states and satisfies the second condition of being radially unbounded.

Finally, taking the derivative of the candidate function yields

$$\dot{L}_3 = m\dot{U}_x U_x + m\dot{U}_y U_y + I_z \dot{r} r + \dot{V}_3 \quad (4.11)$$

Substituting the dynamics from Equation 4.3 gives

$$\dot{L}_3 = \dot{q}_3^T f_3(\dot{q}_3) - 2kx_{la}\psi^2 U_x - 2kx_{la}\psi U_y \quad (4.12)$$

From Proposition 2.3.1 we know that the term $\dot{q}_3^T f_3(\dot{q}_3)$ is never adding energy. Because of the inclusion of lookahead, there are additional terms from the potential, V_3 , which are not cancelled. This system, however, still conserves energy. Expanding the derivative of the candidate Lyapunov function

$$\begin{aligned} \dot{L}_3 &= U_y \left[-(C_f + C_r) \frac{U_y}{U_x} + (C_r b - C_f a) \frac{r}{U_x} \right] + r \left[(C_r b - C_f a) \frac{r}{U_x} - (C_f a^2 + C_r b^2) \frac{r}{U_x} \right] \\ &\quad - 2kx_{la}\psi^2 U_x - 2kx_{la}\psi U_y \end{aligned} \quad (4.13)$$

To check the sign of this equation, the lateral and rotational velocities are transformed to road fixed coordinates using the following relationships

$$\dot{e} = U_y \cos\psi + U_x \sin\psi \approx U_y + U_x \psi \quad (4.14)$$

$$\dot{\psi} = r \quad (4.15)$$

Using these coordinate transformations

$$\dot{L}_3 = - \begin{bmatrix} \dot{e} & \dot{\psi} & \psi \end{bmatrix} \begin{bmatrix} \frac{C_f + C_r}{U_x} & \frac{C_f a - C_r b}{U_x} & kx_{la} - (C_f + C_r) \\ \frac{C_f a - C_r b}{U_x} & \frac{C_f a^2 + C_r b^2}{U_x} & C_r b - C_f a \\ kx_{la} - (C_f + C_r) & C_r b - C_f a & (C_f + C_r) U_x \end{bmatrix} \begin{bmatrix} \dot{e} \\ \dot{\psi} \\ \psi \end{bmatrix} \quad (4.16)$$

Utilizing Sylvester's criterion the matrix in the above expression is positive definite as long as the lookahead distance satisfies

$$0 < x_{la} < \frac{2C_f C_r (a + b)^2}{k(C_f a^2 + C_r b^2)} \quad (4.17)$$

With this constraint on the lookahead as well as a control force location that is positive, the candidate function satisfies the Lyapunov conditions. Since the derivative is always decreasing, the function at time $t > 0$ is bounded by the function value at time

$t = 0$. The initial value of the Lyapunov function, therefore, defines the reachable set for the system in the absence of driver inputs.

□

This Lyapunov function provides a bound on the system states that can be used to guarantee the lanekeeping ability of the system. In reality, however, this result is extremely conservative as a bound on the lateral motion of the vehicle. This conservatism results from including the large amount of longitudinal kinetic energy in the bounding function. During normal lanekeeping maneuvers, very little of the vehicle's longitudinal energy is transferred into the lateral and rotational directions. However, with slightly more restrictive constraints on the control force location and the lookahead distance, it is possible to create a passive system using only the subset of the dynamics that is pertinent for lanekeeping: the lateral and rotational vehicle dynamics.

To create a passive system using a subset of the dynamics, pertaining to the lateral and heading error, requires two constraints. Not surprisingly, the first constraint requires the control force from the potential function to be applied in front of the neutral steer point.

$$x_{cf} > \frac{aC_f - bC_r}{C_f + C_r} \quad (4.18)$$

This is one of the conditions necessary for lateral stability (Chapter 3) that ensures the vehicle rotates in the direction of the control force. The second constraint is the choice of a specific lookahead distance in Equation 4.1, based on the tire cornering stiffnesses and the potential field gain.

$$x_{la} = \frac{C_f + C_r}{2k} \quad (4.19)$$

The need for this constraint is discussed in the following section.

4.2.2 A New Bound for Lanekeeping

In order to bound the lateral motion of the vehicle relative to the lane, the vehicle dynamics developed in Chapter 2 are transformed to the road fixed coordinates,

$w = \begin{bmatrix} s & e & \psi \end{bmatrix}^T$, shown in Figure 4.2. The transformation between the road fixed

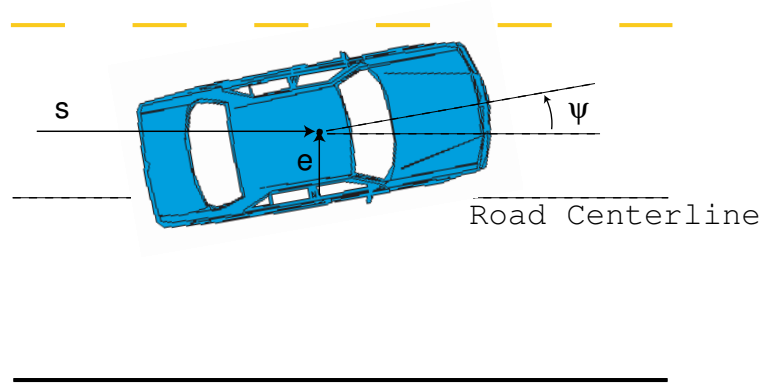


Figure 4.2: Global Coordinates

frame, w , and the vehicle fixed frame, q_3 is given by

$$\frac{\partial \dot{w}}{\partial \dot{q}_3} = \frac{\partial w}{\partial q_3} = \begin{bmatrix} \cos \psi & -\sin \psi & 0 \\ \sin \psi & \cos \psi & 0 \\ 0 & 0 & 1 \end{bmatrix} \quad (4.20)$$

Using this transformation between the vehicle fixed velocities, \dot{q}_3 , and the road fixed velocities, \dot{w} , the equations of motion given in Equation 4.3 are written in terms of the longitudinal velocity, lateral error relative to road center, and heading error relative to road center. From the transformation matrix

$$\dot{e} = U_y \cos \psi + U_x \sin \psi \quad (4.21)$$

Solving for the lateral velocity, U_y , and using the transformation between the yaw rate, r , and the heading error, ψ , gives the following relationships.

$$U_y = \frac{\dot{e}}{\cos \psi} - \frac{U_x \sin \psi}{\cos \psi} \quad (4.22)$$

$$r = \dot{\psi} \quad (4.23)$$

In order to bound the motion in the absence of driver commands these substitutions are used for the vehicle dynamics from Equation 4.3 with the assumption that all the driver commands are zero. The longitudinal velocity is left in terms of the body fixed velocity, U_x . This is done because this velocity appears in the denominator of certain terms in the lateral and heading error dynamics, which play an important role in the following analysis as will be shown shortly.

$$m\dot{U}_x = -\frac{\partial V_c(e_{la})}{\partial e} \sin\psi + m\frac{\dot{\psi}\dot{e}}{\cos\psi} - m\dot{\psi}U_x \tan\psi \quad (4.24)$$

$$\begin{aligned} m\ddot{e} &= -\frac{\partial V_c(e_{la})}{\partial e} - \frac{\dot{e}(C_r + C_f)}{U_x} + (C_f + C_r) \sin\psi \\ &+ \frac{\dot{\psi}(bC_r - aC_f) \cos\psi}{U_x} \end{aligned} \quad (4.25)$$

$$\begin{aligned} I_z\ddot{\psi} &= -\frac{\partial V_c(e_{la})}{\partial e} x_{cf} \cos\psi + \frac{\dot{e}(bC_r - aC_f)}{U_x \cos\psi} + (aC_f - bC_r) \tan\psi \\ &- \frac{\dot{\psi}(b^2C_r + a^2C_f)}{U_x} \end{aligned} \quad (4.26)$$

With our knowledge of lanekeeping stability from the previous chapter, the heading angle of the vehicle remains small relative to the road (hopefully, or you better hope your vehicle has stability control!) so small angle approximations are used for the following development.

$$m\dot{U}_x = -\frac{\partial V_c(e_{la})}{\partial e} \psi + m\dot{\psi}\dot{e} - m\dot{\psi}U_x \psi \quad (4.27)$$

$$m\ddot{e} = -\frac{\partial V_c(e_{la})}{\partial e} - \frac{\dot{e}(C_r + C_f)}{U_x} + (C_f + C_r)\psi + \frac{\dot{\psi}(bC_r - aC_f)}{U_x} \quad (4.28)$$

$$\begin{aligned} I_z\ddot{\psi} &= -\frac{\partial V_c(e_{la})}{\partial e} x_{cf} + \frac{\dot{e}(bC_r - aC_f)}{U_x} + (aC_f - bC_r)\psi \\ &- \frac{\dot{\psi}(b^2C_r + a^2C_f)}{U_x} \end{aligned} \quad (4.29)$$

From Proposition 4.2.1, these dynamics are bounded by a Lyapunov function that consists of the overall kinetic energy of the vehicle and a potential energy-like term (Equation 4.4). The following approach creates a new Lyapunov function that

only consists of the kinetic energy in the lateral and heading error directions and a slightly modified potential function, removing the conservatism from including the longitudinal energy in the bound. The underlying philosophy of this approach is to find a potential, V_2 , that allows a Lagrangian formulation of the lateral and heading error dynamics given in Equations 4.28 and 4.29.

$$M_2 \ddot{q}_2 = f_2(\dot{q}_2) - \left(\frac{\partial V_2}{\partial q_2} \right)^T \quad (4.30)$$

where q_2 consists of the lateral and heading error directions and M_2 is a subset of the overall mass matrix pertaining to the lateral and heading error dynamics.

$$M_2 = \begin{bmatrix} m & 0 \\ 0 & I_z \end{bmatrix} \quad (4.31)$$

Once in this form, if the velocity dependent forces contained in $f_2(\dot{q}_2)$ are dissipative, the sum of the kinetic energy in the lateral and heading directions and the potential, V_2 , are guaranteed to be non-increasing.

To use a Lagrangian formulation for the lateral and heading error dynamics requires the configuration dependent terms to be derivable from a potential. This potential, V_2 , must satisfy

$$-\frac{\partial V_2}{\partial e} = -\frac{\partial V_c(e_{ta})}{\partial e} + (C_f + C_r)\psi \quad (4.32)$$

$$-\frac{\partial V_2}{\partial \psi} = -\frac{\partial V_c(e_{ta})}{\partial e} x_{cf} + (aC_f - bC_r)\psi \quad (4.33)$$

Since the control potential given in Equation 4.1 is quadratic, the forces in the above equations are linear functions of the positional states. Therefore, the new potential is assumed to have the general quadratic form

$$V_2 = c_1 e^2 + c_2 e \psi + c_3 \psi^2 \quad (4.34)$$

Satisfying Equation 4.32 and 4.33 with a potential of this form requires the lookahead of the system to be equal to the ratio of the sum of the lateral cornering stiffnesses

and the potential field gain as previously described in Equation 4.19. This constraint on the lookahead is necessary to cancel out a portion of the tire force that can be adding energy in the lateral and heading error directions. This is the force term that is dependent on the vehicle heading from Equation 4.28 $((C_f + C_r)\psi)$.

This constraint on the lookahead, however, does give realistic values for typical cornering stiffnesses and potential function gains. For general operating conditions and vehicle parameters it gives lookahead values that provide well damped responses. Although this equality constraint may seem restrictive, especially since the cornering stiffnesses may not be known exactly, this lookahead distance is not a critical point for stability. In fact, with the extension of this bounding technique to handle time-varying disturbance (Section 4.4), any deviation from this lookahead value can be treated as a disturbance to the system and the lanekeeping performance can still be bounded. Using this constraint on the lookahead, the coefficients of the new potential are

$$c_1 = k \quad (4.35)$$

$$c_2 = 2kx_{cf} \quad (4.36)$$

$$c_3 = kx_{cf}(x_{la} + x_{cf}) + \frac{1}{2}(bC_r - aC_f) \quad (4.37)$$

The final goal is to show that the remaining velocity dependent terms dissipate energy. In matrix form, these terms are given by

$$f_2(\dot{q}_2) = -\Phi\dot{q}_2 = - \begin{bmatrix} \frac{C_f+C_r}{U_x} & \frac{aC_f-bC_r}{U_x} \\ \frac{aC_f-bC_r}{U_x} & \frac{b^2C_r+a^2C_f}{U_x} \end{bmatrix} \begin{bmatrix} \dot{e} \\ \dot{\psi} \end{bmatrix} \quad (4.38)$$

In order to dissipate energy

$$\dot{q}_2^T f_2(\dot{q}_2) = - \begin{bmatrix} \dot{e} & \dot{\psi} \end{bmatrix} \begin{bmatrix} \frac{C_f+C_r}{U_x} & \frac{aC_f-bC_r}{U_x} \\ \frac{aC_f-bC_r}{U_x} & \frac{b^2C_r+a^2C_f}{U_x} \end{bmatrix} \begin{bmatrix} \dot{e} \\ \dot{\psi} \end{bmatrix} \leq 0 \quad (4.39)$$

The term $\dot{q}_2^T f_2(\dot{q}_2)$ is negative if the matrix Φ is positive definite. Once again, this

is shown using Sylvester's theorem. Since the cornering stiffnesses and longitudinal velocity are positive, the first component in the matrix is positive. Taking the determinant of the matrix yields

$$|\Phi| = \frac{(C_f + C_r)(a^2 C_f + b^2 C_r)}{U_x^2} - \frac{(a C_f - b C_r)^2}{U_x^2} = \frac{C_f C_r (a + b)^2}{U_x^2} > 0 \quad (4.40)$$

$$\Rightarrow \dot{q}_2^T f_2(\dot{q}_2) \leq 0 \quad (4.41)$$

It is important to note that the longitudinal velocity, U_x , only appears in the denominator of the damping terms. Since the longitudinal velocity is bounded by Proposition 4.2.1, these terms will always be removing energy and changes in the velocity only affect the magnitude of the damping.

The equations of motion in the lateral and heading error direction can be derived from the kinetic energy in these directions, T_2 , and the new potential, V_2 .

$$T_2 = \frac{1}{2} \dot{q}_2^T M_2 \dot{q}_2 \quad (4.42)$$

$$V_2 = \frac{1}{2} q_2^T V_{2m} q_2 \quad (4.43)$$

The mass matrix M_2 is a subset of the original mass matrix pertaining to the lateral and heading error dynamics, and V_{2m} contains all the positional dependent terms.

$$M_2 = \begin{bmatrix} m & 0 \\ 0 & I_z \end{bmatrix} \quad (4.44)$$

$$V_{2m} = \begin{bmatrix} 2c_1 & c_2 \\ c_2 & 2c_3 \end{bmatrix} \quad (4.45)$$

The equations of motion for the lateral and heading error dynamics are now composed of dissipation terms and conservative forces derivable from the new potential function, V_2 .

$$M_2 \ddot{q}_2 = f_2(\dot{q}_2) - \left(\frac{\partial V_2}{\partial q_2} \right)^T \quad (4.46)$$

The following proof uses Lyapunov theory to show that the sum of the kinetic

energy in the lateral and rotational directions and the new potential is decreasing. This bounding function is useful for several reasons. Although we know about the lanekeeping stability from Chapter 3, this function guarantees that with the constraint on lookahead and the control force in front of the neutral steer point, this system is stable at all speeds. More importantly, the Lyapunov function provides a bound for the lateral motion of the vehicle, allowing the potential function gain to be chosen in order to avoid lane departures.

Proposition 4.2.2 *Assuming a control force in front of the neutral steer point such that $x_{cf} > \frac{aC_f - bC_r}{C_f + C_r}$, a Lyapunov function for the system given in Equation 4.46 is*

$$L_2(q_2, \dot{q}_2) = T_2 + V_2 = \frac{1}{2} \dot{q}_2^T M_2 \dot{q}_2 + \frac{1}{2} q_2^T V_{2m} q_2 \quad (4.47)$$

The initial value of the Lyapunov function at time, $t = 0$, defines the reachable set for the lateral and heading error states.

$$\mathfrak{R} = \left\{ \left[\begin{array}{cc} q_2 & \dot{q}_2 \end{array} \right]^T \mid L_2(q_2(t), \dot{q}_2(t)) \leq L_2(q_2(0), \dot{q}_2(0)) \right\} \quad (4.48)$$

Proof: This candidate function must satisfy the same conditions used in Proposition 4.2.1. The sign of the candidate function is checked by verifying that the mass matrix, M_2 , and the potential matrix, V_{2m} , are positive definite. By definition, the mass matrix is positive definite. The positive definiteness of V_{2m} is shown using Sylvester's theorem. The first term of V_{2m} consists of the potential field gain and is positive. Taking the determinant of V_{2m} yields

$$|V_{2m}| = 4c_1c_3 - c_2^2 = 2kx_{cf}(C_f + C_r) + 2k(bC_r - aC_f) \quad (4.49)$$

$$\begin{aligned} |V_{2m}| &> 0 \quad \text{if and only if} \\ x_{cf} &> \frac{aC_f - bC_r}{C_f + C_r} \end{aligned} \quad (4.50)$$

Not surprisingly, this is the neutral steer point condition discussed previously.

The candidate function is radially unbounded for the states corresponding to the lateral and rotational motion. Although the longitudinal velocity is not included in

this candidate function it is bounded by Proposition 4.2.1.

Taking the derivative of the candidate Lyapunov function

$$\dot{L}_2 = \dot{q}_2^T M_2 \ddot{q}_2 + \dot{q}_2^T \left(\frac{\partial V_2}{\partial q_2} \right)^T \quad (4.51)$$

Substituting the equations of motion gives

$$\dot{L}_2 = \dot{q}_2^T \left[f_2(\dot{q}_2) - \left(\frac{\partial V_2}{\partial q_2} \right)^T \right] + \dot{q}_2^T \left(\frac{\partial V_2}{\partial q_2} \right)^T \quad (4.52)$$

$$= \dot{q}_2^T f_2(\dot{q}_2) \quad (4.53)$$

$$\leq 0 \quad (4.54)$$

As long as the control force is in front of the neutral steer point, L_2 is a Lyapunov function. Since the derivative is always decreasing, the function at time $t > 0$ is bounded by the function value at time $t = 0$. The initial value of the Lyapunov function defines the reachable set for the system.

□

This Lyapunov function is extremely powerful because it can be used to bound the lateral position of the vehicle given any initial configuration. Since the initial energy in the Lyapunov function is never increasing, the maximum possible positional states occur when all the initial energy is transferred into the potential.

$$V_2 \leq L_2(q_2(t), \dot{q}_2(t)) \leq L_2(q_2(0), \dot{q}_2(0)) \quad (4.55)$$

In order to bound the lateral position, e , it is necessary to determine the configuration with the maximum lateral displacement that satisfies the following level set.

$$V_2 = L_2(q_2(0), \dot{q}_2(0)) \quad (4.56)$$

Since the new potential contains cross terms, the maximum lateral error does not occur when the heading is equal to zero. Figure 4.3 shows a level set for the potential,

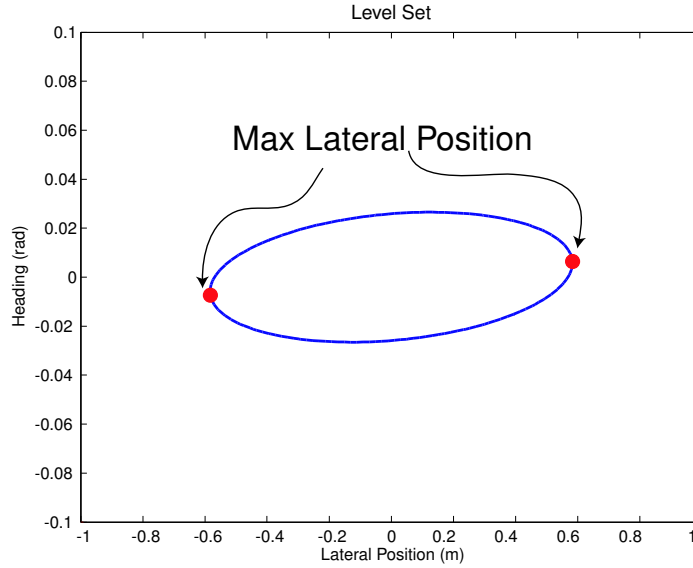


Figure 4.3: Level Set

V_2 , along with the maximum lateral error. The maximum lateral error is found by calculating the point on the level set where the lateral error is not changing relative to the heading error.

$$\frac{\partial e}{\partial \psi} = \frac{\frac{\partial V_2}{\partial \psi}}{\frac{\partial V_2}{\partial e}} = \frac{c_2 e + 2c_3 \psi}{2c_1 e + c_2 \psi} = 0 \quad (4.57)$$

The maximum displacement occurs when the numerator of the above expression is zero. Therefore, the relationship between the heading error and the lateral error at the maximum lateral displacement is

$$\psi = -\frac{c_2}{2c_3} e \quad (4.58)$$

Plugging this into the potential gives an expression for the maximum lateral error which satisfies the level set given in Equation 4.56.

$$\left(c_1 - \frac{c_2^2}{4c_3} \right) e^2 = L_2(q_2(0), \dot{q}_2(0)) \quad (4.59)$$

This expression gives a bound on the lateral position achievable by the vehicle. This

m (kg)	1450
I_z (N/m ²)	2500
C_f (N/rad)	110000
C_r (N/rad)	100000
a (m)	1.3
b (m)	1.3

Table 4.1: Vehicle Parameters for Simulation 1

same bound can also be used to scale the potential field gain in order to avoid reaching a certain lateral position. If, for example, there is a lane edge at $e = e_{edge}$, the gain can be chosen such that this lateral position is never achieved by satisfying

$$\left(c_1 - \frac{c_2^2}{4c_3} \right) = \frac{L_2(q_2(0), \dot{q}_2(0))}{e_{edge}^2} \quad (4.60)$$

The Lyapunov function provides a safety guarantee for the lanekeeping system and is illustrated in the following example.

4.2.3 Simulation Example

The simulation uses the three degree of freedom bicycle model with the parameters for our Corvette test vehicle given in Table 4.1. The vehicle is simulated starting at the lane center, $e(0) = 0m$, with an initial longitudinal velocity of $30m/s$. The initial heading is varied from 1 to 5 degrees and the potential gain is chosen so that the vehicle will never exceed a lateral offset of $1.0m$ (representing the side of the vehicle crossing a lane edge). As in our test vehicle, the control force location is constrained to act at the front axle ($x_{cf} = a$). Using the relationship given in Equation 4.60 the gain necessary to avoid a lane edge at $e_{edge} = 1m$ is

$$k = 7,160 \quad (4.61)$$

This yields a necessary lookahead value of

$$x_{la} = \frac{C_f + C_r}{2k} = 14.7m \quad (4.62)$$

which is similar to the lookahead used in the driver model from Chapter 2.

Figure 4.4 shows the Lyapunov function in time and as expected it is always decreasing. Of course, as the initial heading is increased the initial energy (or hazard) is also larger. Figure 4.5 shows the lateral position of the vehicle on the roadway. The gain was chosen so that in the worst case ($\psi(0) = 5$ Degrees) a lateral obstacle at $1.0m$ will be avoided. The results show that this lateral position is never achieved and the bound is fairly tight, especially compared with using the vehicle's total energy (Equation 4.4), which yields a result that is orders of magnitude conservative.

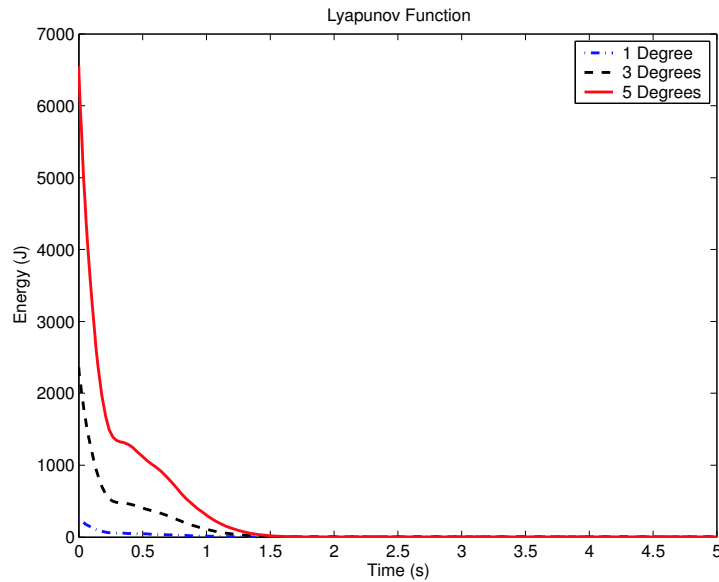


Figure 4.4: Lyapunov Function

Although extremely useful for designing the potential field gain, this Lyapunov function only bounds the system motion in the absence of disturbances. This function does, however, provide an excellent basis for extending the bound to handle time-varying disturbances. During normal driving a vehicle is subjected to a wide variety of disturbances such as road curvature, side winds, and road bank angle. The next

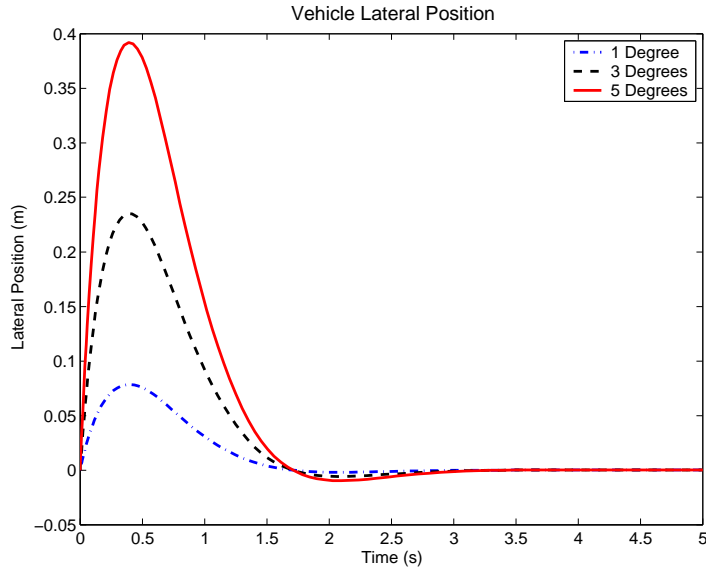


Figure 4.5: Vehicle Lateral Position

section develops a novel and powerful technique for bounding the vehicle motion in the presence of time-varying disturbances with application to road curvature, which is generally the largest disturbance experienced by a vehicle.

4.3 Road Curvature

The potential field framework passively couples the vehicle to the environment. By design, this approach does not attempt to track a desired trajectory and disturbances, such as road curvature, will alter the path of the vehicle. This concept is illustrated in Figure 4.6 with the controller abstracted as a spring attached to the road edge. The magnitude of the disturbance depends on the road curvature and the longitudinal velocity of the vehicle. If a vehicle is travelling on a road with a radius of curvature, ρ , the yaw rate error between the vehicle and the road is a function of the vehicle's yaw rate and the road curvature (Figure 4.7).

$$\dot{\psi} = r - U_x \rho \quad (4.63)$$

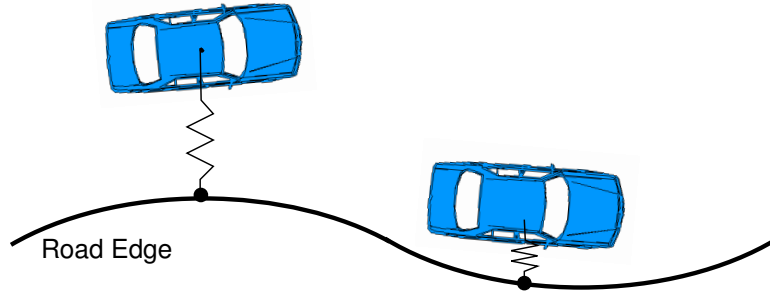


Figure 4.6: Road Curvature Disturbance

where r is the yaw rate of the vehicle, ρ is simply defined as the inverse of the curve radius, R , and $\dot{\psi}$ is the yaw rate error between the vehicle and the road.

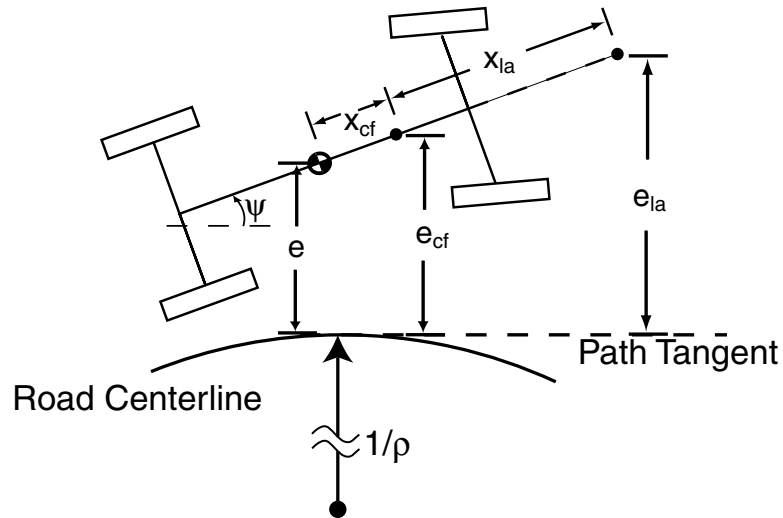


Figure 4.7: Road Curvature

The transformation between vehicle velocities and road fixed velocities must take the road's curvature into account.

$$U_x = \dot{s}\cos\psi + \dot{e}\sin\psi \quad (4.64)$$

$$U_y = \dot{e}\cos\psi - \dot{s}\sin\psi \quad (4.65)$$

$$\dot{\psi} = r - U_x\rho \quad (4.66)$$

$$\ddot{\psi} = \dot{r} - U_x\dot{\rho} - \dot{U}_x\rho \quad (4.67)$$

Substituting in to the body fixed equations of motion and using small angle approximations

$$\begin{aligned}
m\ddot{e} &= -\frac{\partial V(e_{la})}{\partial e} + (C_f + C_r)\psi - \frac{(C_f + C_r)}{U_x}\dot{e} + \frac{(bC_r - aC_f)}{U_x}\dot{\psi} \\
&+ (bC_r - aC_f)\rho(t) - mU_x^2\rho(t)
\end{aligned} \tag{4.68}$$

$$\begin{aligned}
I_z\ddot{\psi} &= -\frac{\partial V(e_{la})}{\partial e}x_{cf} + (aC_f - bC_r)\psi + \frac{(bC_r - aC_f)}{U_x}\dot{e} \\
&- \frac{(a^2C_f + b^2C_r)}{U_x}\dot{\psi} - (a^2C_f + b^2C_r)\rho + I_z(U_x\dot{\rho} + \dot{U}_x\rho)
\end{aligned} \tag{4.69}$$

These equations are similar to those developed in the previous section with the added disturbance terms related to the road curvature. These dynamics can be written in the Lagrangian formulation of Equation 4.46 with additional disturbance terms:

$$M_2\ddot{q}_2 = f_2(\dot{q}_2) - \left(\frac{\partial V_2}{\partial q_2}\right)^T + B_d\bar{\rho} \tag{4.70}$$

where $\bar{\rho} = \begin{bmatrix} \rho & \dot{\rho} \end{bmatrix}^T$ and the disturbance matrix is given by

$$B_d = \begin{bmatrix} (bC_r - aC_f) - mU_x^2 & 0 \\ -(a^2C_f + b^2C_r) + I_z\dot{U}_x & I_zU_x \end{bmatrix} \tag{4.71}$$

The Lyapunov function presented in the last section provides a bound in the absence of disturbances ($\bar{\rho} = 0$). With this added disturbance from road curvature, energy will be added to the system and the Lyapunov function will not necessarily decrease for all time. The next section presents a novel bounding method that slightly modifies the original Lyapunov function and bounds the function with an exponential related to the maximum frequency of the disturbance.

4.4 Bounding Time-Varying Disturbances

This section provides a bounding technique for time-varying disturbances. The following development treats a more general Lagrangian structure that can be applied to

the lanekeeping system as well as being applicable to a wide class of dynamic systems. The equations used in the following analysis are given by

$$M(q)\ddot{q} + C(q, \dot{q})\dot{q} + f(\dot{q}) + \left(\frac{\partial V}{\partial q}\right)^T = r(t) \quad (4.72)$$

where q is the system configuration, $M(q)$ is a configuration dependent mass matrix, $C(q, \dot{q})$ contains the coriolis and centrifugal force terms, $f(\dot{q})$ contains damping forces, V is the potential energy, and $r(t)$ is the disturbance or input to the system. The potential is assumed to have a quadratic form

$$V(q) = q^T D q \quad (4.73)$$

where D is a positive definite, symmetric matrix.

To tackle the time-varying disturbance problem it is illustrative to consider the case of a constant disturbance with known magnitude such as a constant radius turn. Here the solution is fairly straight forward because the equilibrium configuration is easily found from the equations of motion. For example, if the disturbance in Equation 4.72 is a constant, $r(t) = R$, then the equilibrium is simply

$$q = D^{-1}R \quad (4.74)$$

The Lyapunov function developed in the previous section (Equation 4.47) can be used for this case by using a change of variables to account for the equilibrium point. The change of variables is given by

$$q_{eq} = q - D^{-1}R \quad (4.75)$$

which is the new state used in the Lyapunov function.

If the disturbance is time-varying the problem becomes more difficult because the disturbance now has a frequency component. If the disturbance, however, is changing slowly relative to the system dynamics this intuition about the equilibrium configuration provides excellent bounds on the system motion. The following technique uses

a change of variables to account for the equilibrium configuration the system would attain if the input were constant.

$$q_{eq} = q - D^{-1}r(t) \quad (4.76)$$

Using this change of variables, the energy addition is now related to the frequency of the disturbance as will be shown shortly. Similar approaches have been used by Khalil [33] and Vidyasagar [68] to bound dynamic systems subject to slowly varying inputs. The following technique, however, follows the approach of Chang et al. [8], but utilizes this change of variables.

The ensuing proof also uses the following facts for damped mechanical systems. The first is the well known skew-symmetric property [44].

$$\dot{q}^T \left(\frac{d}{dt} M(q) - 2C(q, \dot{q}) \right) \dot{q} = 0 \quad (4.77)$$

For the second property, we define the matrix $A(q)$

$$A_{ij}(q) = \frac{1}{2} \sum_{k=1}^n \left(\frac{\partial^2 V}{\partial q_k \partial q_i} M_{jk}(q) + \frac{\partial^2 V}{\partial q_j \partial q_k} M_{ki}(q) - \frac{\partial V}{\partial q_k} \frac{\partial M_{i,j}}{\partial q_k}(q) \right) \quad (4.78)$$

This matrix satisfies the following expression which simplifies the upcoming proof [8].

$$\dot{q}^T A(q) \dot{q} = \dot{q}^T \frac{\partial^2 V}{\partial q^2} M(q) \dot{q} + \frac{\partial V}{\partial q} \left(\frac{d}{dt} M(q) - C(q, \dot{q}) \right) \dot{q} \quad (4.79)$$

The proof also utilizes the following Lemma for the extremum of the ratio of quadratic forms.

Lemma 1 *Suppose $P, Q \in \mathbb{R}^{n \times n}$ are symmetric, and P is positive definite. Then*

$$\min_{z \in \mathbb{R}^n, z \neq 0} \frac{z^T Q z}{z^T P z} = \lambda_{\min}(P^{-1}Q) \quad (4.80)$$

$$\max_{z \in \mathbb{R}^n, z \neq 0} \frac{z^T Q z}{z^T P z} = \lambda_{\max}(P^{-1}Q) \quad (4.81)$$

Proof Taking the derivative of the ratio of quadratic forms and setting it to zero yields

$$-\frac{z^T Qz}{(z^T Pz)^2} Pz + \frac{Qz}{z^T Pz} = 0 \quad (4.82)$$

rearranging the equations

$$\left(\frac{z^T Qz}{z^T Pz} \right) Pz = Qz \quad (4.83)$$

multiplying the right and left sides by P^{-1} gives

$$\left(\frac{z^T Qz}{z^T Pz} \right) z = P^{-1} Qz \quad (4.84)$$

This is simply an eigenvalue problem. Since P is assumed to be positive definite, the maximum of the ratio of the quadratic forms is the largest eigenvalue of $P^{-1}Q$. Similarly, the minimum of the ratio corresponds to the smallest eigenvalue of $P^{-1}Q$.

□

The proof also requires that the following bounds can be placed on the system where the constants, μ_1 , μ_2 , γ_1 , γ_2 , b_1 , b_2 , and a_1 are all positive.

$$\mu_1 \|\dot{q}\|^2 \leq \dot{q}^T M \dot{q} \leq \mu_2 \|\dot{q}\|^2 \quad (4.85)$$

$$\gamma_1 \|q_{eq}\|^2 \leq q_{eq}^T D q_{eq} \leq \gamma_2 \|q_{eq}\|^2 \quad (4.86)$$

$$b_1 \|\dot{q}\|^2 \leq \dot{q}^T f(\dot{q}) \quad (4.87)$$

$$b_2 \|\dot{q}\| \geq \|f(\dot{q})\| \quad (4.88)$$

$$a_1 \|\dot{q}\|^2 \geq \dot{q}^T A(q_{eq}) \dot{q} \quad (4.89)$$

The first two bounds described in Equations 4.85 and 4.86 bound the kinetic and potential energies by the velocity and configuration norms of the system. The next pair of bounds given in Equations 4.87 and 4.88 bound the dissipation function by velocity norms. The final bound simply puts an upper bound based on the norm of the velocity on the quadratic form $\dot{q}^T A(q_{eq}) \dot{q}$. This last requirement will be clear in the following proof and is used to bound the derivative of the energy-like function.

Proposition 4.4.1 *For the system in Equation 4.72, given an $\epsilon \in \mathcal{E} = \left\{ x \in \mathbb{R} \mid 0 < x < \min \left\{ \sqrt{\frac{\mu_1 \gamma_1}{\mu_2^2 \gamma_2^2}}, \frac{4\gamma_1^2 b_1}{4a_1 \gamma_1^2 + \gamma_2^2 b_2^2} \right\} \right\}$ and a bound on the disturbance's rate of change, $\|\dot{r}(t)\| \leq U_{max}$, the function*

$$L(\dot{q}, q_{eq}) = \frac{1}{2} \dot{q}^T M(q) \dot{q} + \frac{1}{2} q_{eq}^T D q_{eq} + \epsilon \dot{q}^T M(q) D q_{eq}$$

is bounded by an exponential.

$$L(\dot{q}(t), q_{eq}(t)) \leq \left(e^{-\sigma t} (\sqrt{L(\dot{q}(0), q_{eq}(0))} - \kappa U_{max}) + \kappa U_{max} \right)^2 \quad (4.90)$$

where σ and κ are positive constants. The system energy can be approximated by this Lyapunov function providing a bound on the energy of the system.

$$E(\dot{q}, q_{eq}) = \frac{1}{2} \dot{q}^T M \dot{q} + \frac{1}{2} q_{eq}^T D q_{eq} \leq \eta L(\dot{q}, q_{eq}) \quad (4.91)$$

where η is a positive constant.

Proof Defining the following positive definite symmetric matrices

$$P_{1,\epsilon} = \begin{bmatrix} \frac{1}{2} \mu_1 & -\frac{\mu_2 \gamma_2}{2} \epsilon \\ -\frac{\mu_2 \gamma_2}{2} \epsilon & \frac{\gamma_1}{2} \end{bmatrix}$$

$$P_{2,\epsilon} = \begin{bmatrix} \frac{1}{2} \mu_2 & \frac{\mu_2 \gamma_2}{2} \epsilon \\ \frac{\mu_2 \gamma_2}{2} \epsilon & \frac{\gamma_2}{2} \end{bmatrix}$$

and using the bounds from Equation 4.85 and 4.86 along with the Cauchy-Schwarz inequality gives upper and lower bounds for L .

$$L(\dot{q}, q_{eq}) \geq \begin{bmatrix} \|\dot{q}\| & \|q_{eq}\| \end{bmatrix} P_{1,\epsilon} \begin{bmatrix} \|\dot{q}\| \\ \|q_{eq}\| \end{bmatrix} \quad (4.92)$$

$$L(\dot{q}, q_{eq}) \leq \begin{bmatrix} \|\dot{q}\| & \|q_{eq}\| \end{bmatrix} P_{2,\epsilon} \begin{bmatrix} \|\dot{q}\| \\ \|q_{eq}\| \end{bmatrix} \quad (4.93)$$

Taking the derivative of L yields

$$\dot{L} = \dot{q}^T M \ddot{q} + \frac{1}{2} \dot{q}^T \frac{d}{dt} M \dot{q} + q_{eq}^T D \dot{q}_{eq} + \epsilon q_{eq}^T D^T M \ddot{q} + \epsilon q_{eq}^T D^T \frac{d}{dt} M \dot{q} + \epsilon \dot{q}^T M D \dot{q}_{eq}$$

Substituting in the dynamics from Equation 4.72 gives

$$\begin{aligned} \dot{L} &= \dot{q}^T (-Dq - f(\dot{q}) - C(\dot{q}, q)\dot{q} + r(t)) + \frac{1}{2} \dot{q}^T \frac{d}{dt} M \dot{q} + q_{eq}^T D \dot{q}_{eq} \\ &+ \epsilon q_{eq}^T D^T (-Dq - f(\dot{q}) - C(\dot{q}, q)\dot{q} + r(t)) + \epsilon q_{eq}^T D^T \frac{d}{dt} M \dot{q} + \epsilon \dot{q}^T M D \dot{q}_{eq} \end{aligned}$$

Utilizing the definition of q_{eq} , the relations given in Equations 4.77 and 4.79 along with the fact that D is symmetric yields the following reduction.

$$\begin{aligned} \dot{L} &= \dot{q}^T (-Dq - f(\dot{q}) - C(\dot{q}, q)\dot{q} + r(t)) + \frac{1}{2} \dot{q}^T \frac{d}{dt} M \dot{q} + (q - D^{-1}r(t))^T D (\dot{q} - D^{-1}\dot{r}(t)) \\ &+ \epsilon q_{eq}^T D^T (-Dq - f(\dot{q}) - C(\dot{q}, q)\dot{q} + r(t)) + \epsilon q_{eq}^T D^T \frac{d}{dt} M \dot{q} + \epsilon \dot{q}^T M D (\dot{q} - D^{-1}\dot{r}(t)) \\ \dot{L} &= -\dot{q}^T f(\dot{q}) - \dot{r}(t)^T q + \dot{r}(t)^T D^{-1}r(t) + \epsilon [-q_{eq}^T D^T Dq - q_{eq}^T D^T f(\dot{q}) + q_{eq}^T D^T r(t)] \\ &+ \epsilon \dot{q}^T A(q_{eq})\dot{q} - \epsilon \dot{q}^T M \dot{r}(t) \\ \dot{L} &= -\dot{q}^T f(\dot{q}) - \epsilon q_{eq}^T D^T D q_{eq} - \epsilon q_{eq}^T D^T f(\dot{q}) + \epsilon \dot{q}^T A(q_{eq})\dot{q} - \dot{r}(t)^T q_{eq} - \epsilon \dot{q}^T M \dot{r}(t) \end{aligned}$$

Using the positive definite matrix

$$Q_\epsilon = \begin{bmatrix} b_1 - \epsilon a_1 & -\frac{1}{2}\epsilon b_2 \gamma_2 \\ -\frac{1}{2}\epsilon b_2 \gamma_2 & \epsilon \gamma_1^2 \end{bmatrix}$$

an upper bound can be placed on \dot{L} .

$$\frac{d}{dt} L \leq - \begin{bmatrix} \|\dot{q}\| & \|q_{eq}\| \end{bmatrix} Q_\epsilon \begin{bmatrix} \|\dot{q}\| \\ \|q_{eq}\| \end{bmatrix} + \|\dot{r}(t)\| \begin{bmatrix} \epsilon \mu_2 & 1 \end{bmatrix} \begin{bmatrix} \|\dot{q}\| \\ \|q_{eq}\| \end{bmatrix}$$

Utilizing the upper bound on L given in Equation 4.93 along with Lemma 1

$$\frac{d}{dt} L \leq -\lambda_{\min}(P_{2,\epsilon}^{-1} Q_\epsilon) L + \|\dot{r}(t)\| \begin{bmatrix} \epsilon \mu_2 & 1 \end{bmatrix} \begin{bmatrix} \|\dot{q}\| \\ \|q_{eq}\| \end{bmatrix}$$

The contribution from the rate of change of the disturbance is bounded using the fact that $\frac{d}{dt}L = 2\sqrt{L}\frac{d}{dt}\sqrt{L}$.

$$2\sqrt{L}\frac{d}{dt}\sqrt{L} \leq -\lambda_{\min}(P_{2,\epsilon}^{-1}Q_\epsilon)L + \|\dot{r}(t)\| \sqrt{\begin{bmatrix} \|\dot{q}\| & \|q_{eq}\| \end{bmatrix} F \begin{bmatrix} \|\dot{q}\| \\ \|q_{eq}\| \end{bmatrix}}$$

where,

$$F = \begin{bmatrix} \epsilon^2\mu_2^2 & \epsilon\mu_2 \\ \epsilon\mu_2 & 1 \end{bmatrix}$$

Finally, dividing through by $2\sqrt{L}$, using the lower bound on L given in Equation 4.92 and utilizing Lemma 1

$$\frac{d}{dt}\sqrt{L} \leq -\frac{\lambda_{\min}(P_{2,\epsilon}^{-1}Q_\epsilon)}{2}\sqrt{L} + \frac{U_{max}}{2}\sqrt{\lambda_{\max}(P_{1,\epsilon}^{-1}F)}$$

The solution for this first order differential equation is

$$\sqrt{L} \leq e^{-\sigma t}(\sqrt{L(\dot{q}(0), q_{eq}(0))} - \kappa U_{max}) + \kappa U_{max}$$

where $\sigma = \frac{\lambda_{\min}(P_{2,\epsilon}^{-1}Q_\epsilon)}{2}$ and $\kappa = \frac{\sqrt{\lambda_{\max}(P_{1,\epsilon}^{-1}F)}}{\sigma^2}$. Squaring the above result gives the exponential bound for L .

$$L \leq \left(e^{-\sigma t}(\sqrt{L(\dot{q}(0), q_{eq}(0))} - \kappa U_{max}) + \kappa U_{max} \right)^2$$

Finally, by using the relationships in Equation 4.85 and 4.86, a bound can be placed on the system energy.

$$E \leq \begin{bmatrix} \|\dot{q}\| & \|q_{eq}\| \end{bmatrix} P_{energy} \begin{bmatrix} \|\dot{q}\| \\ \|q_{eq}\| \end{bmatrix} \quad (4.94)$$

where,

$$P_{energy} = \begin{bmatrix} \frac{1}{2}\mu_2 & 0 \\ 0 & \frac{\gamma_2}{2} \end{bmatrix} \quad (4.95)$$

Using this along with the upper bound for L given in Equation 4.93 and Lemma 1

$$E \leq \eta L \leq \eta \left(e^{-\sigma t} (\sqrt{L(\dot{q}(0), q_{eq}(0))} - \kappa U_{max}) + \kappa U_{max} \right)^2 \quad (4.96)$$

where $\eta = \lambda_{max}(P_{2,\epsilon}^{-1} P_{energy})$

□

This proof is extremely powerful because it can be used for general nonlinear systems and gives an analytical form for the Lyapunov function that is related to the systems kinetic and potential energies. Using the change of variables for the system configuration provides tight bounds if the system disturbance is changing slowly relative to the dynamics. The next section uses this technique to bound the lateral position of the vehicle system with time-varying curvature disturbances, providing a safety guarantee for the lanekeeping system.

4.5 Application for Lanekeeping

Recall that the equations of motion for the lanekeeping system with road curvature disturbances are given by

$$M_2 \ddot{q}_2 - f_2(\dot{q}_2) + V_{2m} q_2 = B_d \bar{\rho} \quad (4.97)$$

The change of variables that accounts for the equilibrium configuration of this system is defined by q_{2eq} .

$$q_{2eq} = q_2 - V_{2m}^{-1} B_d \bar{\rho} \quad (4.98)$$

In order to use the bounding technique presented in the previous section, the bounds given in Equations 4.85 to 4.89 must be satisfied. The first two bounds are related to the maximum and minimum eigenvalues of the mass matrix, M_2 , and the potential matrix, V_{2m} . These eigenvalues are guaranteed to be positive because the

matrices are positive definite.

$$\lambda_{min}(M_2)\|\dot{q}_2\|^2 \leq \dot{q}_2^T M_2 \dot{q}_2 \leq \lambda_{max}(M_2)\|\dot{q}_2\|^2 \quad (4.99)$$

$$\lambda_{min}(V_{2m})\|q_{2eq}\|^2 \leq q_{2eq}^T V_{2m} q_{2eq} \leq \lambda_{max}(V_{2m})\|q_{2eq}\|^2 \quad (4.100)$$

The damping of the system, f_2 is given by

$$f_2(\dot{q}_2) = -\Phi \dot{q}_2 = - \begin{bmatrix} \frac{(C_f+C_r)}{U_x} & \frac{(aC_f-bC_r)}{U_x} \\ \frac{(aC_f-bC_r)}{U_x} & \frac{(a^2C_f+b^2C_r)}{U_x} \end{bmatrix} \dot{q}_2 \quad (4.101)$$

Bounds on the damping, related to the system velocity, can be found using the maximum and minimum eigenvalues of the damping matrix, Φ . Since the longitudinal velocity, U_x , is bounded the minimum and maximum eigenvalues of Φ are positive.

$$\lambda_{min}(\Phi)\|\dot{q}_2\|^2 \leq \dot{q}_2^T \Phi \dot{q}_2 \quad (4.102)$$

$$\lambda_{max}(\Phi)\|\dot{q}_2\| \geq \|\Phi \dot{q}_2\| \quad (4.103)$$

Finally, the last bound in Equation 4.89 requires a bound on the quadratic form $\dot{q}^T A(q_{eq}) \dot{q}$. For the vehicle system this is given by

$$\dot{q}_2^T M_2 V_{2m} \dot{q}_2 = \dot{q}_2^T \begin{bmatrix} 2c_1 m & \frac{1}{2}c_2(m + I_z) \\ \frac{1}{2}c_2(m + I_z) & 2c_3 I_z \end{bmatrix} \dot{q}_2 \quad (4.104)$$

where c_1 , c_2 , and c_3 are the terms appearing in the potential given in Equations 4.35 to 4.37. Using the above matrix for the product $M_2 V_{2m}$ the bound from Equation 4.89 can be satisfied as follows.

$$\lambda_{max}(M_2 V_{2m})\|\dot{q}_2\|^2 \geq \dot{q}_2^T M_2 V_{2m} \dot{q}_2 \quad (4.105)$$

The modified energy function used for bounding the vehicle's lateral motion is given by

$$L(\dot{q}_2, q_{2eq}) = \frac{\dot{q}_2^T M_2 \dot{q}_2}{2} + \frac{q_{2eq}^T V_{2m} q_{2eq}}{2} + \epsilon \dot{q}_2^T M_2 V_{2m} q_{2eq} \quad (4.106)$$

The proof from the previous section gives a range of ϵ values that can be used. In order to find the least conservative bound, an ϵ value within the allowable range is found that minimizes the product $\eta\kappa^2$. This value determines the magnitude of the exponential bound as time gets large.

Proposition 4.4.1 gives a bound for the entire energy of the system. As in the previous bounding case with no disturbances (Section 4), the worst case lateral position is achieved when all the energy is transferred into the potential. Using the conditions for the maximum lateral error in Equation 4.60

$$e_{eq}^2 \left(c_1 - \frac{c_2^2}{4c_3} \right) \leq E(t) \leq \eta \left(e^{-\sigma t} (\sqrt{L(0)} - \kappa U_{max}) + \kappa U_{max} \right)^2 \quad (4.107)$$

To determine a bound on the actual lateral error instead of the transformed variable, a substitution is made using the change of variables given in Equation 4.98. Since

$$q_{2eq} = q_2 - V_{2m}^{-1} B_d \bar{\rho} \quad (4.108)$$

the relationship for the lateral error is given by

$$e_{eq} = e - (V_{2m}^{-1} B_d)_{1x2} \bar{\rho} \quad (4.109)$$

where $(V_{2m}^{-1} B_d)_{1x2}$ denotes the first row of the matrix $V_{2m}^{-1} B_d$. Bounding the lateral error requires a bound on the disturbance term $(V_{2m}^{-1} B_d)_{1x2} \bar{\rho}$ to guarantee that the sign of this term does not flip the inequality in the bound. This is accomplished using the Cauchy-Schwarz inequality.

$$e(t) \leq \frac{1}{\sqrt{\left(c_1 - \frac{c_2^2}{4c_3} \right)}} \sqrt{E_{bound}} + \|(V_{2m}^{-1} B_d)_{1x2}\| \|\bar{\rho}(t)\| \quad (4.110)$$

where E_{bound} is the exponential bound on the energy. If the road disturbance profile is not known for all time, the norm can simply be bounded by the maximum norm that is encountered (i.e. $\sup \|\bar{\rho}(t)\| \leq R_{max}$).

This bound is remarkably powerful because it can handle general time-varying disturbance and only requires knowledge of the maximum value of the disturbance

m (kg)	1450		
I_z (N/m ²)	2500		
C_f (N/rad)	110000		
C_r (N/rad)	100000		
a (m)	1.3		
b (m)	1.3		
		k	5000
		x_{cf} (m)	1.3
		x_{la} (m)	21

Table 4.2: Vehicle and Controller Parameters for Simulation 2

and the disturbance frequency. For road curvature disturbances these are easily determined and the resulting bound produces excellent results for typical curvature profiles.

4.5.1 Simulation with Lateral Bounds

A simulation example illustrates this bounding technique for the lanekeeping system subjected to time-varying road curvature disturbances. The simulation uses the lateral and heading error dynamics presented in Equations 4.68 and 4.69 and assumes a constant longitudinal velocity of $U_x = 30m/s$, representing a typical freeway speed. The parameters used for this simulation are given in Table 4.2 and represent our test vehicle, a 1997 Chevrolet Corvette.

The bounds required on the system energy, the damping, and the quadratic form involving $A(q_{eq})$ are calculated as described in the previous section. The ϵ value is chosen to give the least conservative bound on the lateral position of the vehicle. Proposition 4.4.1 gives a range of allowable ϵ values. This space is searched to find the value that minimizes $\eta\kappa^2$. Figure 4.8 shows the value of $\sqrt{\eta\kappa^2}$ compared with a range of ϵ values for the parameters used in this simulation. The circle shows that $\eta\kappa^2$ is minimized with an ϵ value of around 1.58×10^{-5} .

The road profile for the simulation consists of straight sections and one constant radius turn with a radius of $500m$ (Figure 4.9). The transitions between the straight sections and the curve are accomplished using cubic polynomials. The curvature profile is shown in Figure 4.10. The bound developed in Proposition 4.4.1 can be used in a number of ways for a time-varying road disturbance. One approach is to bound

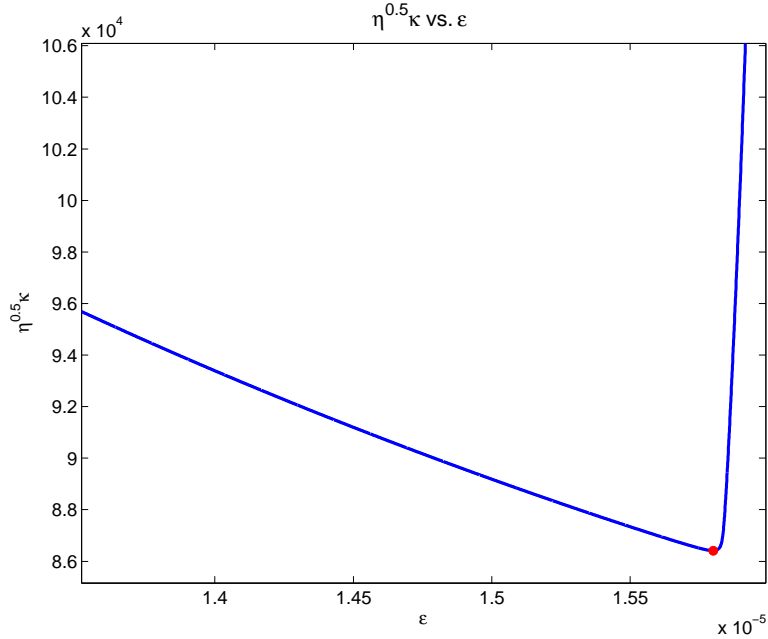


Figure 4.8: Optimal ϵ

the entire section of road using the worst case disturbance. This is a good technique if the designer does not know the entire road profile in time. However, this technique will obviously lead to some conservatism, especially when the road disturbance is not near the maximum disturbance used in the bound. For the simulation case, the bound is split into segments based on the road profile. There is a bound for the initial and final straight sections, the transition sections (where the road curvature is changing in time), and the constant curvature section. The bounding technique developed in Proposition 4.4.1 requires a bound on the time rate of change of the disturbance. For each section, the bound used on the disturbance derivative is

$$\begin{aligned}
 \text{Straight Sections:} & \quad \|\dot{\tilde{\rho}}(t)\| = 0 \\
 \text{Constant Radius Turn:} & \quad \|\dot{\tilde{\rho}}(t)\| = 0 \\
 \text{Transition Sections:} & \quad \|\dot{\tilde{\rho}}(t)\| \leq U_{max} = 7.7 \times 10^{-4}
 \end{aligned}$$

Figure 4.11 shows the lateral error of the vehicle with no driver input. As expected, the vehicle drifts to the outside of the turn and moves back to the center of the lane in

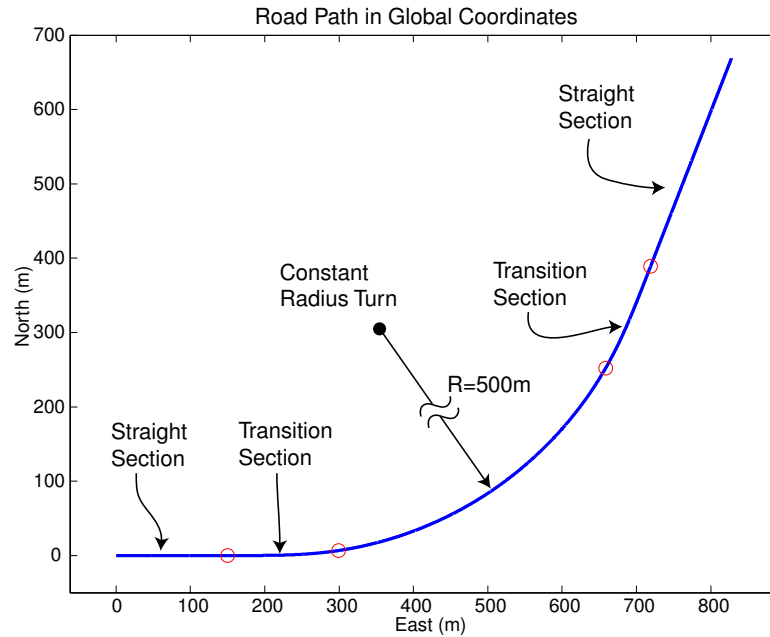


Figure 4.9: Road Profile

the straight sections. The unshaded region depicts the reachable set for the vehicle's lateral position. During the straight segments and the constant radius portion of the road, the exponential bound approaches the actual lateral error of the vehicle. In these time invariant sections, the vehicle achieves a steady state configuration determined by the conservative force and the magnitude of the road curvature (recall the spring analogy in Figure 4.6). The change of variables used in the bound accounts for this steady state configuration, which results in a tight steady state bound (i.e. the value the bound attains as $t \rightarrow \infty$).

As expected, the bound becomes slightly more conservative during the transition sections when the curvature disturbance is changing in time. The bounds, however, are not extremely conservative because the curvature disturbance is changing slowly relative to the system dynamics. Therefore, during the transitions the vehicle is always close to the transformed configuration (q_{2eq}), which accounts for the equilibrium position the vehicle would attain if the disturbance were constant. This bounding technique provides fairly tight bounds for time-varying disturbances that are realistic for scaling the potential function for lanekeeping (i.e. the bounds are within a lane

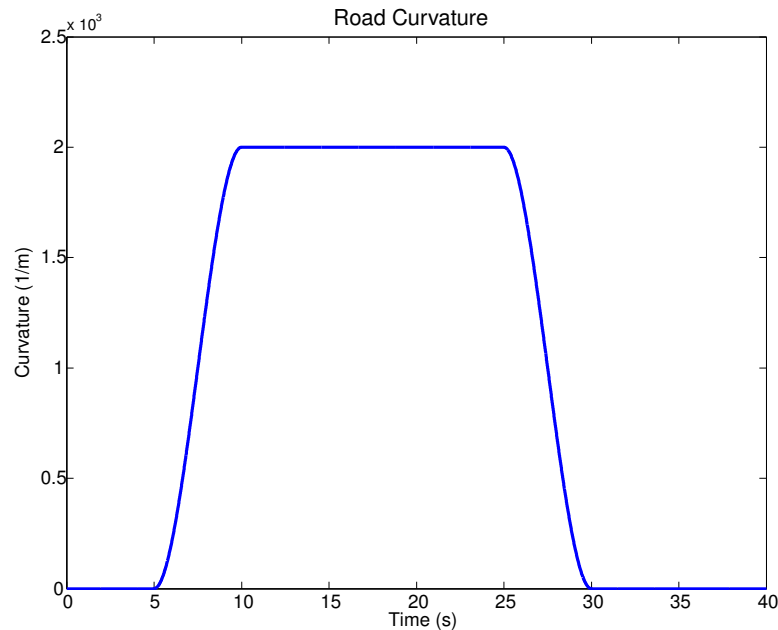


Figure 4.10: Road Curvature

width). These bounds also provide a mathematical way of guaranteeing the nominal safety of the lanekeeping system.

4.6 Concluding Remarks

This chapter presented a method of incorporating the design rules for obtaining stable, well-behaved lanekeeping performance to form a passive system using only the lateral and heading error dynamics. Using Lyapunov theory the sum of a new potential energy-like term and the kinetic energy (in the lateral and rotational directions of interest) is dissipative. Creating a bounding function that does not include the large amount of kinetic energy in the longitudinal direction provides excellent bounds for the lateral position of the vehicle.

The potential field framework passively couples the vehicle to the road and disturbances such as road curvature add energy to the system. Utilizing the slow-varying nature of certain disturbances along with the structure of Lagrangian systems provides an exponential bound on the system energy. This is a novel approach for obtaining

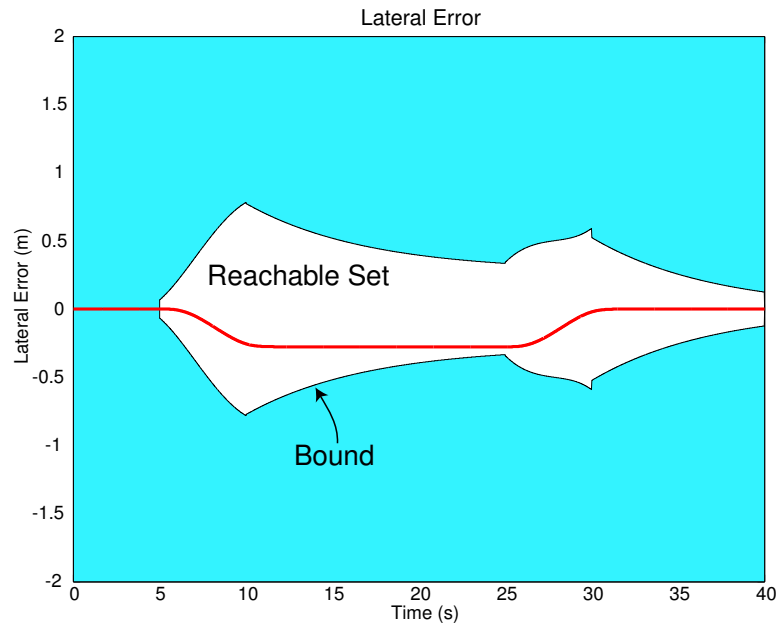


Figure 4.11: Lateral Error with Bounds

non-conservative bounds for any disturbance that changes slowly relative to the system dynamics. Although previous work has utilized a change of variables to account for analyzing slow-varying inputs, the Lagrangian approach provides an analytical structure for the Lyapunov function and the resulting bound. This technique is also remarkably general and can be used for any dynamic system that can be expressed in a Lagrangian framework.

The tools presented in this chapter are extremely powerful, providing a safety guarantee for the lanekeeping system. With knowledge of the maximum frequency of the road curvature disturbance, gains can be chosen to guarantee the lanekeeping ability of the system while not being overly conservative (as in the case of using the vehicle's total energy). For lanekeeping assistance this is paramount because the potential field can be scaled to keep the vehicle in the lane while not being overly intrusive during normal driving. The following chapter presents the experimental testbed and results for the potential field lanekeeping system.

Chapter 5

Implementation of the Lanekeeping System

In theory, the potential field framework provides a nominally safe lanekeeping system that smoothly combines the commands from the potential field controller and the driver. One big question still remains: Will this framework work in a real vehicle? The experimental results presented in this chapter verify that the system performance is closely matched by simulation predictions and the vehicle stays within the theoretical bounds presented in the last chapter.

This chapter discusses the potential field control algorithm used in the tests, controller implementation on the steer-by-wire Corvette test bed (Figure 5.2), and experimental results. The results show that the vehicle remains in the lane without driver inputs. The experimental data matches simulation results remarkably well, giving confidence in both the vehicle model and the theoretical bounding results. The bounds on the lateral motion of the vehicle are relatively tight and provide a realistic safety guarantee for the lanekeeping performance of the system.

5.1 Potential Field Control with Front Steering

The lanekeeping potential used for the testing is a simple quadratic function. As discussed in previous chapters, the potential function value is based on a projected

lateral offset, e_{la} .

$$V_c(e_{la}) = k(e_{la})^2 = k(e + (x_{cf} + x_{la}) \sin \psi)^2 \quad (5.1)$$

where x_{la} is the projected distance in front of the vehicle's front axle, x_{cf} is the control force location (which is at the front axle for this test vehicle), and k is the potential field gain.

The original controller development in Chapter 2 assumed a fully by-wire vehicle with differential braking capability. Since only the steering can be controlled in the test vehicle, the driver controls the longitudinal forces using the accelerator and brake pedals as in a conventional vehicle. With the quadratic potential function described in Equation 5.1 the overall control vector, $g(u_c)$, is composed of driver controlled terms and control terms related to the potential function. Assuming small angle approximations for the front steering angle and front slip angle yields

$$g(u_c) = g(u_{driver}) + g(u_{pf}) = \begin{bmatrix} F_{xr} + F_{xf} \\ C_f \delta_{driver} \\ a C_f \delta_{driver} \end{bmatrix} - \begin{bmatrix} 0 \\ \frac{\partial V_c}{\partial e} \cos \psi \\ a \frac{\partial V_c}{\partial e} \cos \psi \end{bmatrix} \quad (5.2)$$

The desired wheel angle is accomplished through the steer-by-wire system which must combine the driver's desired steering angle, δ_{driver} , along with the additional steering angle related to the potential field. The total commanded steering angle is given by

$$\delta = \delta_{driver} - \frac{1}{C_f} \frac{\partial V_c}{\partial e} \cos \psi \quad (5.3)$$

This steering angle, δ , is produced by the steer-by-wire controller described by Yih et al. [69]. All of the analysis presented in Chapter 4 is used to guarantee the lanekeeping ability of the system. Once you have a potential function, however, the controller implementation is extremely simple.

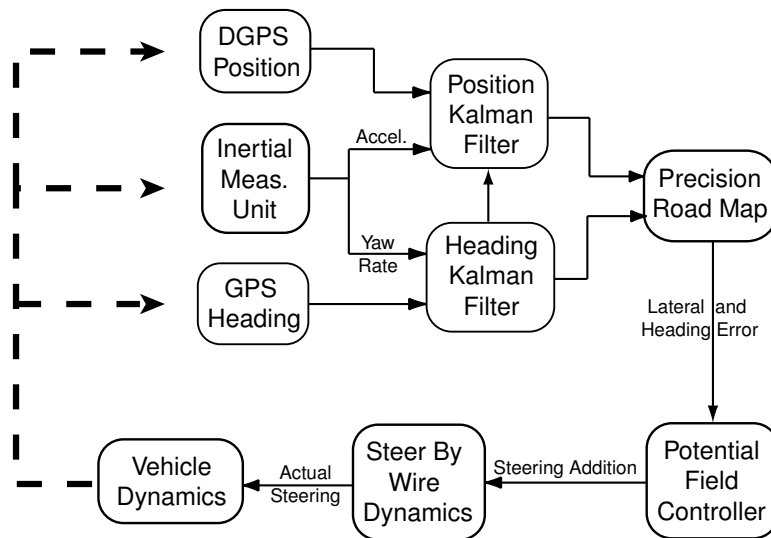


Figure 5.1: Control Structure for Vehicle Lanekeeping

5.2 Control System Structure

As shown in Equations 5.1-5.3, the potential field controller requires an accurate estimation of the vehicle's position and heading relative to lane center. Although there are other methods to obtain this information (i.e. vision, magnetometers, etc.) our control strategy uses a unique combination of Global Positioning System (GPS) data and precision digital maps. The control structure used is shown in Figure 5.1. Sensors include differential GPS (DGPS) for position and a two-antenna GPS unit for heading. These measurements are accurate but have a slow update rate, so they are combined with accelerations and yaw rate from Inertial Navigation System (INS) sensors to obtain an accurate estimate of the vehicle states between GPS updates. A Kalman filter combines the two sources of measurement to estimate and remove bias from the inertial measurement sensor data. The Kalman filters output the vehicle's position and heading which are compared to a precision map of the road to determine the error in lateral position and heading. These errors are used by the potential field controller to calculate a steering angle (Equation 5.3), which is produced by the experimental steer-by-wire system.



Figure 5.2: Steer-by-Wire Corvette

5.3 Sensing and Actuation

5.3.1 Position and Attitude Sensing

The test vehicle uses GPS to determine position and heading. GPS receivers are becoming more common on production vehicles and current applications focus on positioning information for navigation or as a locator for fast emergency response. Utilizing differential corrections and accurate maps, GPS can be combined with other sensors for lanekeeping applications. DGPS systems rely on a stationary reference receiver to cancel out most of the atmospheric error associated with ordinary GPS. The reference receiver uses its known position to calculate timing corrections to the satellite signals being received by the vehicle's GPS system. The use of DGPS as a sensing system for autonomous vehicle control has been demonstrated by several groups. In 1992, Crow and Manning [11] used DGPS for low speed autonomous vehicle control. DGPS based systems were also developed and tested by Farrell and Barth [13], Omae and Fujioka [43] as well as Schiller et al. [58]. A novel multi-antenna system for attitude was combined with DGPS for low speed autonomous control of a farm tractor by Rekow et al. [50]. Our work combines a multi-antenna system with accurate DGPS to give independent measurements of position and heading. The heading measurement from this setup is not corrupted by vehicle sideslip (the

angle between the vehicle's velocity vector and its longitudinal axis), which allows the estimation problem to be separated into two regular Kalman filters (described in Section 5.4) as opposed to using an extended Kalman filter.

For our experimental system, a carrier phase Differential Global Positioning System (DGPS) provides accurate global position information at an update rate of 10Hz. A wireless serial link sends the differential corrections from the reference receiver to the vehicle receiver, once per second. With this setup, the position is accurate to a circular error precision (CEP) of 1cm. Two Novatel OEM4 GPS receiver are used: one for the reference station and one on the vehicle. The Novatel Pinwheel antenna is also used on both ends to ensure proper phasing of both GPS frequencies.

A Novatel Beeline two-antenna system is used to provide absolute vehicle heading. The system uses the difference in the relative phasing of signals between each antenna and the satellites to determine the angle of the antenna array relative to an earth fixed frame. With a 2m baseline between the two antennae, the accuracy is 0.2° with an update rate of 5Hz.

Two Bosch automotive grade INS units are used to measure lateral and longitudinal acceleration and yaw rate. Each of these units consists of an accelerometer and an angular rate gyro, with a guaranteed bandwidth of 30Hz. The signals from these inertial sensors are corrupted by bias and drift, but these errors are estimated and removed by combining these sensors with GPS (sec. 5.4).

5.3.2 Steer-by-wire

The term 'steer-by-wire' refers to a steering system where the actuation of the front wheels is accomplished electronically and is mechanically decoupled from the driver's steering input. Steer-by-wire systems open many new horizons for automotive control including improved stability control, active handling modification, collision avoidance, and lanekeeping. Automotive manufacturers are currently developing robust steer-by-wire systems, which are not currently available on production vehicles (eg. [6], [12], [30]).

For experimental implementation of the lanekeeping system, our lab has converted

a 1997 Corvette C5 to a steer-by-wire setup [69]. This system uses a brushless DC motor to drive the input shaft of the power steering unit. The maximum steering speed is approximately 39 degrees/sec at the road wheels with a bandwidth of about 2Hz. The steering inputs needed for lanekeeping are a function of the shape of the road. For highway road profiles, the required steering angles are less than a few degrees and the road variations are much less than 2Hz. Therefore, the steering dynamics do not significantly influence the performance of the lanekeeping system.

5.3.3 Computing

The lanekeeping controller and the steer-by-wire system are run on a Versallogic Single Board Computer (VSBC8). This machine uses an 850MHz Pentium 3 processor and has 128MB Ram, which is used for both the operating system and the data collection. The control is developed in Matlab's Simulink environment and is compiled to run on the xPC operating system. xPC is a realtime operating system with a user configurable sampling rate. The entire control loop shown in Figure 5.1 is closed at 100Hz.

5.4 Kalman Filters

5.4.1 Overview

As shown in Figure 5.1, the control structure uses two Kalman filters to integrate INS sensors with GPS information for high update heading and position values. Typical GPS updates are around 10Hz compared to the sampling rate of 100Hz used to read the analog output of the inertial sensors. With differential corrections, GPS provides accurate position information that is not corrupted by the same bias and scale factor errors common in inertial sensors. Although corrupted by these terms, inertial sensors provide a much higher update rate more suitable for control. Combining these sensors together provides an estimate of the inertial sensor biases and then uses information from these sensors to fill in the gaps between GPS updates.

Because the filters used are purely kinematic, they do not rely on any vehicle model that might contain inaccuracy. The “model” used simply captures the relationships between acceleration, yaw rate and position for a rigid body, which only depends on the geometry of the measurement setup. This can be measured very accurately and does not change during operation. The GPS heading system allows the estimation problem to be separated into two Kalman filters instead of one extended Kalman filter. The traditional Kalman filter is comprised of a measurement update and a time update [63]. Since the GPS measurements come in at a lower rate, the measurement update is only performed when GPS is available to estimate the sensor bias and zero out the state estimate error. The measurement update is described by:

$$x_+(t) = x_-(t) + K[y(t) - Cx_-(t)] \tag{5.4}$$

$$K = P_-(t)C^T[CP_-(t)C^T + R]^{-1} \tag{5.5}$$

$$P_+(t) = [I - KC]P_-(t) \tag{5.6}$$

where:

$x_-(t)$ = prior estimate of the system state at time t

$x_+(t)$ = updated estimate of the system state at time t

$P_-(t)$ = prior error covariance matrix at time t

$P_+(t)$ = updated error covariance matrix at time t

K = Kalman gain

$y(t)$ = new measurement

C = observation matrix

R = measurement noise covariance

x represents the vehicle states of interest and y represents the measurements. Simple Euler integration of the inertial sensors is performed during the time update as

described below.

$$x_-(t + 1) = x_+(t) + \Delta t \dot{x}_+(t) \tag{5.7}$$

$$P_-(t + 1) = A_d P_+(t) A_d^T + Q \tag{5.8}$$

where A_d represents the discretized dynamics and Q is the process noise covariance. This is the Kalman filter structure used to estimate the vehicle position and heading for implementation of the potential field controller.

The GPS data used to calculate the heading and position information has an inherent latency due to computation and data transfer delays. Therefore, the time tags in the GPS measurement and the synchronizing pulse per second (PPS) from the receiver are used to align the GPS information with the inertial sensor measurements. Upon a GPS measurement, the time tags are used to calculate the time to which the GPS measurement corresponds. The integrated inertial value at the identified time and the GPS value are used for the measurement update. From this measurement update, the accelerometer measurements are then used to integrate forward in time until the next GPS update becomes available. This synchronizing process is extremely important when trying to get real-time estimates of the vehicle states [55].

5.4.2 Heading

For the heading Kalman filter, a linear dynamic system is constructed using the gyro's yaw rate as an input and the heading from a two-antenna GPS system for the measurement update.

$$\begin{bmatrix} \dot{\psi} \\ \dot{r}_{bias} \end{bmatrix} = \begin{bmatrix} 0 & -1 \\ 0 & 0 \end{bmatrix} \begin{bmatrix} \psi \\ r_{bias} \end{bmatrix} + \begin{bmatrix} 1 \\ 0 \end{bmatrix} r_m + \text{noise} \tag{5.9}$$

$$\psi_m^{GPS} = \begin{bmatrix} 1 & 0 \end{bmatrix} \begin{bmatrix} \psi \\ r_{bias} \end{bmatrix} + \text{noise} \tag{5.10}$$

where ψ is the heading, r_m is the measured yaw rate, r_{bias} is the yaw rate sensor bias, and ψ_m^{GPS} is the GPS heading from the two-antenna GPS system. A portion of the process noise covariance matrix is based on the covariance of the gyro (determined

using static data) while the remaining part is chosen to give an appropriate filter response. The measurement noise covariance is based on the standard deviation given in the GPS data sheet. The process and measurement noise covariances used in the Kalman filter are

$$Q_{heading} = \begin{bmatrix} 0.0286 & 0.0 \\ 0.0 & 0.01 \end{bmatrix} \tag{5.11}$$

$$R_{heading} = 0.2 \tag{5.12}$$

Figure 5.3 shows the raw (unsynchronized in time) GPS measurement from the Beeline system along with the Kalman filter output. At the macro scale the two are indistinguishable. The bottom plot shows a zoomed in section of the heading. The Kalman filter output leads the GPS output as expected because of the latency in the GPS signal discussed earlier. The filter gives smooth heading information between GPS updates, ideal for high speed vehicle control.

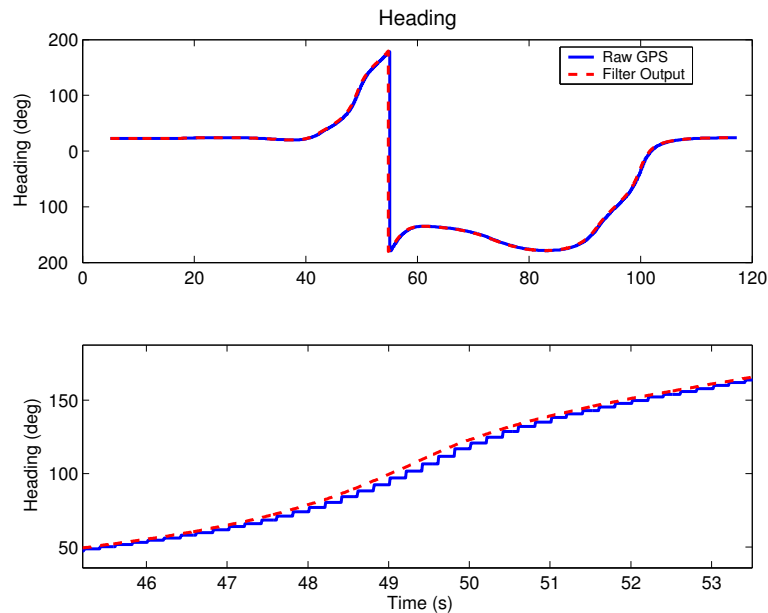


Figure 5.3: Heading: GPS and Kalman filter Output

5.4.3 Position

The position Kalman filter uses lateral and longitudinal accelerations along with DGPS position information to obtain a high update global position of the vehicle. For this Kalman filter the linear dynamic system uses the vehicle's lateral and longitudinal accelerations as inputs and the DGPS east and north positions for the measurement update. The heading output of the first filter is used to transform the accelerations from body fixed to global coordinates.

$$\begin{bmatrix} \dot{P}_N \\ \ddot{P}_N \\ \dot{a}_{xbias} \\ \dot{P}_E \\ \ddot{P}_E \\ \dot{a}_{ybias} \end{bmatrix} = A \begin{bmatrix} P_N \\ \dot{P}_N \\ a_{xbias} \\ P_E \\ \dot{P}_E \\ a_{ybias} \end{bmatrix} + B \begin{bmatrix} a_{xm} \\ a_{ym} \end{bmatrix} + \text{noise} \quad (5.13)$$

where P_N and P_E are the north and east position of the vehicle, respectively, a_{xbias} is the longitudinal accelerometer bias, a_{ybias} is the lateral accelerometer bias, a_{xm} is the measured longitudinal acceleration, and a_{ym} is the measured lateral acceleration. The matrices A and B are

$$A = \begin{bmatrix} 0 & 1 & 0 & 0 & 0 & 0 \\ 0 & 0 & -\cos\psi & 0 & 0 & \sin\psi \\ 0 & 0 & 0 & 0 & 0 & 0 \\ 0 & 0 & 0 & 0 & 1 & 0 \\ 0 & 0 & \sin\psi & 0 & 0 & \cos\psi \\ 0 & 0 & 0 & 0 & 0 & 0 \end{bmatrix} \quad (5.14)$$

$$B = \begin{bmatrix} 0 & 0 \\ \cos\psi & -\sin\psi \\ 0 & 0 \\ 0 & 0 \\ -\sin\psi & -\cos\psi \\ 0 & 0 \end{bmatrix} \quad (5.15)$$

with the heading, ψ , coming from the heading Kalman filter. The measurement update equation is

$$\begin{bmatrix} P_N^{GPS} \\ P_E^{GPS} \end{bmatrix} = \begin{bmatrix} 1 & 0 & 0 & 0 & 0 & 0 \\ 0 & 0 & 0 & 1 & 0 & 0 \end{bmatrix} \begin{bmatrix} P_N \\ \dot{P}_N \\ a_{xbias} \\ P_E \\ \dot{P}_E \\ a_{ybias} \end{bmatrix} + \text{noise} \quad (5.16)$$

where P_N^{GPS} and P_E^{GPS} are the north and east position measurements from DGPS. The process and measurement noise covariances are determined in a similar fashion to the heading filter and are given by

$$Q_{position} = \begin{bmatrix} 1e^{-6} & 0 & 0 & 0 & 0 & 0 \\ 0 & 1e^{-3} & 0 & 0 & 0 & 0 \\ 0 & 0 & 1e^{-6} & 0 & 0 & 0 \\ 0 & 0 & 0 & 1e^{-6} & 0 & 0 \\ 0 & 0 & 0 & 0 & 1e^{-3} & 0 \\ 0 & 0 & 0 & 0 & 0 & 1e^{-6} \end{bmatrix} \quad (5.17)$$

$$R_{position} = \begin{bmatrix} 1e^{-4} & 0 \\ 0 & 1e^{-4} \end{bmatrix} \quad (5.18)$$

Figure 5.4 and 5.5 compare the east and north position from DGPS measurements with the Kalman filter output. Similar to the heading case the Kalman filter data

fills in the gaps between the DGPS measurements providing a smooth, clean signal.

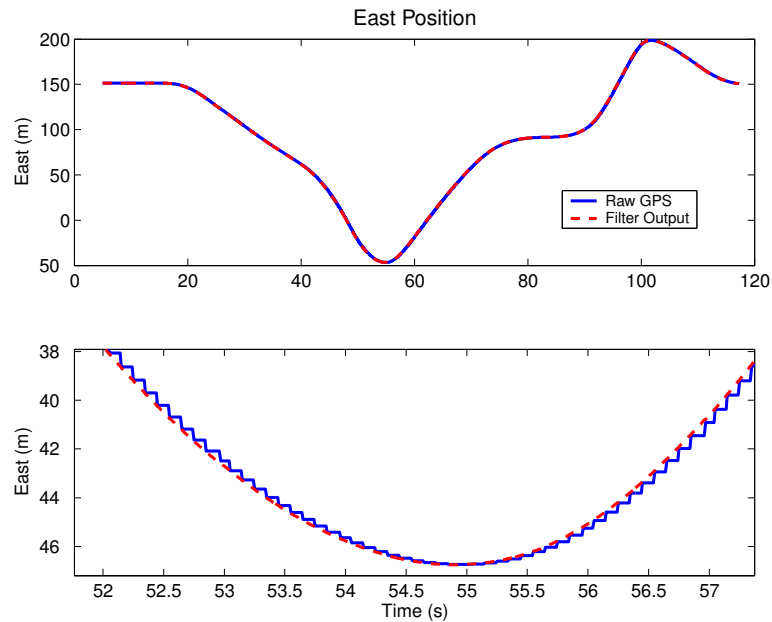


Figure 5.4: East Position: Raw GPS and Kalman Filter Output

The Kalman filter approach to GPS/INS integration proposed here is novel in that the output of the heading filter is used by the position filter. Using a GPS heading system allows this decoupling of the heading and position Kalman filters. This is not an extended Kalman filter, it is instead a combination of two ordinary Kalman filters and thus does not require linearization. With this structure the tuning of the filters can also be performed independently.

5.5 Precision Maps

The combination of GPS and INS provides an accurate and high bandwidth measurement of global position and attitude. Lanekeeping assistance requires knowledge of the vehicle's deviation from the lane center. Using a digital road map, the vehicle's current position is used to calculate the lateral and heading error of the vehicle. Road maps are already available for virtually every road in the United States, but not with sufficient accuracy for lanekeeping. High precision maps will soon be available from

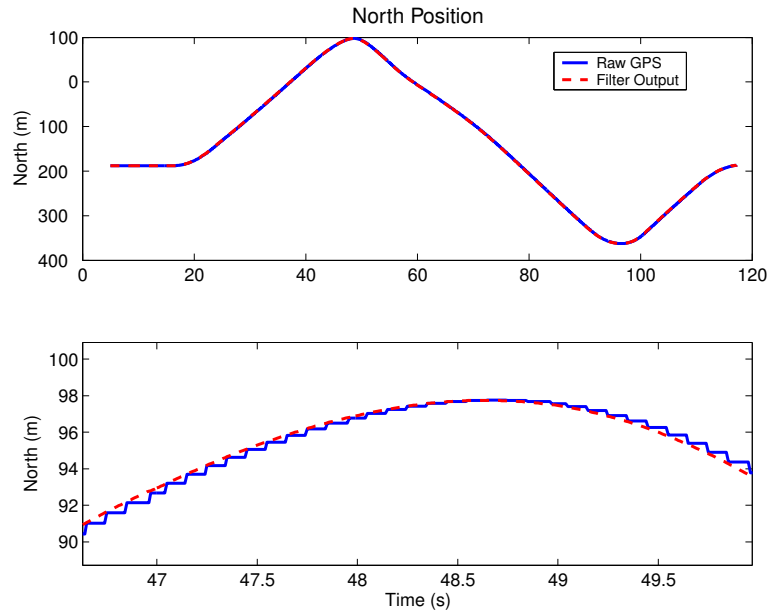


Figure 5.5: North Position: Raw GPS and Kalman Filter Output

commercial firms with the necessary accuracy for lanekeeping. Research is underway both in academia and industry on automated ways to generate high precision road maps. One approach by Rogers et al. [51] based on averaging the trajectories of many vehicles over the same stretch of road to create digital maps. For the purposes of experimental validation of this lanekeeping system, maps are created manually for the specific test area needed.

The map making process consists of driving the road loop at constant speed and recording position measurements from DGPS. A smooth map is generated from this data using constrained least squares. This map consists of a predetermined number of segments, each of which is a parametric polynomial function of a distance parameter, σ [59]. Figure 5.6 shows the map used for the experimental testing at Moffett Federal Airfield. This mapping technique was developed by Switkes [54] and more details are shown in Appendix C.

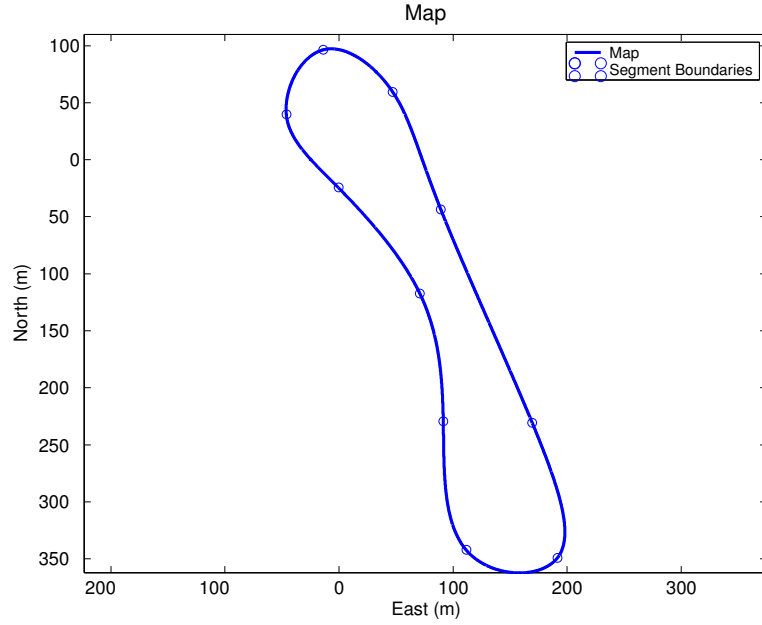


Figure 5.6: Moffett Map with Segment Boundaries

5.5.1 Error Finding

For lanekeeping, it is necessary to determine the lateral and heading deviation from the road map in real-time. The digital map gives the east and north position of the desired trajectory for some distance along the given map segment, σ , while the vehicle's east and north position is obtained from the Kalman filter output discussed in Section 5.4. Assuming that the radius of curvature for each segment is large compared to the lateral deviation of the vehicle (as it is for highway lanekeeping), the shortest distance from the vehicle to the path is perpendicular with the path tangent. This is found when the dot product between the vehicle's position relative to the map and the slope of the map is zero (Figure 5.7).

$$((X(\sigma) - P_E^{GPS}), (Y(\sigma) - P_N^{GPS})) \bullet (\dot{X}(\sigma), \dot{Y}(\sigma)) = 0 \quad (5.19)$$

If the polynomial used for the map segment is of order, n , this dot product polynomial is order $2n - 1$ and can be solved for the distance down the segment, σ_{veh} , which

corresponds to the point on the segment closest to the vehicle. Once σ_{veh} is found, it is used to find the distance between the vehicle and the point on the path identified by σ_{veh} . Similarly, the heading error between the vehicle and the path is found by comparing the heading from the Kalman filter output with the slope of the path at the point σ_{veh} . Since the point when the vehicle switches segments is unknown, the error finding algorithm assumes that the car is always moving forward and checks the segment from the previous solution along with the upcoming segment when solving for the lateral and heading errors.

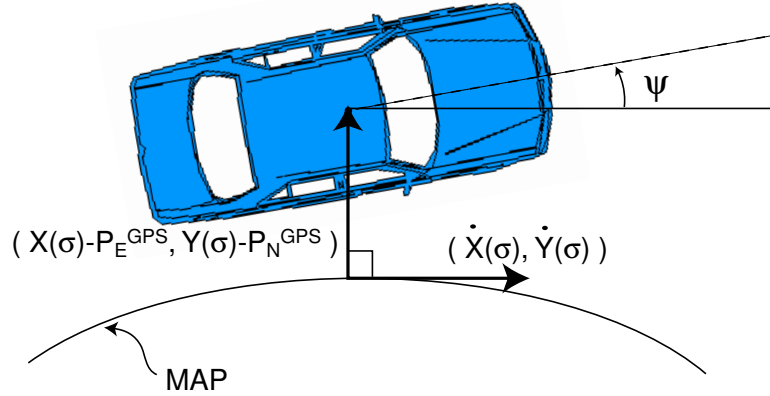


Figure 5.7: Error Finding

5.6 Results and Simulation

5.6.1 Test Setup

Experimental testing of the lanekeeping system was conducted on the West Ramp and West Parallel of Moffett Federal Airfield. Figure 5.8 shows the test vehicle at the Moffett Field test site. The map used for the experimental tests is given in Figure 5.6 along with the segment boundaries. Using this map and the bounding results from Chapter 4, the potential field gain is chosen so that the vehicle stays within a lane at a speed of $12m/s$ ($25mph$). The pertinent vehicle, map, and controller parameters are given in Tables 5.1 and 5.2.



Figure 5.8: Corvette Test Vehicle at Moffett Field

For the purposes of implementing the system, an accurate determination of the front cornering stiffness, C_f , is needed to calculate the steering angle necessary for a given potential field control force, as described in Equation 5.3. To compare experimental results to simulation, all the parameters in the equations of motion (Equation 2.17) are needed. Some of these can be directly measured, such as mass and distance from the center of gravity to each axle, while the cornering stiffnesses are estimated as in [55]. The yaw moment of inertia, I_z , is estimated to be the mass times the product of the distances from the CG to the front and rear axle [19].

5.6.2 Lanekeeping Performance

Figure 5.9 shows the lateral error at the GPS antenna location (Table 5.2) of the vehicle for one loop around the map with no driver steering input. This is compared with a simulation using the simple vehicle model and the Corvette parameters from Table 5.2. The match between the two is quite remarkable with a peak difference of around 10cm but much smaller errors for most of the run, as shown in Figure 5.10. The close match to simulation is impressive considering the simple model used as well as the absence of noise and steering dynamics in the simulation. The simulation does not take into account the surface of the testing area, which contains numerous

Antenna Location Behind C.G. (m)	0.7
m (kg)	1450
I_z (N/m ²)	2500
C_f (N/rad)	110000
C_r (N/rad)	100000
a (m)	1.3
b (m)	1.3
ρ_{max} (1/m)	$\frac{1}{25}$
$\dot{\rho}_{max}$ (1/ms)	0.01
$\ddot{\rho}_{max}$ (1/ms ²)	0

Table 5.1: Test Vehicle and Road Parameters

	Figure 5.9	Figure 5.11
P.F. gain k	15000	10000
x_{la} (m)	7	10.5

Table 5.2: Controller Parameters for Moffett Field Testing

pavement seams and rectangular holes for aircraft tie-downs.

From the highway design manual published by the California Department of Transportation [42], a standard freeway lane is 3.6m, leaving 0.85m on each side of the 1.9m wide Chevrolet Corvette. The experimental results verify that the vehicle remains in the lane without driver steering commands, achieving a maximum lateral error of around 0.6m. The repeatability of the vehicle motion during cornering is significant because it creates a response that is easily predicted by the driver. There are no unexpected motions that might force the driver to make unnatural steering commands to remain on the path (i.e. the driver steering the wrong direction around a corner).

The simple simulation’s close match to the experimental results gives great confidence in the bounds obtained in the previous chapter. Figure 5.9 shows the lateral error from the experiment and simulation along with the bounds used for the potential field design. The unshaded region defines the reachable set for the vehicle’s lateral position, which represents the maximum excursion from lane center at a speed

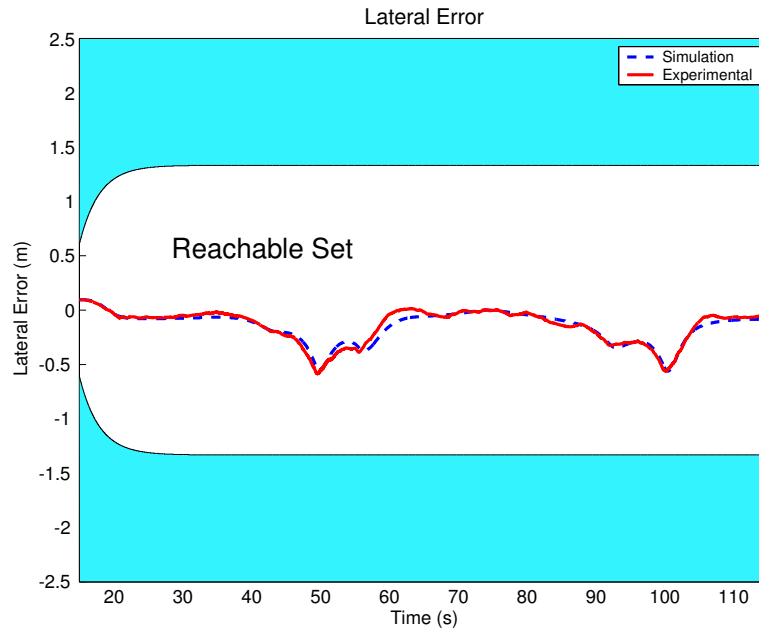


Figure 5.9: Lateral Error: Simulation vs. Experiment with $k=15000$

of $12m/s$ on this map. The bound is slightly conservative because it is based on the maximum geometric characteristics of the map, however it still provides a useful method to choose the gain of the potential field.

Figure 5.11 shows the lateral error for a two-lap test run with a lower potential field gain. As expected the vehicle drifts further into the potential around each turn. The mathematical bound on the vehicle's motion also extends further as a result of the lower gain. This demonstrates how the potential field gain can be chosen to bound the motion of the vehicle within a lane. Again the simulation matches the experiment quite closely. This bounding technique is a powerful tool, providing a quantitative safety guarantee for the potential field lanekeeping system.

5.7 Concluding Remarks

This chapter presented experimental results for the potential field assistance system. The system performed extremely well and almost exactly as predicted by simulation.

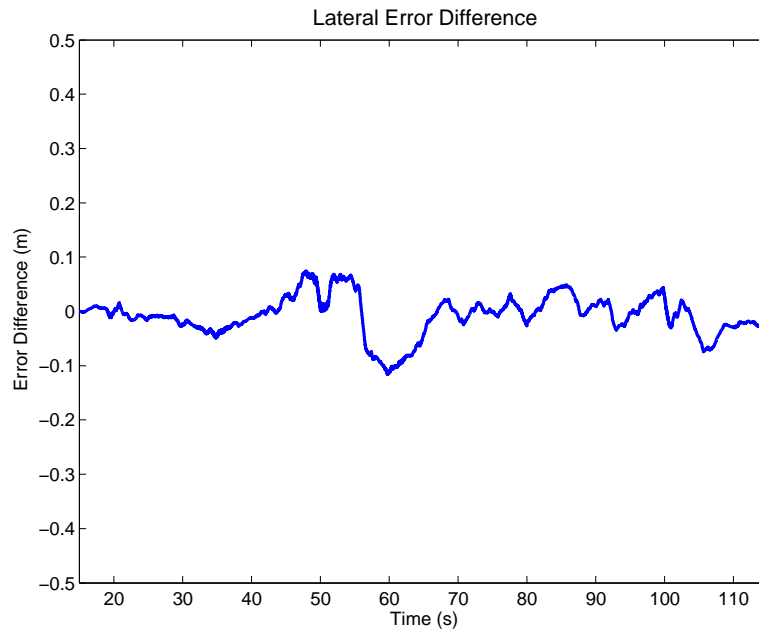
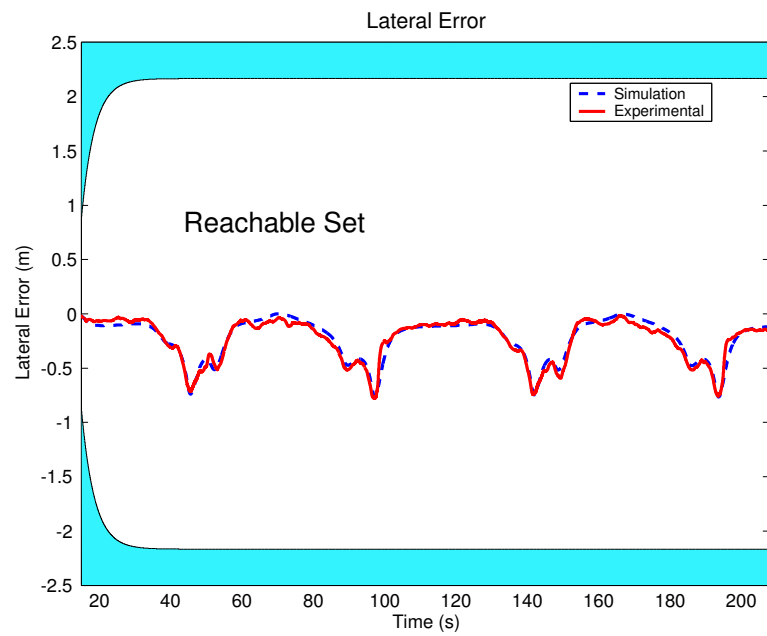


Figure 5.10: Difference in Lateral Error between Simulation and Experiment

The success of these experiments confirm that the theoretical bounds provide a potential field gain capable of keeping the vehicle within lane boundaries in the absence of driver input. The bounds also provide a safety guarantee for the lanekeeping system without too much conservatism. Using the bounding technique for the design of the potential field gains, provides a system that will remain in the lane, while not being so large that the controller overpowers the drivers steering inputs.

The test setup also verifies the feasibility of using GPS data and INS sensors to detect lane position for smooth and comfortable lanekeeping assistance. Although it was not presented, the lanekeeping system was tested at speeds up to 50mph along the straight sections of the map and continued to operate smoothly. This provides some level of confidence that this setup could be used in combination with other sensors for a robust and comfortable lanekeeping system.

Figure 5.11: Lateral Error with $k=10000$

Chapter 6

Conclusion

This chapter concludes the thesis and provides a summary of the major results and contributions of this work. A discussion of directions for future work concludes the thesis.

6.1 Summary

This work presented a controller framework for incorporating active lanekeeping as a driver assistance system. Unlike autonomous systems where the primary goal may be accurate and high performance tracking, an assistance system has different design objectives, summarized below.

- The system must integrate well with the driver, and not be overly obtrusive during normal driving
- The system must provide a stable, well behaved response that is predictable for the driver
- In the absence of driver commands, the assistance system must keep the vehicle in the lane

To achieve these goals, a potential field approach is used to passively couple the vehicle to the environment. This approach has several key advantages. It provides a

natural and intuitive way of representing hazards - The larger the potential, the more hazardous the obstacle. The general approach also utilizes the natural damping of the tires to leave all the uncontrolled vehicle dynamics and simply adds the control forces from the potential. This is a key advantage for driver assistance because the underlying handling characteristics of the vehicle remain, presenting a familiar set of dynamics to the driver.

Although the general approach dissipates overall energy, the performance and local stability of the vehicle's lateral dynamics depend on the underlying handling characteristics and the passive connection with the environment. Treating the potential field controller as a 'virtual' force applied to the vehicle is a unique way of looking at the stability of the lanekeeping system. This approach showed that two important conditions must be satisfied for lateral stability. First, the control force must be applied in front of the neutral steer point of the vehicle. Once this condition is satisfied an appropriate response can be obtained by basing the control force on a projected lateral error. This approach to vehicle stability provides a unique way of obtaining simple stability criterion that encompasses a wide variety of vehicle actuator and sensing configurations.

Incorporating the stability results from the linear analysis into the potential field framework results in a control force that is not strictly derivable from the lanekeeping potential. The controlled system dynamics still maintain passive properties, but this bound on the total system energy provides extremely conservative bounds for the lateral motion of the vehicle. With a constraint on the lookahead distance, a subset of the dynamics (pertaining to the lateral and heading error dynamics) is also passive. The Lyapunov function bounding this subset of the dynamics provides an excellent bound for the vehicle's lateral motion. This function is useful for appropriately scaling the potential function or bounding the lanekeeping performance of the system.

The potential field approach passively couples the vehicle to the environment and does not attempt to track a desired trajectory. Therefore, disturbances such as road curvature will alter the path of the vehicle. A general Lyapunov based method provides a quantitative method for bounding the vehicle motion in the presence of disturbances. This bounding technique is extremely general and applies to a wide

variety of Lagrangian systems. The bounding method utilizes a change of variables to give realistic bounds for slowly varying disturbances (such as road curvature). This bound works remarkably well for the lanekeeping system and provides an analytical method for guaranteeing the nominal safety of the potential field system.

Finally, experimental results verified the feasibility of the potential field approach for lanekeeping and the theoretical bounds for the system performance. The lateral error from experimental results matches simulation results remarkably well. The results also show that the bounding technique can be used to design a potential field controller that remains within the lane without being overly conservative.

6.2 Future Work

A successful driver assistance system has to increase the vehicle safety and be acceptable for the user. A natural direction for this work is to focus on driver acceptance issues. One major area affecting driver comfort is the type of steering wheel feedback given to the user. With steer-by-wire, there is a wealth of options for the type of feedback used. Forces can be added based on the vehicle states, the position in the potential, as well as the states of the steering wheel itself. Incorporating force feedback requires actuation at the steering wheel. Since the steering wheel controls part of the overall steering command, the stability of the lanekeeping system will be altered. When designing a force feedback system, the stability conditions for the overall system must be considered, in a variety of situations. With the driver steering normally the feedback should feel intuitive to the driver. With hands off the steering wheel, the system must still be stable and maintain the vehicle within the lane. Another intriguing avenue of study is the stability of the system with the user in the loop. For example, if there is sufficient delay in the feedback system, the driver may not be able to stabilize the vehicle.

Determining driver intent may also play a role in the user acceptance of active driver assistance system. For example, if a driver decides to change lanes or pull over and stop on the lane shoulder the system should not prevent this. One solution is to scale the potential function to allow these types of maneuvers. If it is possible

to know what the driver is planning, however, the potential field could be modified to accommodate a driver's desire. For example, if a driver wants to change lanes into an adjacent lane that is free of obstacles, the most unobtrusive system would simply remove the potential between lanes. Upon successful completion of the lane change, the lanekeeping potential can be reinstated. Studies of driver intent could utilize driver cues such as steering movements along with head and eye positions. There are many intriguing avenues for future work in active driver assistance. These systems hold the potential of saving thousand of lives while preserving the autonomy and freedom that have made cars an inexorable part of daily life.

Appendix A

The Dugoff Tire Model

The Dugoff tire model captures the nonlinear behavior of tires near saturation and accounts for the coupling that occurs between lateral and longitudinal forces [28]. Recalling that the tire slip and slip angle are defined as

$$s_w = \frac{V_x - R\omega}{V_x} \quad (\text{A.1})$$

$$\alpha = \tan^{-1} \left(\frac{V_y}{V_x} \right) \quad (\text{A.2})$$

where V_x and V_y are the longitudinal and lateral velocity at the tire center, R is the tire radius, and ω is the angular velocity of the tire as shown in Figure A.1.

The forces from the Dugoff tire model can be specified at each tire in terms of the longitudinal tire slip, s_w , slip angle, α , normal force, F_n , and friction coefficient, μ :

$$F_x = -\frac{C_x s_w}{1 - s_w} f(\lambda) \quad (\text{A.3})$$

$$F_y = -\frac{C_y \tan \alpha}{1 - s_w} f(\lambda) \quad (\text{A.4})$$

where,

$$\lambda = \frac{\mu F_n (1 - s_w)}{2[F_x^2 + F_y^2]^{1/2}} \quad (\text{A.5})$$

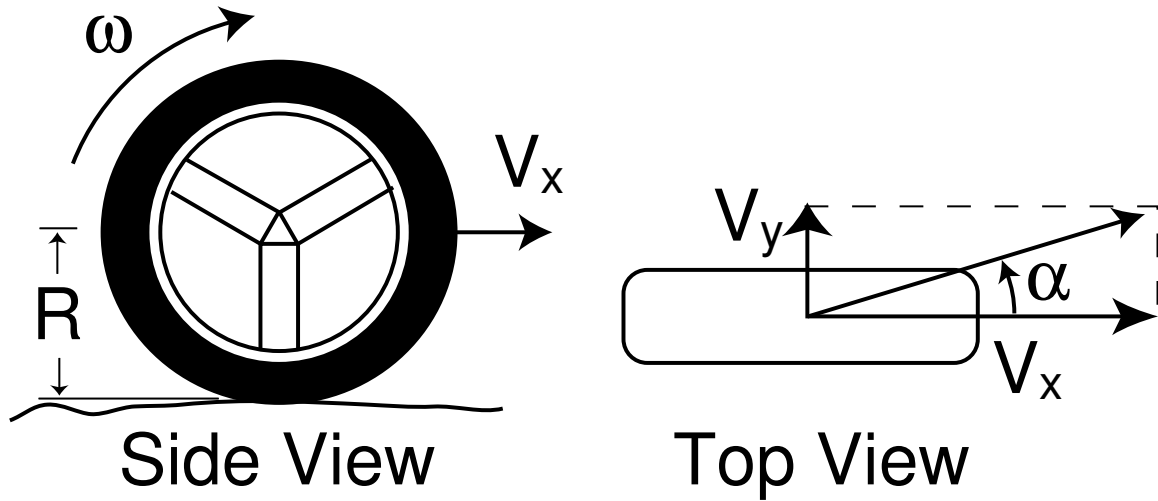


Figure A.1: Tire Velocities

and

$$f(\lambda) = \begin{cases} (2 - \lambda)\lambda & : \lambda < 1 \\ 1 & : \lambda \geq 1 \end{cases} \quad (\text{A.6})$$

The $f(\lambda)$ term accounts for tire saturation, which occurs as the tires begin to slide. Figure A.2 shows the lateral force versus slip angle and longitudinal force plotted against the tire slip.

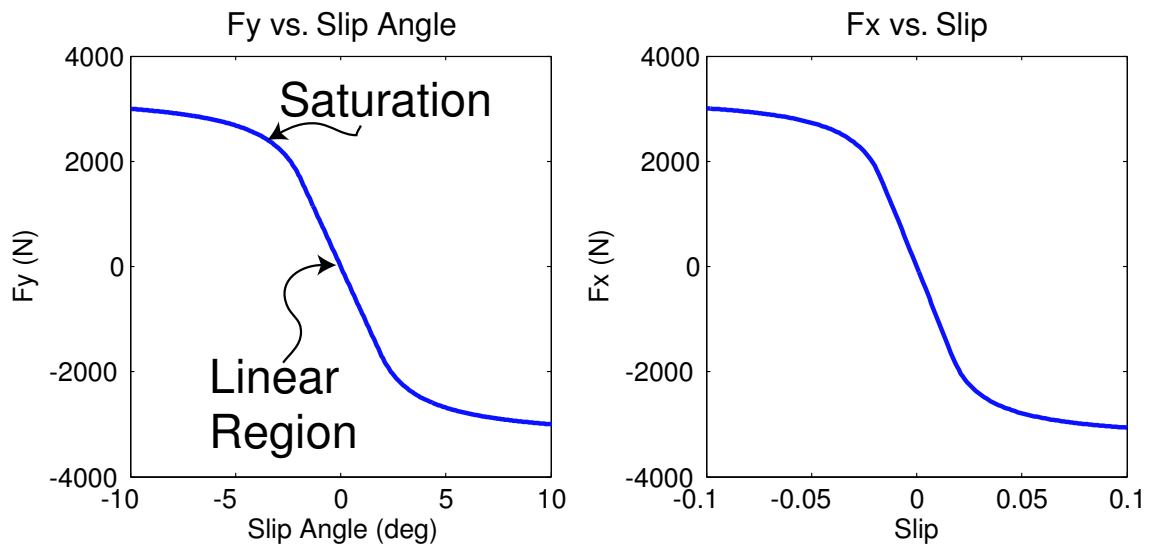


Figure A.2: Lateral and Longitudinal Tire Forces

Appendix B

Solving for the Control Inputs

This section looks at solving for the control vector $g(u_c)$ (first introduced in Chapter 2) using the non-linear Dugoff tire model and assuming a fully x-by-wire vehicle with differential braking. The control vector consists of terms involving the longitudinal forces on the tires and a portion of the lateral force on the front tires involving the steering angle. The potential field control law sets these forces equal to the forces controlled by the driver, $g(u_{driver})$, along with forces and moments from the damping and potential functions. In essence, this can be viewed as setting the control forces at the tires equal to ‘virtual’ control forces and a moment, derived from the potential field controller, that act at the vehicle’s center of gravity. This equivalent forces concept is depicted in Figure B.1 and gives a graphical representation of the following process that solves for the control vector, u_c .

Solving for an appropriate choice of inputs requires the use of a specific tire model. In contrast to the linear model used by Gerdes and Rossetter [21], the following solution for the control vector uses the simplified version of the Dugoff tire model presented in Appendix A. As opposed to the linear tire model, the Dugoff model captures the coupling between lateral and longitudinal forces.

For simplicity in solving for the control vector, it is assumed in this paper that the tires are not near saturation. In this region, the non-linear $f(\lambda)$ term equals one. If saturation is taken into account, a solution for u_c can be found using iterative techniques on the procedure presented below. To get F_y in terms of the control

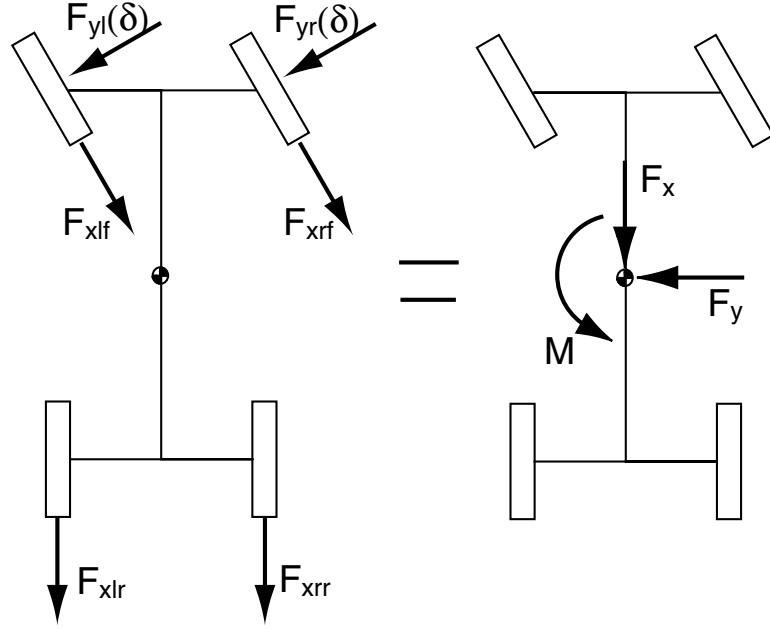


Figure B.1: Equivalent Forces Concept

inputs the slip term has to be eliminated. Assuming a static representation of slip, the longitudinal force equation (Equation A.3) can be solved to give:

$$s = \frac{F_x}{F_x - C_x} \quad (\text{B.1})$$

Substituting this expression into F_y (Equation A.4) and assuming small angles gives the following expression for the front lateral force:

$$F_{yf} = C_{yf}\delta - C_{yf}\left(\frac{ra + U_y}{U_x}\right) - \frac{C_{yf}}{C_{xf}}F_{xf}\delta + \frac{C_{yf}}{C_{xf}}F_{xf}\left(\frac{ra + U_y}{U_x}\right) \quad (\text{B.2})$$

This equation for F_{yf} is substituted into Equation 2.22 to obtain an expression that is solely in terms of the control vector u_c .

$$g(u_c) = \begin{bmatrix} F_{xf} - (C_{yf}\delta - C_{yf}\left(\frac{ra+U_y}{U_x}\right) - \frac{C_{yf}}{C_{xf}}F_{xf}\delta + \frac{C_{yf}}{C_{xf}}F_{xf}\left(\frac{ra+U_y}{U_x}\right))\delta + F_{xr} \\ F_{xf}\delta + C_{yf}\delta - \frac{C_{yf}}{C_{xf}}F_{xf}\delta + \frac{C_{yf}}{C_{xf}}F_{xf}\left(\frac{ra+U_y}{U_x}\right) \\ (\Delta F_{xr} + \Delta F_{xf})\frac{d}{2} + F_{xf}\delta a + (C_{yf}\delta - \frac{C_{yf}}{C_{xf}}F_{xf}\delta + \frac{C_{yf}}{C_{xf}}F_{xf}\left(\frac{ra+U_y}{U_x}\right))a \end{bmatrix} \quad (\text{B.3})$$

To solve for u_c , the above vector equation is set equal to the generalized force terms of Equation 2.27. Solving for the controlled terms involves manipulation of each equation in the control vector. Therefore, the following notation is introduced to separate Equation 2.27 into the desired force components and equate the terms with those in Equation B.3.

$$\begin{bmatrix} g_{des}(1) \\ g_{des}(2) \\ g_{des}(3) \end{bmatrix} = g(u_{driver}) + F(\dot{q}_3) - \left(\frac{\partial V_c}{\partial w} \frac{\partial w}{\partial q_3} \right)^T \quad (\text{B.4})$$

The components, $g_{des}(1)$ and $g_{des}(2)$ can be thought of as the ‘virtual’ control force in the longitudinal and lateral direction while $g_{des}(3)$ is the control moment to be applied. The controlled dynamics of Equation B.3 are set equal to the above force components to solve for the control vector u_c .

$$F_{xf} - (C_{yf}\delta - C_{yf}\left(\frac{ra + U_y}{U_x}\right) - \frac{C_{yf}}{C_{xf}}F_{xf}\delta + \frac{C_{yf}}{C_{xf}}F_{xf}\left(\frac{ra + U_y}{U_x}\right))\delta + F_{xr} = g_{des}(1) \quad (\text{B.5})$$

$$F_{xf}\delta + C_{yf}\delta - \frac{C_{yf}}{C_{xf}}F_{xf}\delta + \frac{C_{yf}}{C_{xf}}F_{xf}\left(\frac{ra + U_y}{U_x}\right) = g_{des}(2) \quad (\text{B.6})$$

$$(\Delta F_{xr} + \Delta F_{xf})\frac{d}{2} + F_{xf}\delta a + (C_{yf}\delta - \frac{C_{yf}}{C_{xf}}F_{xf}\delta + \frac{C_{yf}}{C_{xf}}F_{xf}\left(\frac{ra + U_y}{U_x}\right))a = g_{des}(3) \quad (\text{B.7})$$

This system is undertermined, but there exists a variety of techniques that can be used to solve this problem. The approach used in this section adds two extra constraints and is by no means the most elegant solution, but it presents one method of solving for the control inputs with the Dugoff tire model. The first constraint is to assume a differential braking distribution, which is given in Figure B.2. This distribution puts all the differential braking on the front wheels until a magnitude of 500N is reached. If the total differential braking required is above this amount, the extra force is distributed evenly between the front and rear wheels. The value for switching some of the differential load to the rear was chosen based on the lowest coefficient of friction used in simulation. In reality, this value could be based on results from μ estimation. The second constraint, shown in Figure B.3, distributes the total braking

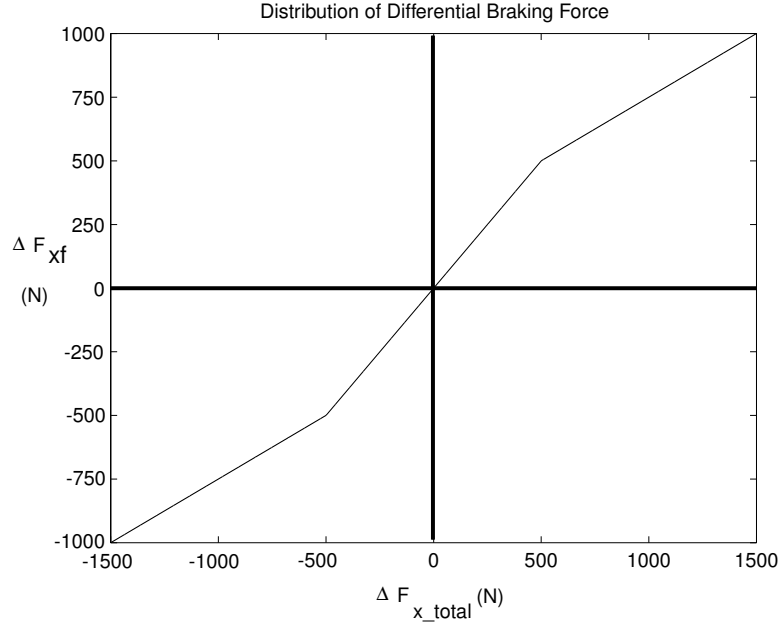


Figure B.2: Differential Braking Distribution

between front and rear. Since we are assuming a rear wheel drive vehicle, the front wheels can only provide braking forces. The minimum amount of braking force is determined by the differential braking needed at the front. Therefore, if the vehicle needs a total force that is larger than the braking force at the front, this must come from the rear wheels. If the total braking force is larger than the force capable by the front tires, the extra braking force required is evenly distributed between the front and rear wheels of the vehicle.

To solve for the control inputs, Equation B.7 is subtracted from Equation B.6 multiplied by the parameter a . This gives an expression for the total differential braking needed in the system:

$$\Delta F_{x_total} = \Delta F_{xr} + \Delta F_{xf} = -\frac{2}{d}(ag_{des}(2) - g_{des}(3)) \quad (\text{B.8})$$

Using the first constraint in Figure B.2, the differential braking at the front and rear is determined.

The total longitudinal force required is estimated by neglecting terms involving δ

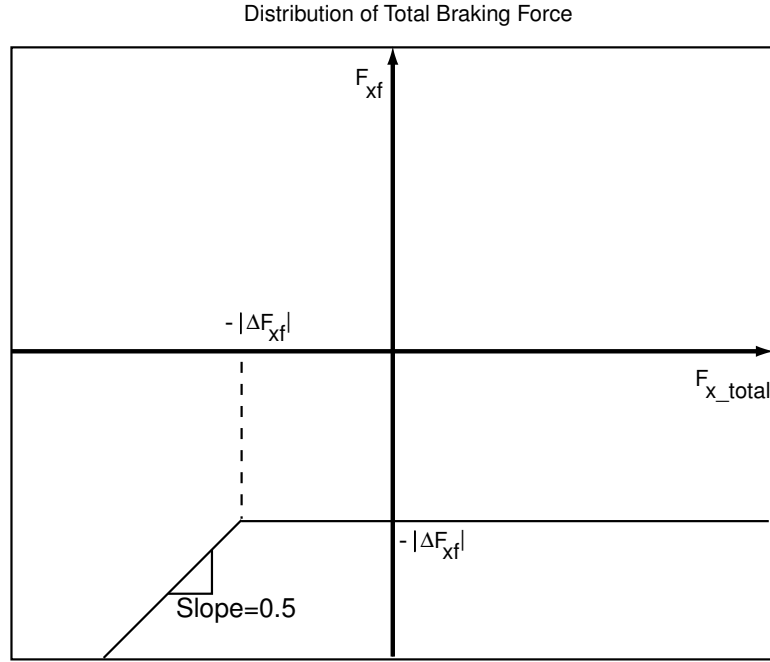


Figure B.3: Front/Rear Brake Distribution

from Equation B.5.

$$F_{xf} + F_{xr} \approx g_{des}(1) \tag{B.9}$$

Using this estimate, the total force at the front can be determined from the second constraint in Figure B.3. This value for F_{xf} is substituted into Equation B.6 and the steering angle, δ , can be found. The steering angle and front longitudinal force are then used in Equation B.5 to solve for the total rear longitudinal force, F_{xr} . With the total and differential longitudinal forces now known for each axle, the longitudinal force at each wheel can be determined.

Appendix C

A Simple Stability Controller

This section develops a simple stability controller in the potential field framework by including a generalized damping term. A stability controller should use the available control inputs to keep the vehicle's yaw rate, r , as close to the desired yaw rate commanded by the driver, r_{des} . Based upon steady state handling results, the desired yaw rate is determined by the driver's steering command, δ_{driver} [25]:

$$r_{des} = \frac{U_x}{L + KU_x^2} \delta_{driver} \quad (\text{C.1})$$

where L is the wheelbase of the vehicle, U_x is the longitudinal velocity, and K is given by

$$K = \frac{W_f}{C_f} - \frac{W_r}{C_r} \quad (\text{C.2})$$

W_f and W_r are the weights on the front and rear of the vehicle and C_f and C_r are the front and rear cornering stiffnesses. The term, K , is the vehicle's understeer gradient and is another way of looking at the handling characteristics of a vehicle (Chapter 3).

The yaw rate controller developed here simply commands a moment on the vehicle based on the error between the desired yaw rate and the actual yaw rate.

$$M_{yaw,des} = \gamma(r_{des} - r) \quad (\text{C.3})$$

where γ is a positive constant. Figure C.1 conceptually divides this controller into

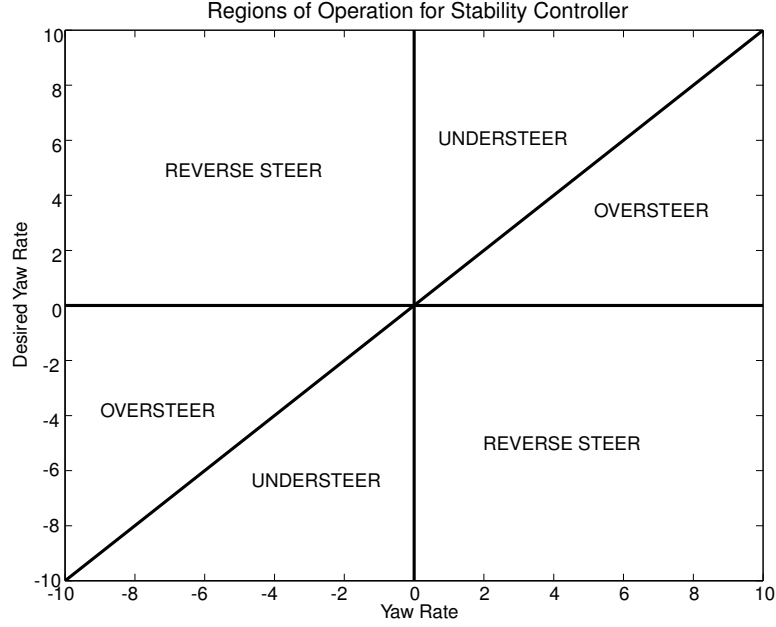


Figure C.1: Stability Control Regions of Operation

six regions, labelled understeer, oversteer, and reverse steer. The understeer case refers to a situation where the vehicle is not rotating as fast as it should, hence it is understeering the desired path. The opposite case occurs when the vehicle is rotating too quickly and oversteering the desired trajectory. The reverse steer case refers to a situation where the vehicle is spinning in a direction opposite of the desired rotation. In the oversteer and reverse steer cases, the desired yaw moment always acts in the opposite direction as the yaw rate, making the damping nature of the controller quite clear. In the understeering case, however, the stability controller increases the yaw rate. If we do not compensate for the effect of the differential braking terms on the longitudinal motion, however, the overall system exhibits a damped response.

Therefore, defining the damping function, F by

$$F(\dot{q}_3, u_{driver}) = \begin{bmatrix} \frac{2}{d}\gamma|r_{des} - r| \\ 0 \\ \gamma(r_{des} - r) \end{bmatrix} \quad (\text{C.4})$$

$$\dot{q}^T F(\dot{q}_3, u_{driver}) = r [\gamma(r_{des} - r)] - 2U_x \gamma |r_{des} - r|/d \quad (C.5)$$

This expression is less than zero whenever the vehicle is operating in the oversteer or reverse steer regions described above or when the vehicle is operating in the understeer region with:

$$|r| \leq \frac{2U_x}{d} \quad (C.6)$$

Physically, this corresponds to an instantaneous turning radius greater than half of the track width. Cases where the vehicle is understeering the desired yaw rate while achieving a turning radius of less than half of the track are, to say the least, rare. From a mathematical standpoint, the controller can be shut off or the driver command limited under these conditions to guarantee damping; from a practical standpoint, such a modification does not impact the stability control at all. The control law used in this simulation uses this stability controller combined with the lanekeeping potential shown in Figure 2.7 (Chapter 2).

$$g(u_c) = g(u_{driver}) + F(\dot{q}_3, u_{driver}) - \left(\frac{\partial V_c}{\partial w} \frac{\partial w}{\partial q_3} \right)^T \quad (C.7)$$

While omitted here for simplicity, more realistic features for a stability control system can be added in this framework. Among such enhancements are braking of the front wheels, a threshold level of mismatch between r and r_{des} before the system activates and ensuring that the system does not attempt to track values of r_{des} that cannot be achieved under the current friction conditions (Alberti and Babbal [2]). Additional stabilization based upon the vehicle sideslip angle can also be added within this framework, since counteracting sideslip is comparable to damping on U_y .

C.0.1 Avoidance Maneuver

To analyze the effect of the stability controller, an avoidance maneuver consisting of a double lane change is examined using the driver model given in Equation 2.31. Figure C.2 shows this maneuver under three sets of conditions. For a high friction road surface corresponding to a dry road, the driver is able to successfully control the vehicle. When the friction is reduced to a peak value $\mu = 0.3$, however, the

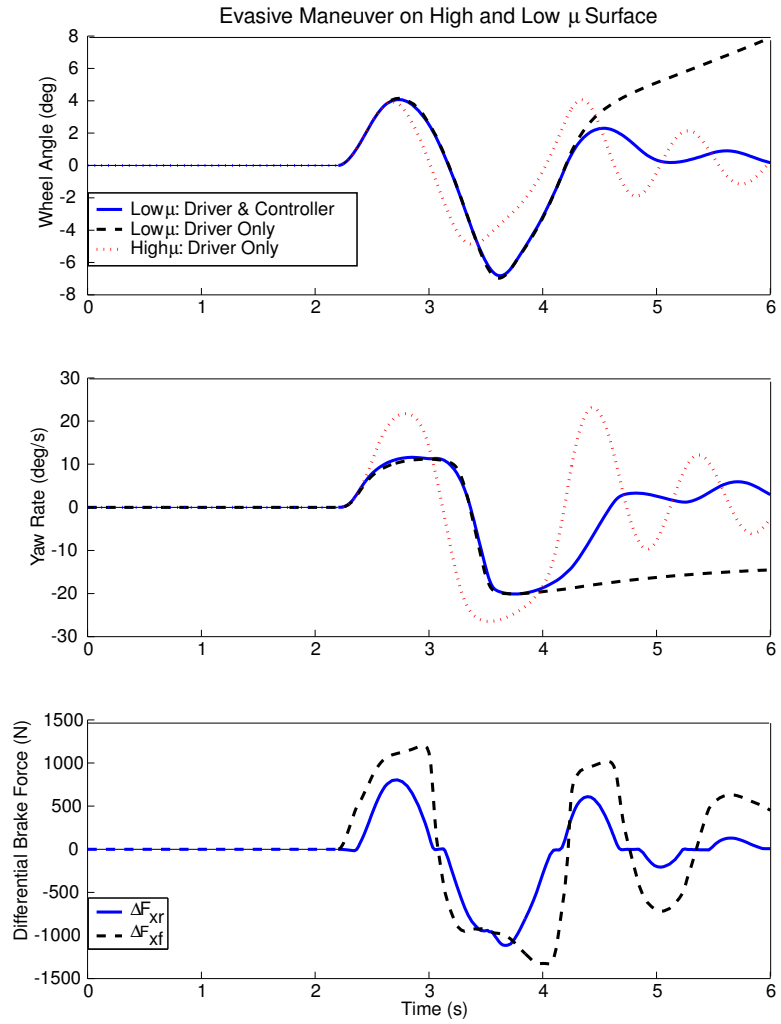


Figure C.2: Avoidance Maneuver Response

vehicle spins, as indicated by the relatively constant yaw velocity of approximately -20 deg/s. With the addition of the stability and potential field controller, the driver is again able to execute the avoidance maneuver with even less oscillation than the high μ , uncontrolled case. Comparison with published results (Alberti and Babbal [2]) shows that the controller response is indeed reasonable. As mentioned previously, the stability control here does not represent a production system due to its simplicity (particularly the lack of a term depending on the slip angle); however, it is illustrative of how control objectives can be merged in this paradigm.

Appendix D

Map Making

The map making process consists of driving the road loop at constant speed and recording position measurements from DGPS. A smooth map is generated from this data using constrained least squares. This map consists of a predetermined number of segments, each of which is a parametric polynomial function of the parameter σ [59](Figure D.1). The number of segments is chosen so that each segment will capture a feature of the road while the constant speed ensures that the density of data points is roughly uniform. For simplicity the segments contain equal numbers of data points. The polynomials describing each segment are given by

$$Y_i(\sigma) = a_{yi}\sigma^3 + b_{yi}\sigma^2 + c_{yi}\sigma + d_{yi} \quad (\text{D.1})$$

$$X_i(\sigma) = a_{xi}\sigma^3 + b_{xi}\sigma^2 + c_{xi}\sigma + d_{xi} \quad (\text{D.2})$$

where a_{yi} and a_{xi} denote the i th coefficient in the polynomial for Y and X , and σ varies from 0 to 1 on each segment.

The determination of the polynomial coefficients is formed as a constrained least squares problem [7]. To setup this problem, the unconstrained least squares solution is needed.

$$x_{in} = Hk_{xls} \quad (\text{D.3})$$

$$y_{in} = Hk_{yls} \quad (\text{D.4})$$

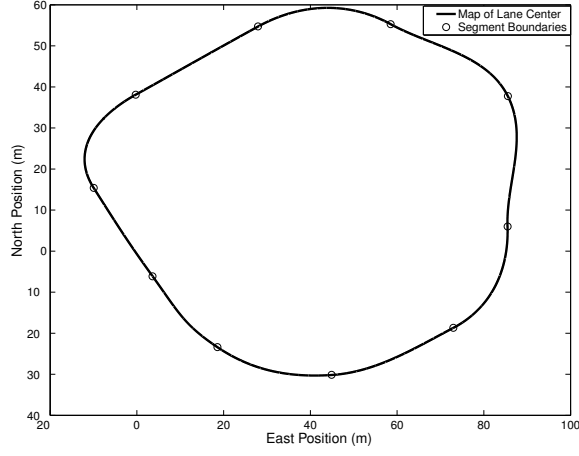


Figure D.1: Map of Lane Center Showing Segment Boundaries

where k_{xls} and k_{yls} contain the best fit polynomial coefficients for all the segments.

$$k_{xls} = \left(a_{x1} \ b_{x1} \ c_{x1} \ d_{x1} \ \dots \ a_{xn} \ b_{xn} \ c_{xn} \ d_{xn} \right)^T \quad (D.5)$$

$$k_{yls} = \left(a_{y1} \ b_{y1} \ c_{y1} \ d_{y1} \ \dots \ a_{yn} \ b_{yn} \ c_{yn} \ d_{yn} \right)^T \quad (D.6)$$

$$H = \begin{pmatrix} \bar{\sigma}^3 & \bar{\sigma}^2 & \bar{\sigma} & 1 & 0 & 0 & 0 & 0 \dots \\ 0 & 0 & 0 & 0 & \bar{\sigma}^3 & \bar{\sigma}^2 & \bar{\sigma} & 1 \dots \\ \vdots & \vdots & \vdots & \vdots & \vdots & \vdots & \vdots & \ddots \end{pmatrix} \quad (D.7)$$

where $\bar{\sigma}$ denotes the entire σ vector, ranging from 0 to 1, of length equal to the number of data points in the segment. The unconstrained solution is then found as the least squares solution of the above, or

$$k_{yls} = (H^T H)^{-1} H^T y_{in} \quad (D.8)$$

$$k_{xls} = (H^T H)^{-1} H^T x_{in} \quad (D.9)$$

The standard least squares solution does not ensure that the map will be continuous or smooth at the segment boundaries.

For a useful map, we must require that it be continuous at segment ends, and that

the slope be continuous at segment boundaries.

$$Y_i(1) = Y_{i+1}(0) \quad (\text{D.10})$$

$$X_i(1) = X_{i+1}(0) \quad (\text{D.11})$$

$$\frac{\partial Y_i}{\partial \sigma}(1) = \frac{\partial Y_{i+1}}{\partial \sigma}(0) \quad (\text{D.12})$$

$$\frac{\partial X_i}{\partial \sigma}(1) = \frac{\partial X_{i+1}}{\partial \sigma}(0) \quad (\text{D.13})$$

$$(\text{D.14})$$

Thus, we must require that

$$a_{yi} + b_{yi} + c_{yi} + d_{yi} = d_{yi+1} \quad (\text{D.15})$$

$$a_{xi} + b_{xi} + c_{xi} + d_{xi} = d_{xi+1} \quad (\text{D.16})$$

$$3a_{yi} + 2b_{yi} + c_{yi} = c_{yi+1} \quad (\text{D.17})$$

$$3a_{xi} + 2b_{xi} + c_{xi} = c_{xi+1} \quad (\text{D.18})$$

Using these constraint equations, the problem can be reformulated as a constrained least squares problem in which these equality constraints are placed on the problem in the form of a matrix equation. This matrix equation is not a minimization, but rather a series of equations that must be satisfied:

$$Ak_{xopt} = 0 \quad (\text{D.19})$$

$$Ak_{yopt} = 0 \quad (\text{D.20})$$

where the A matrix is formed to constrain the continuity and smoothness at segment boundaries.

In order to form a closed map, the last rows of the A matrix must enforce the continuity and smoothness between the final and first segments of the map, in the same way outlined above.

With the problem formulated in this way, we can find the constrained least squares

solution as

$$k_{yopt} = k_{yls} - (H^T H)^{-1} A^T [A(H^T H)^{-1} A^T]^{-1} A k_{yls} \quad (\text{D.21})$$

$$k_{xopt} = k_{xls} - (H^T H)^{-1} A^T [A(H^T H)^{-1} A^T]^{-1} A k_{xls} \quad (\text{D.22})$$

Bibliography

- [1] J. Ackermann. Robust decoupling of car steering dynamics with arbitrary mass distribution. In *Proceedings of the American Control Conference*, pages 1964–1968, 1994.
- [2] V. Alberti and E. Babbel. Improved driving stability by active braking of the individual wheels. In *Proceedings of the International Symposium on Advanced Vehicle Control, Aachen University of Technology*, pages 717–732, 1996.
- [3] A. Alleyne. A comparison of alternative intervention strategies for unintended roadway departure (URD) control. In *Proceedings of the International Symposium on Advanced Vehicle Control, Aachen University of Technology*, pages 485–506, 1996.
- [4] A. Alleyne and M. DePoorter. Lateral displacement sensor placement and forward velocity effects on stability of lateral control of vehicles. In *Proceedings of the American Control Conference*, pages 1593–1597, 1997.
- [5] E. Bakker, L. Nyborg, and H.B. Pacejka. Tyre modelling for use in vehicle dynamics studies. In *Proceedings of the SAE Congress and Exposition*, 1987.
- [6] M. Binfet-Kull, B. Rech, and A. Meyna. Definition of safety/reliability requirements for components of an electronic vehicle system such as steer by wire. In *Proceedings of the 4th European Conference and Exhibition on Vehicle Electronic Systems, Coventry, UK*, 2001.
- [7] Ake Bjorck. *Numerical Methods for Least Squares Problems*. SIAM, Philadelphia, PA, 1996.

- [8] S.Y. Chang, C.R. Carlson, and J.C. Gerdes. A Lyapunov approach to energy based model reduction. In *Proceedings of the ASME International Congress and Exposition*, 2000.
- [9] C. Chen and M. Tomizuka. Passivity-based nonlinear observer for lateral control of tractor-trailer vehicles in automated highway systems. In *Proceedings of the 1996 IFAC, San Francisco, CA*, pages 273–278, 1996.
- [10] R.J. Cooke, D.A. Crolla, and M. Abe. Combined ride and handling modelling of a vehicle with active suspension. In *Proceedings of the International Symposium on Advanced Vehicle Control, Aachen University of Technology*, pages 1037–1053, 1996.
- [11] S.C. Crow and F.L. Manning. Differential GPS Control of Starcar 2. *Journal of the Institute of Navigation*, 39:383–405, Winter 1992.
- [12] E. Dilger, T. Fuhrer, and B. Muller. Distributed fault tolerant and safety critical applications in vehicles—a time-triggered approach. In *Proceedings of the 17th International Conference on Computer Safety, Reliability and Security, Heidelberg, Germany*, 1998.
- [13] J. Farrell and M. Barth. Integration of GPS-aided INS into AVCSS. Technical Report MOU 374, California PATH Program, 2000.
- [14] K. Feng, H. Tan, and M. Tomizuka. Design of vehicle lateral guidance system for driver assistance. In *Proceedings of the American Control Conference*, pages 2553–2557, 2000.
- [15] R. Fenton and R. Mayhan. Automated highway studies at the Ohio State University—an overview. *IEEE Transaction on Vehicular Technology*, 40(1):100–113, 1991.
- [16] R. Fenton, G. Melocik, and K. Olson. On the steering of automated vehicles: Theory and experiment. *IEEE Transactions on Automatic Control*, 21(3):306–315, 1976.

- [17] U. Franke, S. Goerzig, F. Lindner, D. Mehren, and F. Paetzold. Steps towards an intelligent vision system for driver assistance in urban traffic. In *Proceedings of the IEEE Intelligent Transportation Systems*, pages 601–606, 1997.
- [18] T. Fujioka, Y. Shirano, and A. Matsushita. Driver’s behavior under steering assist control system. In *Proceedings of the IEEE Intelligent Transportation Systems*, pages 246–251, 1999.
- [19] W. Riley Garrott, Michael W. Monk, and Jeffrey P. Chrstos. Vehicle inertial parameters measured values and approximations. *SAE Paper No. 881767*.
- [20] S.K. Gehrig, A. Gern, S. Heinrich, and B. Woltermann. Lane recognition on poorly structured roads-the bots dot problem in California. In *Proceedings of the IEEE Intelligent Transportation Systems*, pages 67–71, 2002.
- [21] J.C. Gerdes and E.J. Rossetter. A unified approach to driver assistance systems based on artificial potential fields. In *Proceedings of the 1999 International Mechanical Engineering Congress and Exposition, Nashville, TN.*, 1999.
- [22] J.C. Gerdes and E.J. Rossetter. A unified approach to driver assistance systems based on artificial potential fields. *ASME Journal of Dynamic Systems, Measurement, and Control*, 123:431–438, September 2001.
- [23] J.C. Gerdes, E.J. Rossetter, and U. Saur. Combining lanekeeping and vehicle following with hazard maps. *Vehicle System Dynamics*, 36(4–5):391–411, 2001.
- [24] A. Gern, U. Franke, and P. Levi. Advanced lane recognition-fusing vision and radar. In *Proceedings of the IEEE Intelligent Vehicles Symposium*, pages 45–51, 2000.
- [25] Thomas D. Gillespie. *Fundamentals of Vehicle Dynamics*. Society of Automotive Engineers, Warrendale, PA, 1992.
- [26] J. Guldner, W. Sienel, H. Tan, J. Ackermann, S. Patwardhan, and T. Buente. Robust automatic steering control for look-down reference systems with front

- and rear sensors. *IEEE Transactions on Control Systems Technology*, 7(1):2–11, 1999.
- [27] J. Guldner, H. Tan, and S. Patwardhan. Analysis of automatic steering control for highway vehicles with look-down lateral reference systems. *Vehicle System Dynamics*, pages 243–269, 1996.
- [28] R. Guntur and S. Sankar. A friction circle concept for Dugoff’s tyre friction model. *International Journal of Vehicle Design*, 4(1):373–377, 1980.
- [29] U. Handmann, T. Kalinke, C. Tzomakas, M. Werner, and W. Seelen. Image processing systems for driver assistance. *Journal of Image and Vision Computing*, 18(5):367–376, 2000.
- [30] B. Hedenetz. A development framework for ultra-dependable automotive systems based on a time-triggered architecture. In *Proceedings of the Real-Time Systems Symposium, Madrid, Spain*, 1998.
- [31] M. Hennessey, C. Shankwitz, and M. Donath. Sensor based ‘virtual bumpers’ for collision avoidance: Configuration issues. In *Proceedings of the SPIE*, volume 2592, 1995.
- [32] N. Hogan. Impedance control: An approach to manipulation, parts I-III. *ASME Journal of Dynamic Systems, Measurement, and Control*, 107:1–24, March 1985.
- [33] Hassan K. Khalil. *Nonlinear Systems*. Prentice Hall, Upper Saddle River, New Jersey 07458, 1996.
- [34] O. Khatib. Real-time obstacle avoidance for manipulators and mobile robots. *International Journal of Robotics Research*, 5(1):90–98, 1986.
- [35] B. Koepele and J. Starkey. Closed-loop vehicle and driver models for high-speed trajectory following. In *Transportation Systems - 1990 ASME WAM, Dallas, TX*, pages 59–68, 1990.

- [36] B. Krogh. A generalized potential field approach to obstacle avoidance control. In *Proceedings of the SME Conference on Robotics Research, Bethlehem, PA*, 1984.
- [37] W. Kwon and S. Lee. Performance evaluation of decision making strategies for an embedded lane departure warning system. *Journal of Robotic Systems*, 19(10):499–509, 2002.
- [38] D.J. LeBlanc, P.J. Venhovens, C.-F. Lin, T.E. Pilutti, R.D. Ervin, A.G. Ulsoy, C. MacAdam, and G.E. Johnson. Warning and intervention system to prevent road-departure accidents. *Vehicle System Dynamics*, 25:383–396, 2003.
- [39] S. Lee, W. Kwon, and J. Lee. Vision based lane departure warning system. In *Proceedings of the IEEE International Conference on Intelligent Robots and Systems*, pages 160–165, 1999.
- [40] William Milliken and Douglas Milliken. *Race Car Vehicle Dynamics*. SAE International, 400 Commonwealth Dr. Warrendale, PA 15096-0001, 1995.
- [41] NHTSA. Traffic safety facts 2001. Technical report, National Highway Traffic Safety Administration, 2002.
- [42] California Department of Transportation. The highway design manual, 2001.
- [43] M. Omae and T. Fujioka. DGPS-based position measurement and steering control for automatic driving. In *Proceedings of the American Control Conference*, 1999.
- [44] R. Ortega, A. Loria, P.J. Nicklasson, and H. Sira-Ramirez. *Passivity-based Control of Euler-Lagrange Systems*. Springer, London, England, 1998.
- [45] F. Paetzold, U. Franke, and W. Von Seelen. Lane recognition in urban environment using optimal control theory. In *Proceedings of the IEEE Intelligent Vehicles Symposium*, pages 221–226, 2000.

- [46] H. Peng and M. Tomizuka. Preview control for vehicle lateral guidance in highway automation. *ASME Journal of Dynamic Systems, Measurement, and Control*, 115:679–686, December 1993.
- [47] D. Reichardt. Kontinuierliche Verhaltenssteuerung eines autonomen Fahrzeugs in dynamischer Umgebung. PhD thesis, Fachbereich Informatik der Universitaet Kaiserslautern, May 1996.
- [48] D. Reichardt and J. Schick. Collision avoidance in dynamic environments applied to autonomous vehicle guidance on the motorway. In *Proceedings of the IEEE Intelligent Vehicles Symposium, Paris, France, 1994*.
- [49] W. Reichelt and P. Frank. Driver assistance systems to improve active safety in the closed-loop system driver-vehicle-surroundings. *International Journal of Vehicle Design*, 18(6):639–651, 1997.
- [50] A. Rekow, T. Bell, D. Bevly, and B. Parkinson. System identification and adaptive steering of tractors utilizing differential Global Positioning System. *Journal of Guidance, Control, and Dynamics*, 22:671–674, September-October 1999.
- [51] S. Rogers, P. Langley, and C. Wilson. Mining GPS data to augment road models. In *International Conference on Knowledge Discovery and Data Mining*, 1999.
- [52] E.J. Rossetter and J.C. Gerdes. Performance Guarantees for Hazard Based Lateral Vehicle Control. In *Proceedings of the ASME International Mechanical Engineering Congress and Exposition*, 2002.
- [53] E.J. Rossetter and J.C. Gerdes. A study of lateral vehicle control under a ‘virtual’ force framework. In *Proceedings of the International Symposium on Advanced Vehicle Control, Hiroshima, Japan, 2002*.
- [54] E.J. Rossetter, J.P. Switkes, and J.C. Gerdes. A gentle nudge towards safety: Experimental validation of the potential field driver assistance system. In *Proceedings of the American Control Conference*, 2003.

- [55] J. Ryu, E.J. Rossetter, and J.C. Gerdes. Vehicle sideslip and roll parameter estimation using GPS. In *Proceedings of the International Symposium on Advanced Vehicle Control, Hiroshima, Japan, 2002*.
- [56] Shankar Sastry. *Nonlinear Systems*. Springer, New York, NY, 1999.
- [57] B. Schiller, Y. Du, D. Krantz, C. Shankwitz, and M. Donath. *Vehicle Guidance Architecture for Combined Lane Tracking and Obstacle Avoidance*, chapter 7 in *Artificial Intelligence and Mobile Robots: Case Studies of Successful Robot Systems*, pages 159–192. AIII Press/The MIT Press, Cambridge, MA, 1998.
- [58] B. Schiller, V. Morellas, and M. Donath. Collision avoidance for highway vehicles using the virtual bumper controller. In *Proceedings of the IEEE International Symposium on Intelligent Vehicles*, 1998.
- [59] S. Schrödl, S. Rogers, and C. Wilson. Map refinement from GPS traces. Technical Report 6, Daimler Chrysler RTC North America, 2000.
- [60] L. Segel. Research in the fundamentals of automobile control and stability. In *Proceedings of the SAE National Summer Meeting*, pages 527–540, 1956.
- [61] S. Shladover, C. Desoer, J. Hedrick, M. Tomizuka, J. Walrand, W. Zhang, D. McMahon, H. Deng, S. Sheikholeslam, and N. McKeown. Automatic vehicle control developments in the PATH program. *IEEE Transaction on Vehicular Technology*, 40(1):114–130, 1991.
- [62] Jean-Jacques Slotine and Weiping Li. *Applied Nonlinear Control*. Prentice Hall, Englewood Cliffs, NJ, 1990.
- [63] Robert Stengel. *Optimal Control and Estimation*. Dover Publications, INC., New York, NY, 1994.
- [64] C. Stiller, W. Poechmueller, and B. Huertgen. Stereo vision in driver assistance systems. In *Proceedings of the IEEE Intelligent Transportation Systems*, pages 888–893, 1997.

- [65] K. Stonex. Car control factors and their measurement. *SAE Transactions*, 36:81–93, 1941.
- [66] K. Suzuki and H. Jansson. An analysis of driver’s steering behaviour during auditory or haptic warnings for the design of lane departure warning system. *Journal of the Society of Automotive Engineers of Japan (JSAE)*, 24(1):65–70, 2003.
- [67] D. Swaroop and S. Yoon. Integrated lateral and longitudinal vehicle control for an emergency lane change maneuver design. *International Journal of Vehicle Design*, 21(2):161–174, 1999.
- [68] M. Vidyasagar. *Nonlinear Systems Analysis*. Prentice Hall, Englewood Cliffs, New Jersey, 1993.
- [69] P. Yih, J. Ryu, and J.C. Gerdes. Modification of vehicle handling characteristics via steer-by-wire. In *Proceedings of the American Control Conference*, 2003.
- [70] W. Zhang and R.E. Parsons. An intelligent roadway reference system for vehicle lateral guidance/control. In *Proceedings of the American Control Conference*, pages 281–286, 1990.